Metals and Ceramics Division

Heavy Vehicle Propulsion Materials Program
Quarterly Progress Report for
January through March 2003

D. R. Johnson
Technical Project Manager

Prepared for
U.S. Department of Energy
Assistant Secretary for Energy Efficiency and Renewable Energy
Office of FreedomCAR and Vehicle Technologies Program
EE 07 01 00 0

Prepared by the
OAK RIDGE NATIONAL LABORATORY
Oak Ridge, Tennessee 37831-6066
Managed by
UT-Battelle, LLC
for the Department of Energy
Under contract DE-AC05-00OR22725

CONTENTS

Materials for Fuel Systems

Advanced Materials for Diesel Fuel System Injector (Detroit Diesel Corporation)

Cost-Effective Smart Materials for Diesel Engine Applications (ORNL)

Low-Cost Manufacturing Processes for Ceramic and Cermet Diesel Engine Components (SIU-C)

Intermetallic-Bonded Cermets (ORNL)

Low Cost High Toughness Ceramics (ORNL)

Materials for Exhaust Aftertreatment

Materials for Exhaust Aftertreatment (Caterpillar Inc.)

Development of Materials Analysis Tools for Studying NO_x Adsorber Catalysts (Cummins Engine Company and ORNL)

Development of NO_x Sensors for Heavy Vehicle Applications (ORNL and Ford Motor Company)

Microstructural Changes in NO_x Trap Materials under Lean and Rich Conditions at High Temperatures (ORNL and Ford Motor Company)

Materials for Air Handling, Hot Section, and Structural Components

Lightweight Valve Train Materials (Caterpillar Inc.)

Thick Thermal Barrier Coatings (TTBCs) for Low Emission, High Efficiency Diesel Engine Components (Caterpillar Inc.)

Processing and Characterization of Structural and Functional Materials for Heavy Vehicle Applications (North Carolina A&T State University)

NDE Development for Ceramic Valves for Diesel Engines (Argonne National Laboratory)

Durability of Diesel Engine Component Materials (ORNL)

Life Prediction of Diesel Engine Components (ORNL and Caterpillar)

Diesel Exhaust Filter Temperature Measurement and Cost-Effective Machining of Titanium Alloys (University of Michigan)

Advanced Cast Austenitic Stainless Steels for High-Temperature Components (ORNL and Caterpillar Inc.)

In-Situ TEM Observations of Strain-Induced Interface Instability in TiAl/Ti_3Al Laminate Composite (Lawrence Livermore National Laboratory)

Synthesis of Powders for Titanium Carbide/Nickel Aluminide Cermets (University of Colorado)

Laser Surface Texturing of Lubricated Ceramic Parts (ORNL)

High-Density Infrared Surface Treatment of Materials for Heavy-Duty Vehicles (ORNL)

Test and Materials Standards

Standards for Reliability Testing of Heavy Vehicle Propulsion Materials (NIST)

Implementing Agreement for a Programme of Research and Development on Advanced Materials for Transportation Applications (ORNL)

Mechanical Property Test Development (NIST)

DAIMLERCHRYSLER

DaimlerChrysler Powersystems

ADVANCED MATERIALS FOR FUEL INJECTION SYSTEMS

Progress Report for February 1 - April 30, 2003

Report Contents

- Piezo Stack Test Status
- Amplification Module Fabrication
- Two-Actuator Injection System Reference – Engine Testing
- Two-Actuator Injector Hydraulic Model Improvements
- Demonstrator Piezo Injector Schedule

Summary of Accomplishments

Feb 1 – Apr 30, 2003

- **Piezo Stack Testing Stretched**
  - **Higher Preload Applied to Minimize Internal Tensile Forces**
  - **Higher Voltage Applied to Achieve Higher Displacements and Higher Current for Better Response Times**
  - **Power Consumption Calculations for Energy Savings and/or Cost Reductions**
- **Design of Amplification Module System Completed. Fabrication Initiated.**
- **Two-Actuator Injection System Reference Testing Under Steady State Engine Operation Initiated. Potential Opportunities for Higher Fidelity Injector Performance Identified.**
- **Two-Actuator Injector Hydraulic Model Enhanced.**
  - **Detailed Injector Orifice (Nozzle) Model Created.**
  - **Potential Benefits of Modulated Control Valve Simulated Successfully.**
  - **Excellent Comparison of System Results (Model vs Experiment) Achieved.**

Fixture Design for Amplification System Mounting

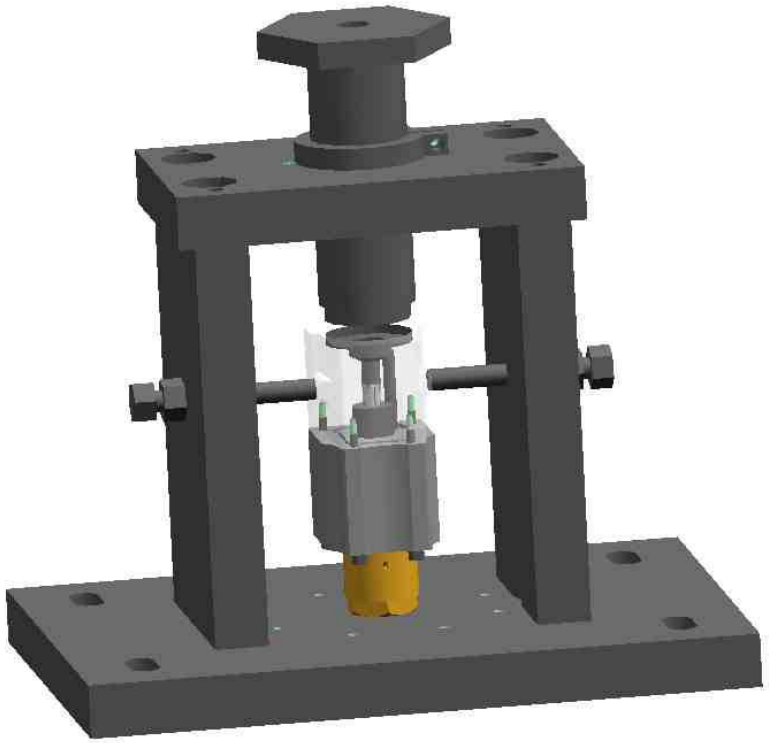

- **Modification in the 3rd Generation Fixture Completed for Mounting the Amplification System**

Testing of Stack B With Higher Preload and Current

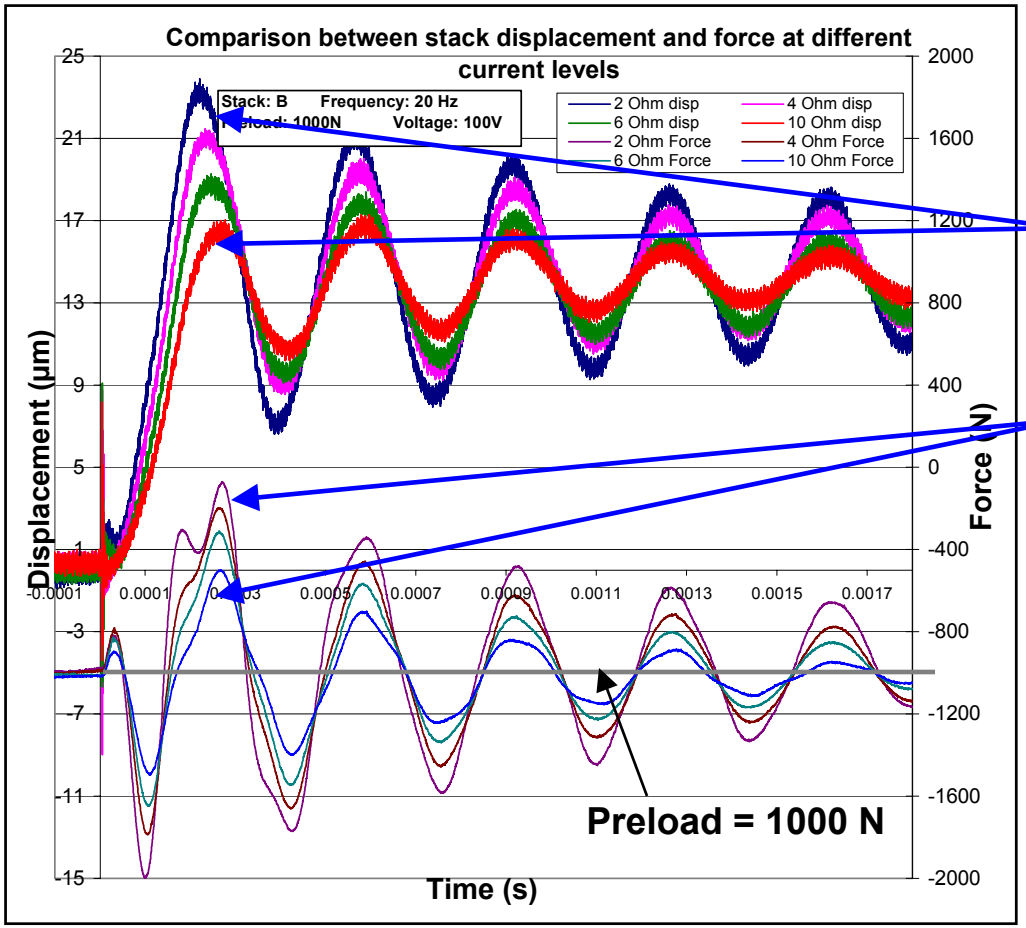

- Testing of Piezo Stack at 100 V With 1000 N Preload and Variable Current.
- Although the Average Stack Displacement Is Constant, the Overshoot Increases With Increase in Current.
- The Internal Tensile Forces in the Stack Also Increase With the Increase in Current.
- Hence, an Optimized Current Value Will Be Used To Trade-off to Avoid Higher Tensile Forces and Achieve Minimum Response Time and Minimize Over-shoot.

Development of Mathematical Equation for System Study

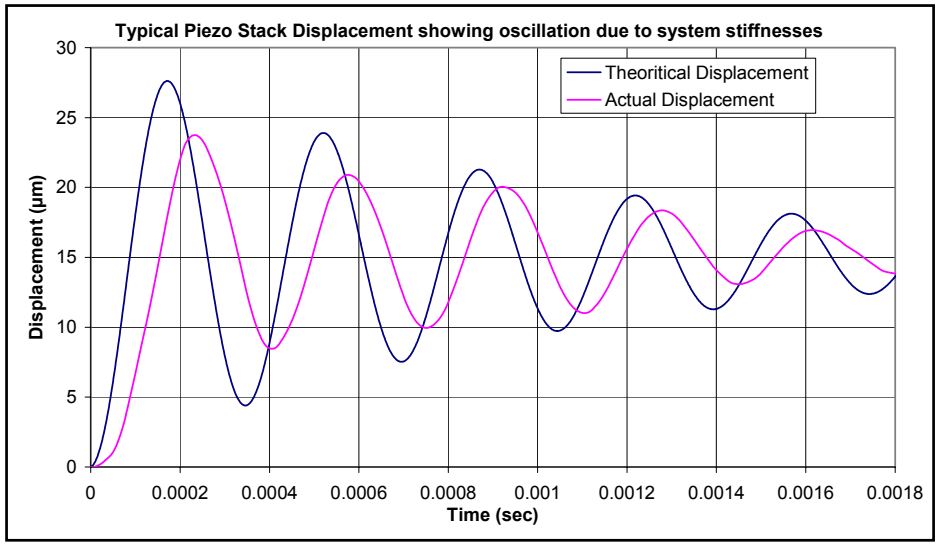

- **Mathematical System Equation Developed to Study Stack Displacement Behavior in Correlation With Experimental Results**

System Equation: $m\ddot{x} + C\dot{x} + kx = F$

Where, m – Mass; C – Damping; k – Stiffness; F – Force; x – Displacement

$$x(t) = A(t)Sin(\omega t) + B$$

Where, $A(t) = ae^{-bt}$ and $\omega = 2\pi f$, here f is stack rise freq. and not the operating freq.

Picking values: ω = 18000 rad/sec; B = 15 µm; a = -15; b = 1000

Comparison of Displacement, Rise and Delay Time

Stack B vs Stack C

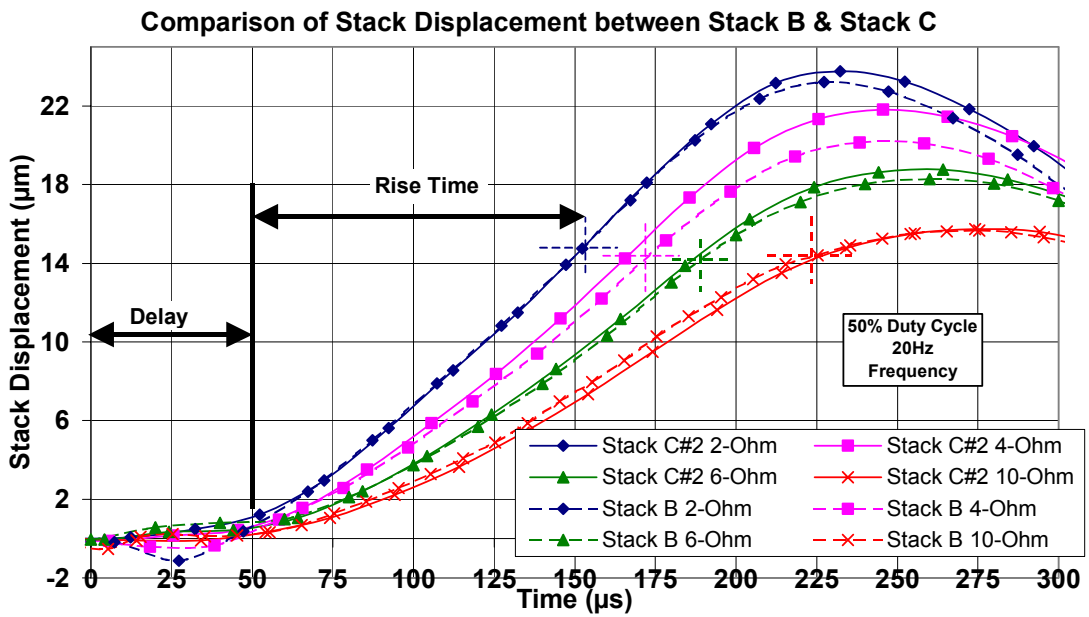

- Tests Were Completed to Measure and Compare the Displacement, Rise Time and Delay Time of Stack B and C at Varying Current With New Mechanical System
- An Average Delay Time of 50 µSec Was Observed
- The Rise Times Were About 100 µSec at Higher Current and 175 µSec at Lower Current for Stack C.
- Stack C Showed Better Performance in Terms of Displacement and Rise Times Compared to Stack B.

Power Requirements of Piezo Stack

Stack: C, Preload: 1500N, Voltage: 200V, Frequency: 20Hz

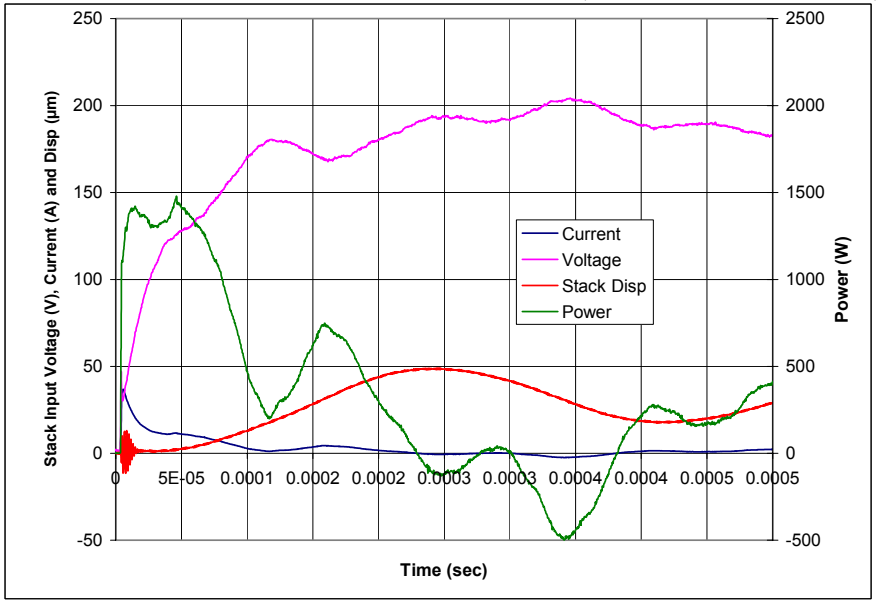

1. Power Curve During the Rise of the Stack/CV Closure in Injector

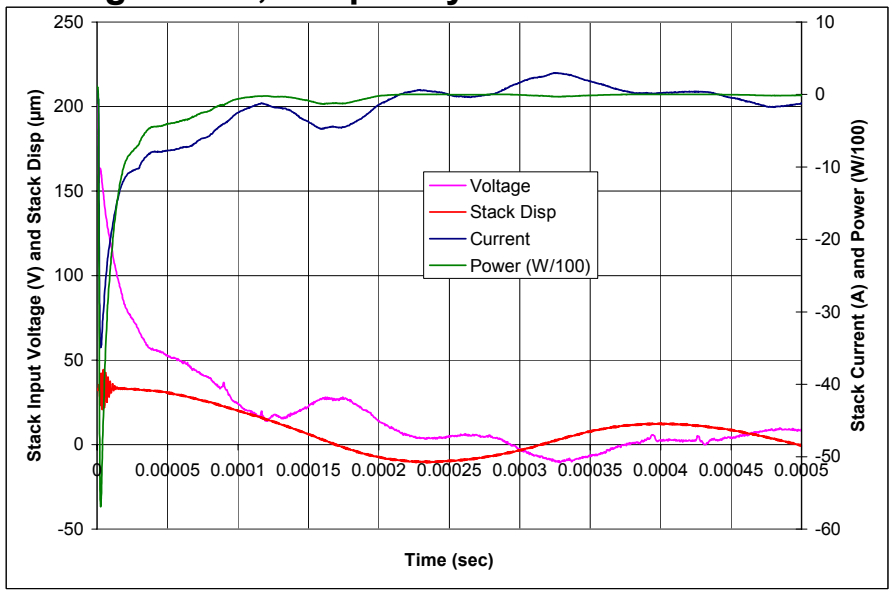

2. Power Curve During the Fall of the Stack/CV Opening in Injector

- **Tests Were Initiated to Calculate the Power Consumption by Stack C. It Was Observed That the Stack Supplies Power Back to the System During the Fall Cycle As Seen in the Right Hand Figure**
- **Also, Since There Is No Holding Current Required for Stack Displacement, the Power Consumption Is Substantially Less Compared to Solenoid Control.**

Piezo Injector Development

Amplification System Design Completed

- Methodologies to Integrate the Amplification System With the Conventional Injector Control Valve Were Developed and Implemented.
- A Control Valve Spring With Higher Stiffness Was Assembled for Higher Preload Application to the Piezo Stack
- Operating and Control Parameters Were Finalized for Piezo Injector Operation
  - Preload on Piezo Stack = 1000 N
  - Operating Voltage = 100 V
  - Operating Current = 20 A
  - Stack Displacement = 14.92 μM
  - Control Valve Displacement = 149 μM (Theoretical)
- Variation in the Above Parameters May Be Necessary Depending Upon the Functional Requirements of the Application Injector

Advantages of Amplification System

- System Designed to Fit DDC Production Injector
- Testing of the Injector Requires No Alterations to Series 60 Engine Cylinder Head
- Amplification Ratio Set to Match the Control Valve Stroke for DDC Production Injector

Two Actuator Injector Reference System

Engine Experimental Results

Investigative Results Illustrated In Following Slides

- Injection Timing Sweep (A100, C100)
- Camshaft Interaction w/ Actuator Type (A100, C100)
- Nozzle Opening Pressure vs Injection Timing (A100, C100)
- Nozzle Closing Pressure Influence (A100, C100)
- Close Coupled Pilot Injection (B50)
- Close Coupled Post Injection (B75)

Reference for Standard 13 Mode Test Procedure

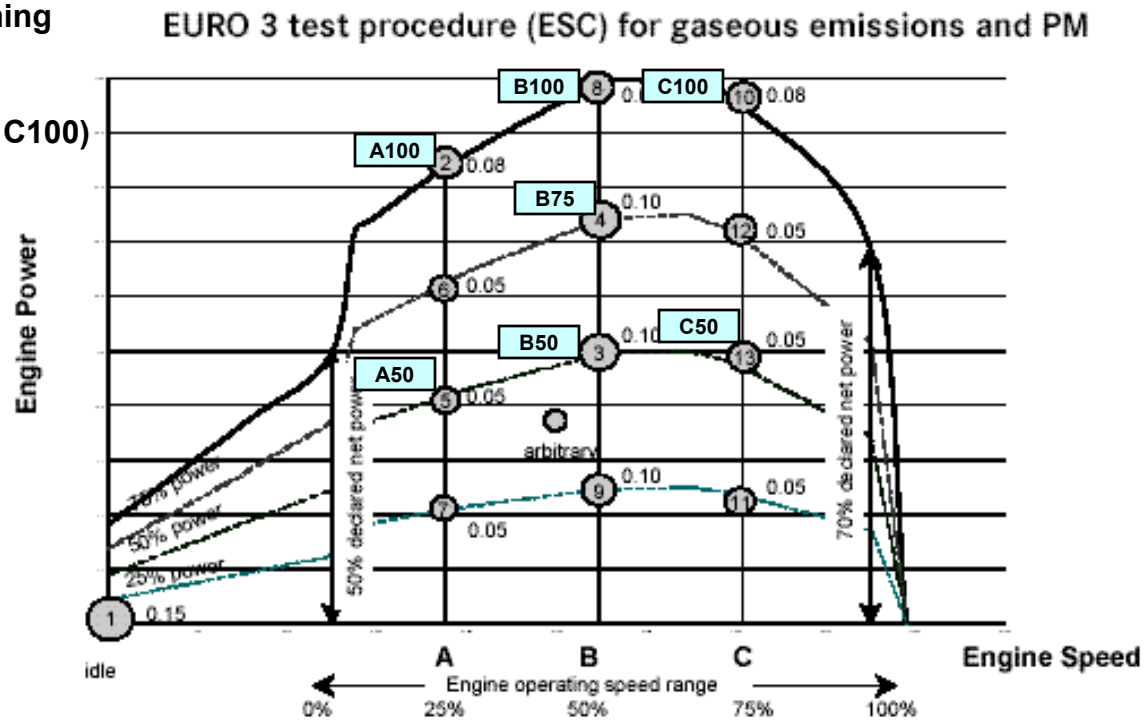

Injection Timing Sweep

A100, C100

Observations

- Best NOx-BSFC Trade-Off with Two-Actuator Injector and Higher Flow (1.7 l/min) Orifice, Slightly Better Than Lower Flow (1.4 l/min) Orifice.
- To Achieve the Same NOx, the Injection Timings of a Higher Flow (1.7l/min) Orifice Must Be More Retarded Than The Lower Flow (1.4 l/min) Orifice.
- The Steady State PM (Particulate) Levels Are Low for Any Combination Tested Here (Without EGR).

Injection Timing Sweep: 3 Points With 3° Timing Increments

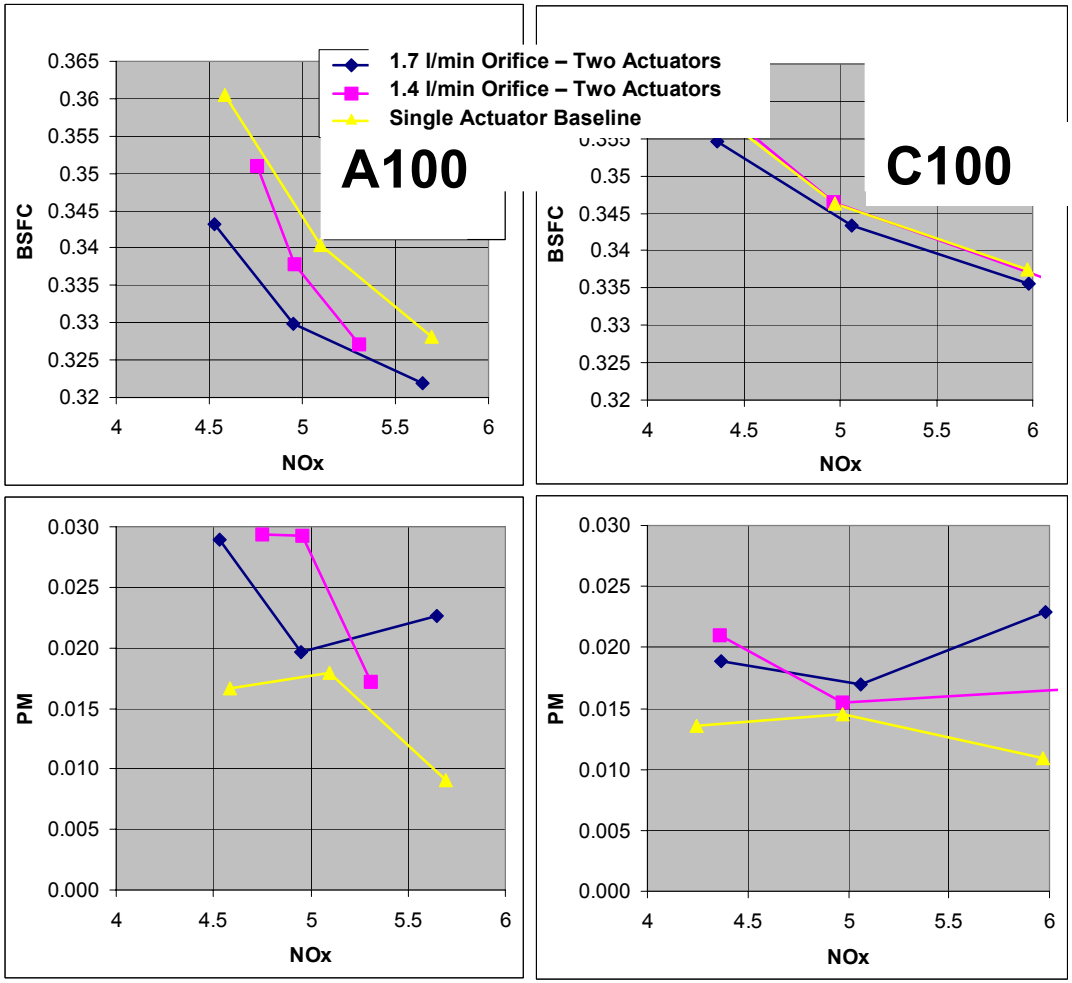

Camshaft Interaction w/ Injector Actuator Type

Observation

- **BSFC/Emissions Results with Two Actuator Injectors Compare Favorably to the Single Actuator Injector Baseline.**
- **BSFC/Emissions Results With The Two Actuator Injector Were Insensitive to The Range of Camshaft Velocity (Cam A, Cam B) Tested for These Engine Operating Conditions (A100, C100).**

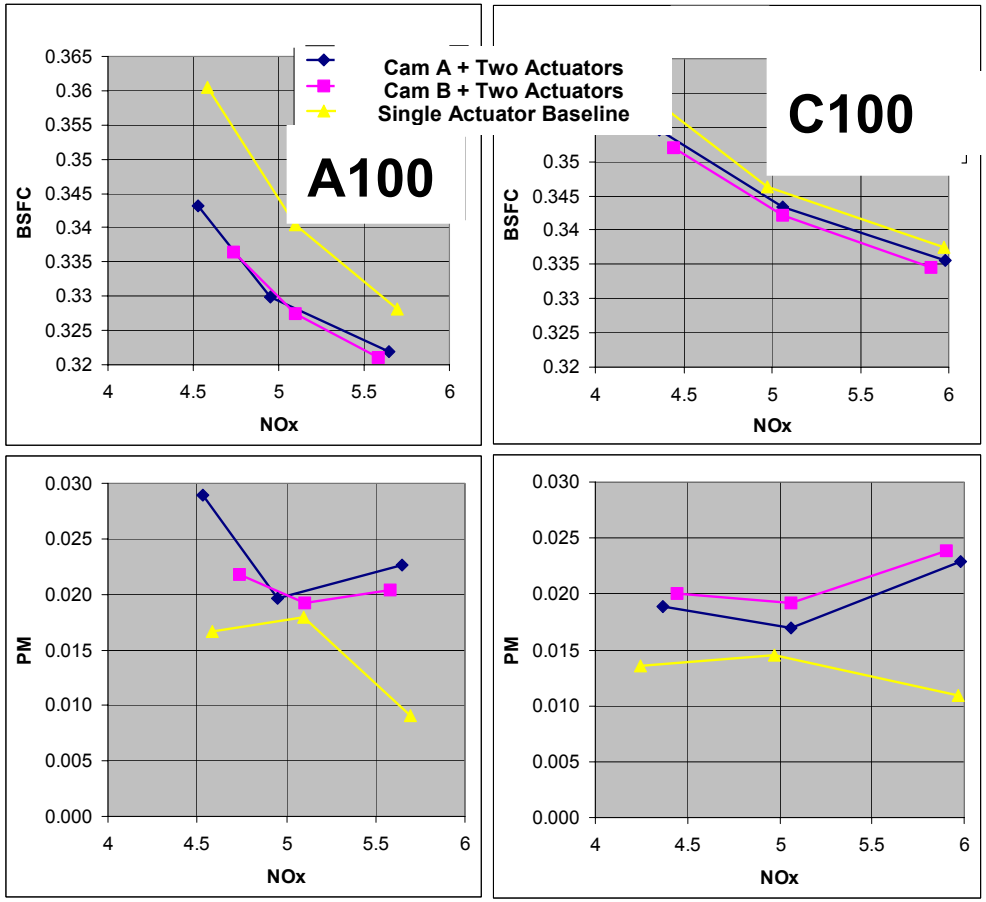

Nozzle Opening Pressure vs Injection Timing

A100, C100

Observations

- Steady State Performance and Emissions Did Not Respond Favorably to High Nozzle Opening Pressure (NOP) Settings At These Conditions (A100, C100).
- With Intermediate NOP Settings, BSFC Is Improved and Comparable To The Single Actuator Baseline.

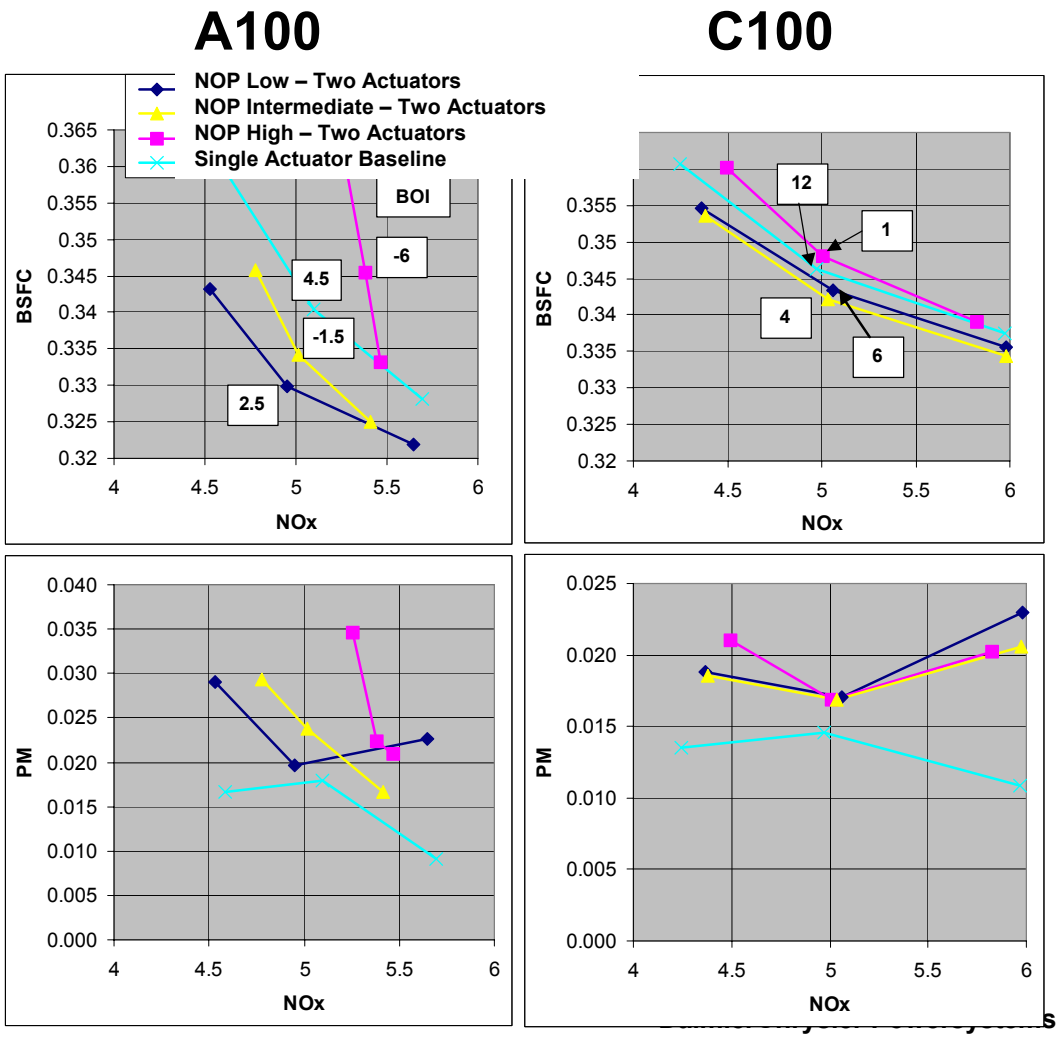

Nozzle Closing Pressure Influence

A100, C100

Observations

- **No Meaningful BSFC/Emission Impact Achieved To-Date by Varying Nozzle Closing Pressure (NCP) with the Two Actuator Injector.**
- **Potential For Higher Fidelity (ex: Piezo) Actuator To Be Investigated with Hydraulic Model.**

Two Actuator Injection

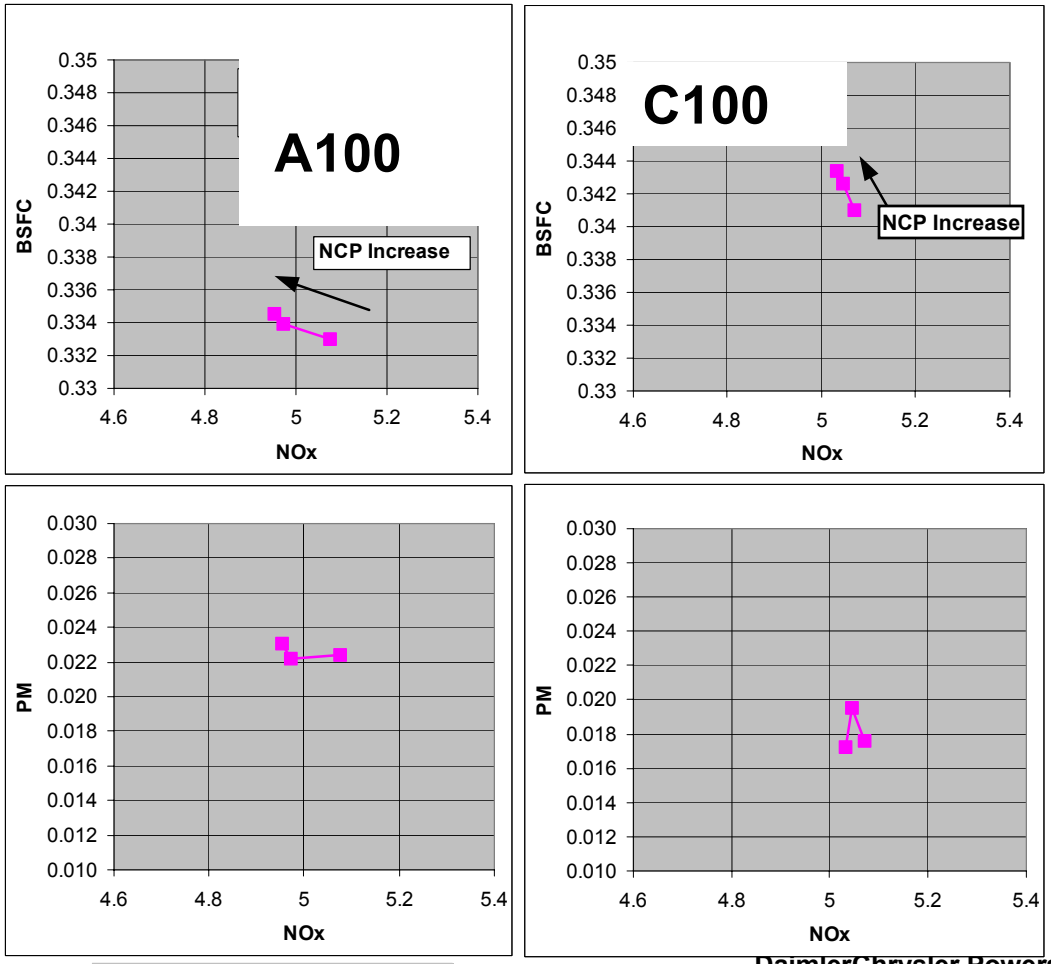

1351	1330	1332

Close Coupled Pilot Injection

B50

Observations

- **At This Test Condition (B50), Pilot Injection Offered Slight NOx and PM Benefits**
- **Shorter Pilot Separation (From Main Injection Event) Was Shown To Provide Slightly Better BSFC, but Slightly Worse PM.**
- **Pilot Injection Promises Incremental Noise and Gaseous Emission Benefits at Moderate to Light Load.**

Two Actuator Injection

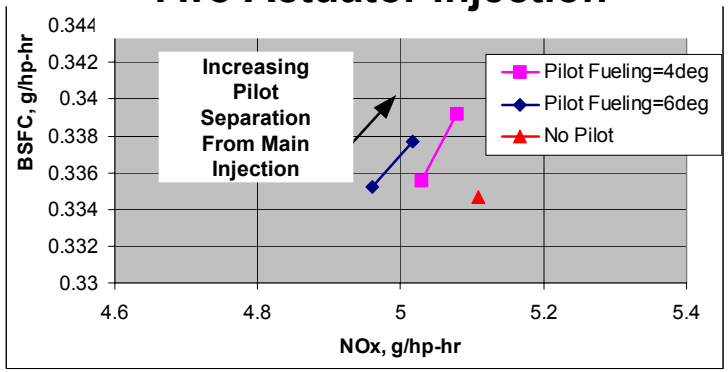

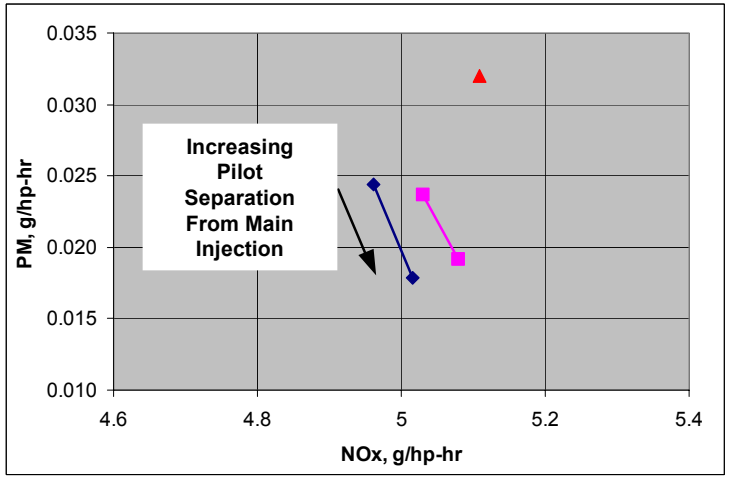

Close Coupled Post Injection

B75

Observations

- **No Strong or Favorable BSFC/Emission Trade-Off With Post Injection Apparent At This Operating Condition With The Present Level of Fidelity Afforded By the Two Actuator Injector.**
- **Variables Included Post Injection Quantity and Post Injection Separation from Main Injection.**

.

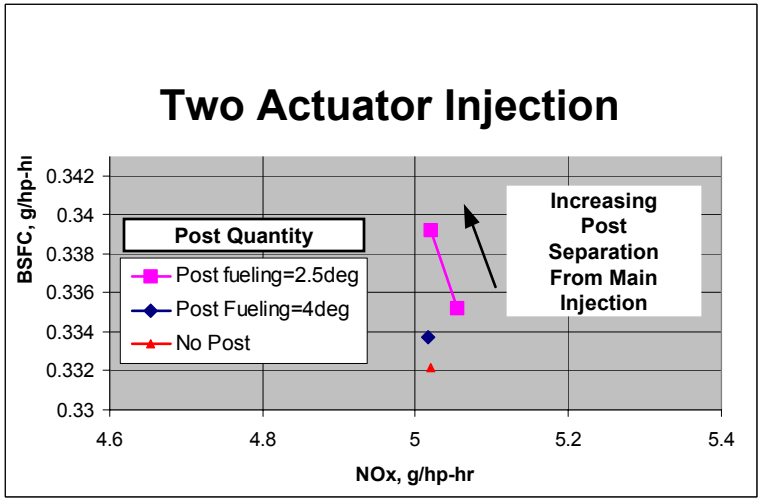

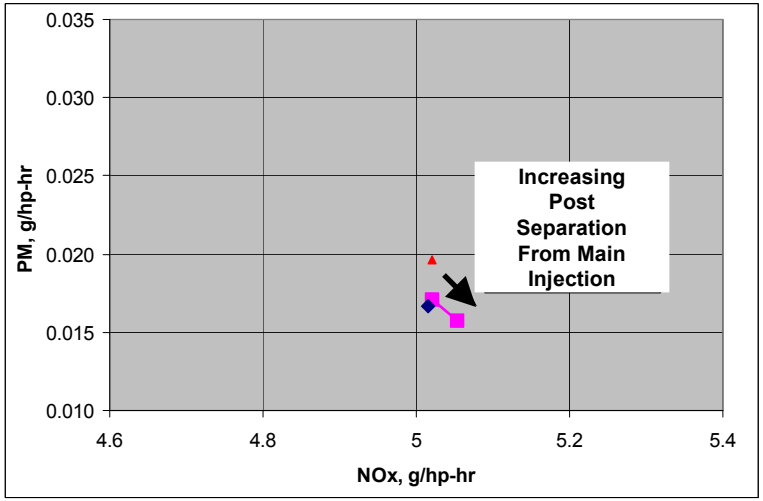

Two Actuator Hydraulic Network

Model Improvement

- Efforts Focused on Improving the Modularity of the Model
- The Nozzle Model Has Been Reevaluated
- Signal Models Are in Progress for More Versatile Multiple Injection Applications
- Extensive Verification Is in Progress for the Engine Data Calibrated Model

Two Actuator Hydraulic Network

Injector Nozzle Model

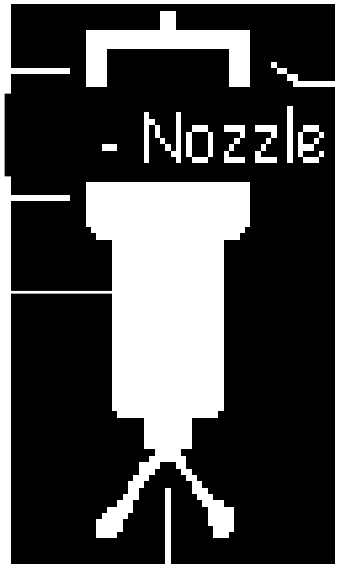

Injector Tip Super-Component

Modular Nozzle Tip Modeling Through Use of Super-Components

Super-Components Improve the Flexibility of Model

Direct Measurement Data Is Used for Tip Model Calibration

Potential of Spill Control Valve Modulation

Two Actuator Hydraulic Simulation

For Multiple Injections, Spill Control Valve Modulation Would Yield Improved Flexibility and A Wider Range of Rate Shaping. Modeling Example Below Illustrates How Pressure (Press) and Rate of Injection (ROI) Are Influenced By Modulated (Light Blue PCV) and Unmodulated (Dark Blue PCV) Spill Control Valve Motion

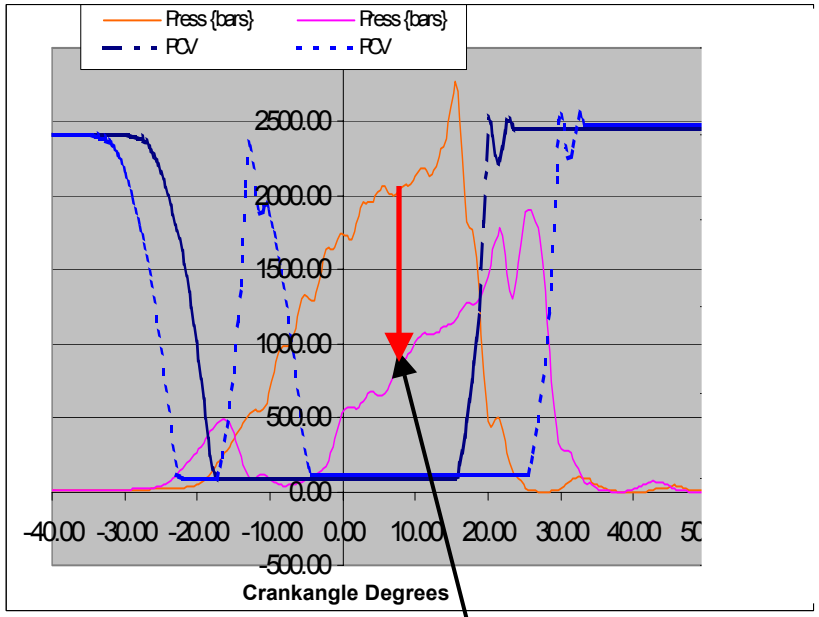

Pressure Is Reduced Due to Control Valve Modulation

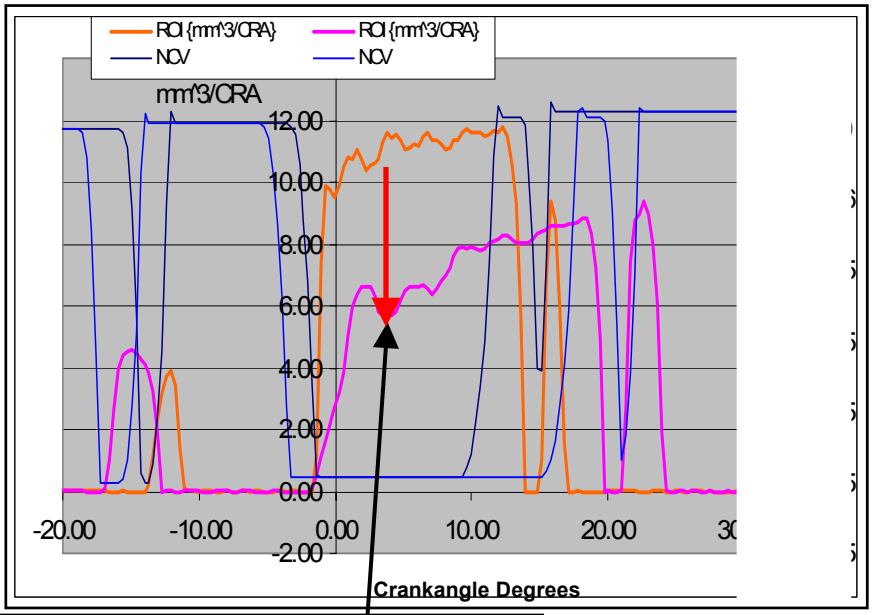

Injection Rate Profile Is Revised Due to Control Valve Modulation

Comparison of Simulation and Experimental Results

Two Actuator Injector @ A100

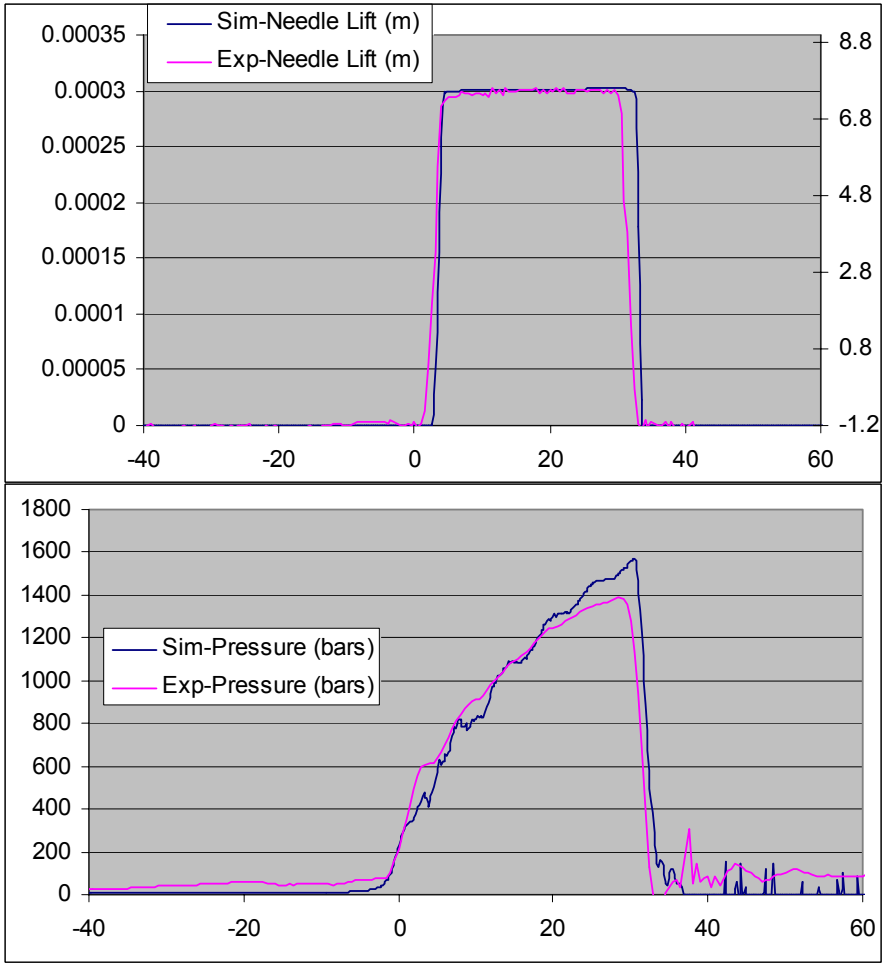

- **Good Correlation Was Achieved for Needle Traces In This Steady State Engine Test.**
- **Slightly Higher Peak Injection Pressure Predicted by Simulation Model As Compared to Experimental Measurements.**
- **Lengthy Debate As To Which Method Provides the Most Repeatable, Absolute Accuracy.**

Comparison of Simulation and Experimental Results

Two Actuator Injector Simulation Across the Steady State (ESC 13 Mode) Test

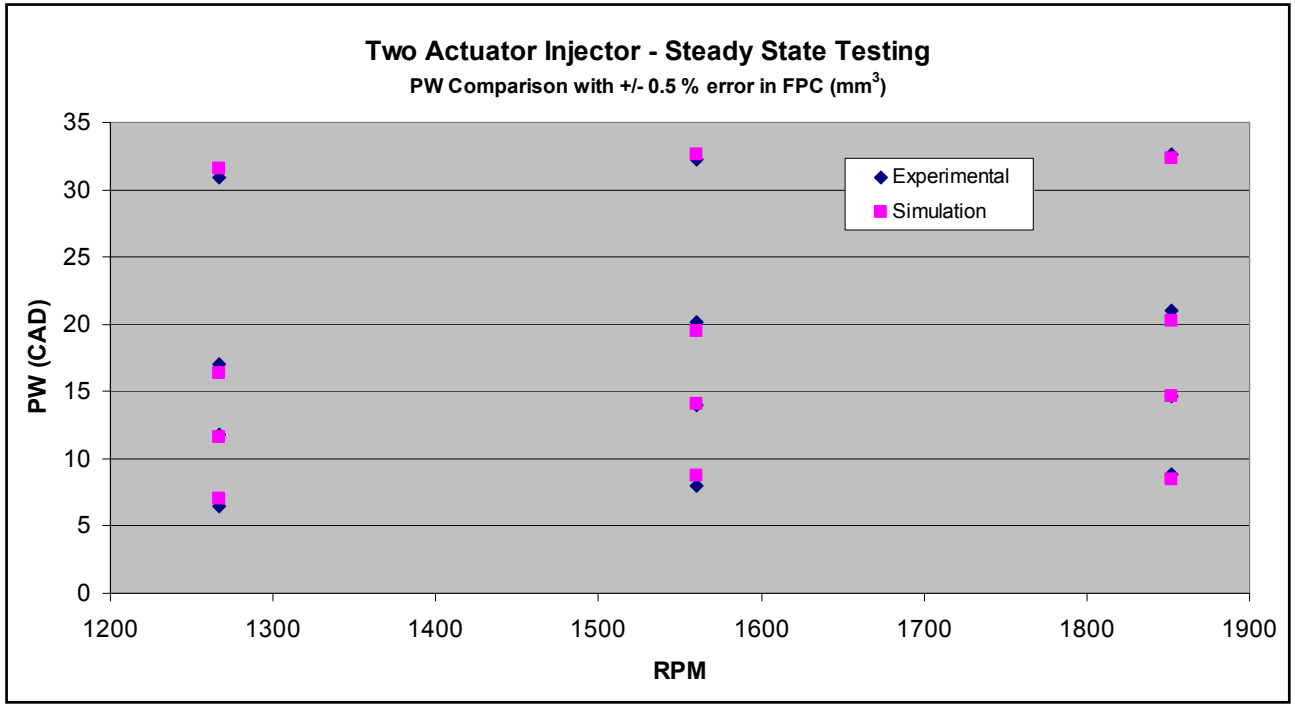

- **The AMESim Simulation Model Developed for the Two Actuator Injector Showed Very Good Correlation With Steady State Experimental Results. The Observed Difference Between Experimentally Measured and Modeled Fuel Delivery Quantity for a Given Electronic Duration (Pulse Width) Throughout The ESC Test RPM Range Was < 0.5%**

Piezo Injector Development and Testing

Schedule Outline

- Stack Testing at Higher Preload, Voltage and Current- 30th April Complete
- Amplification Module System
  - Module Fabrication – 15th May Complete
  - Integration With DDC Injector : Piezo Injector – 30th May Complete
  - Trouble Shooting and Final Assembly – 30th June
- Hardware Requirements for Testing
  - Instrumentation of Injector- 15th July
  - Controls for Piezo Injector – 31th July
  - Measurements for Control Valve Motion and Rate of Injection – 15th Aug
- Testing of Piezo Injector – 31th Aug
  - Main Injection
  - Pilot, Post and Multiple Injection

Cost-Effective Smart Materials for Diesel Engine Applications

J. O. Kiggans, Jr., F. C. Montgomery, T. N. Tiegs,
Oak Ridge National Laboratory

Objective / Scope

There are two objectives for this project. The first is to evaluate the cost-effectiveness and maturity of various "Smart Materials Technologies," which are under consideration for diesel engine applications, such as fuel injection systems. The second is to develop "Smart Materials" to be incorporated into working actuators and sensors.

Task 1 - Multilayer Electroded Laminates

The purpose of this study is to find satisfactory methods for the preparation of PZT laminates with internal electrodes from tape cast materials. There is no new data on this task to include in the present report.

Task 2 – Compositional Alteration of PZT-4

A major task of this project is to develop cost-effective PZT compositions and processing methods that will give PZT powders that will sinter to high density at a temperature below 960ºC. This goal is driven by the need to lower the cost of multilayer PZT actuators by reducing the cost of the interlayer electrodes. Commercial hard PZT powders require sintering at temperatures exceeding 1200ºC and, thus, multilayer devices must use costly Pd/Ag electrodes.

Small amounts of bismuth oxide compounds can lower the PZT sintering temperature sufficiently that Ag or Ag/Pd alloy (70/30) can be used as internal electrodes. PZT-840 sintered with 2 wt % Bi_2O_3 and an acceptor ion oxide reaches greater than 99% of the theoretical density after 1 h at 900ºC and has piezoelectric properties which are as good as the properties of commercial PZT sintered at ~1275ºC. However, the sintered ceramic has poorer mechanical properties than high temperature sintered PZT and could cause actuators with a PZT element to have low reliability. In an attempt to improve the mechanical properties, we have added a second phase to the ceramic. In the last quarterly we showed that 0.5 vol % of SiC, BN or Al_2O_3 did not enhance the strength or toughness of the low temperature sintered ceramic. However, since literature reports show that Al_2O_3 additions can increase the strength of PZT[1], we have continued this study with a material containing the sintering aid and 2 vol % of nanophase Al_2O_3.

Experimental

A powder was formulated with PZT-840 and a sintering aid containing 3 wt % of Bi_2O_3 and 0.5 wt % Mn_3O_4. The powder was prepared by attrition milling for 6 h with ZrO_2 media in a 50 vol % ethanol/xylene mixture. After drying, 1.06 wt % (2 vol %) of boehmite alumina (Dispal 23N4-80 boehmite, Sasol Chemical Industries) was dispersed in the powder by ball milling in ethanol with ZrO_2 media for 24 h.

Disks 1.2 mm thick by 28.7 mm diameter were obtained by cold compaction of the powers in a steel die at 103 MPa. The organic binders were removed by heating in air to 600 ^{o}C at 1 ^{o}C/min with a 1 h hold at 300°C and a 2 h hold at 600°C. Dimensional and weight measurements showed that the samples after binder removal were between 59% and 62% of the theoretical density based on the reported value of 7.6 g/cm^3 for PZT-840.

The disks were sintered for 3 or 24 h at 900°C and 950°C in closed alumina crucibles. The samples rested on a platinum setter with a mixture containing 10 wt % ZrO_2 and 90 wt % $PbZrO_3$ added to the crucible to control the PbO vapor pressure above the samples. After sintering, the densities were measured using the Archimedes method by immersion in ethyl alcohol.

To measure the piezoelectric properties, Ag paste (Metech 3288) was screen printed on both sides of the sintered disks and the electrodes were cured at 600°C for 10 minutes. The disks were poled at 1.5 kV/mm for 10 minutes in a silicone oil bath at 120°C. The current required to obtain 1.5 kV/mm was calculated by measuring the voltage drop across a series resistor in the high voltage contact line. The piezoelectric properties were measured at room temperature after a 24 h stabilization period. Capacitances were measured at 1 kHz and the resonant frequencies of the radial mode were measured using an impedance gain phase analyzer (Agilent 4194A).

Results and Discussion

In the following discussion the effects of increasing the second phase Al_2O_3 to 2 vol % on the ceramic properties are compared with data we reported earlier for samples with 0.5 vol % Al_2O_3. Samples with 3 wt % of the Bi_2O_3 sintering aid, but without any second

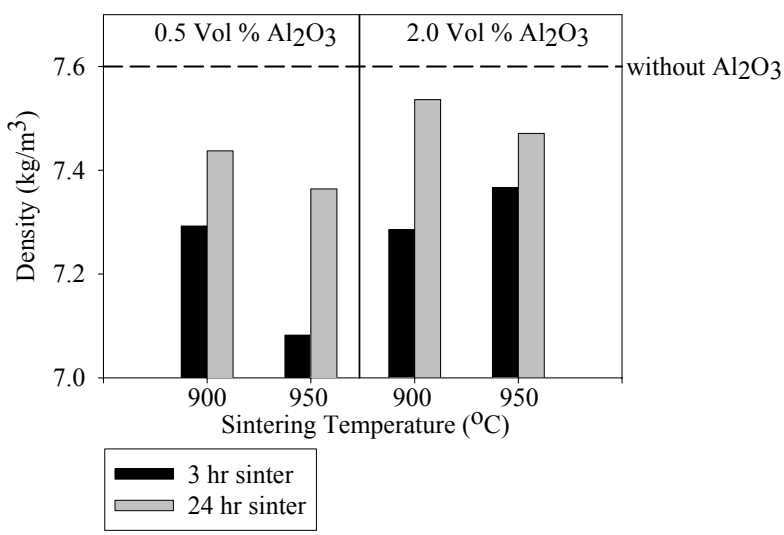

Figure 1. Effect of temperature and concentration of second phase Al_2O_3 on the density of PZT after sintering with 3 wt % Bi_2O_3 and 0.5 wt % Mn_3O_4.

phase additive, reach a density slightly greater than 7.6 kg/m^3 after sintering for 3 h at 900°C. Sintering at 950°C does not increase the density. As shown in Figure 1, the presence of Al_2O_3 as a second phase reduces the density of the sintered samples especially when the sintering time is only 3 h. Sintering for 24 h increases the density. Increasing the sintering temperature to 950°C tends to reduce the density. The density increases as the Al_2O_3 concentration increases from 0.5 vol % to 2 vol %. This is significant since the calculated density for this PZT material is reduced from 7.6 to 7.3 kg/m^3 when 2 vol % Al_2O_3 is added because Al_2O_3 has a lower density than PZT.

The samples were poled with an applied voltage of 1.5 kV/mm. The samples containing 2 vol % Al_2O_3 are harder to pole because they are more conductive than samples without Al_2O_3. Dense PZT which has been formulated with only the Bi_2O_3 sintering aid requires a current of 1-3 µA when poled at 1.5 kV/mm. With 0.5 vol % Al_2O_3 the current increases to 4-8 µA and with 2 vol % a current of 100-150 uA is necessary. Because of this increased conductivity it is not possible to pole the material with 2 vol % Al_2O_3 at higher applied fields.

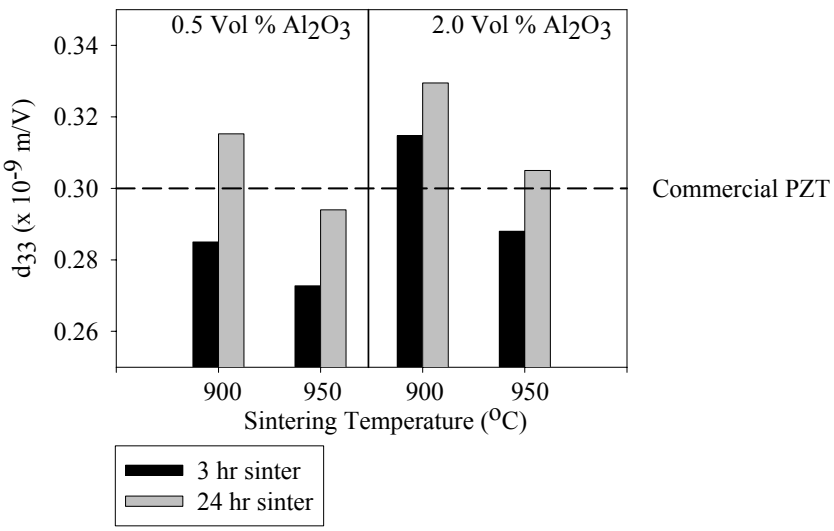

Figure 2. Effect of temperature and concentration of second phase Al_2O_3 on d of PZT-840 after sintering with 3 wt % Bi O and 0.5 wt % Mn O .

Shown in Figure 2, Figure 3, and Figure 4 are the piezoelectric constant (d_{33}), the radial coupling coefficient (k_r), and the mechanical Q (Q_m), respectively, for the PZT-840 with sintering aid and with the second phase Al_2O_3. It is apparent from Figure 2 that, for a given sintering temperature, the d_{33} increases when the sintering time increases from 3 to 24 h. However, for a given sintering time, the d_{33} decreases when the sintering temperature increases from 900 to 950 °C. Since the number of piezoelectric layers required to produce a specific displacement in a multilayer actuator is inversely related to the d_{33}, our goal is to keep the d_{33} around 0.3 x 10^{-9} m/V.

The radial coupling coefficient is a measure of the efficiency for converting electrical energy to mechanical energy. For all of the samples tested, k_r exceeds 0.5. Commercially sintered PZT-840 has a k_r of about 0.6. The coefficient in samples with

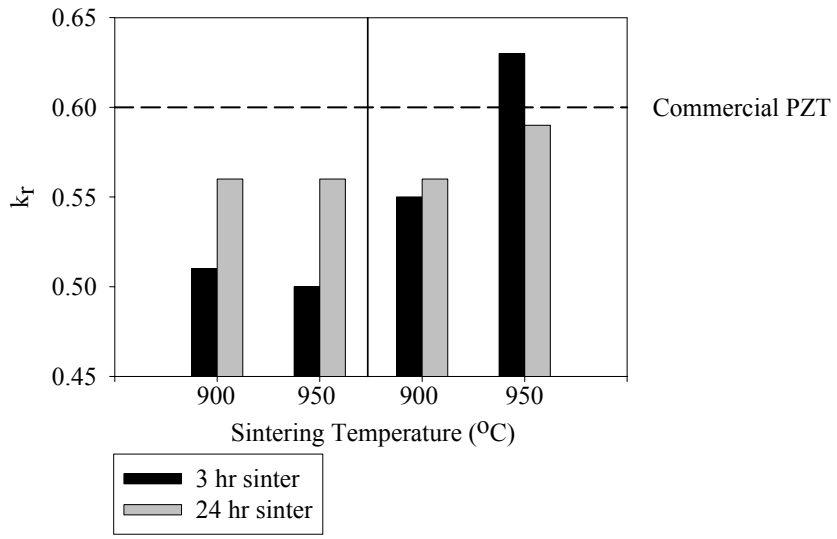

the second phase Al_2O_3 (Figure 3) is similar to that of the PZT doped with only the Bi_2O_3 sintering aid and annealed at 900 to 950°C (k_r of 0.45-0.55)

Commercial PZT-840 sintered at >1200°C has a reported mechanical Q of 400[2]. The addition of 3 wt % of the Bi_2O_3 sintering aid increases Q_m to 950-1200 for samples

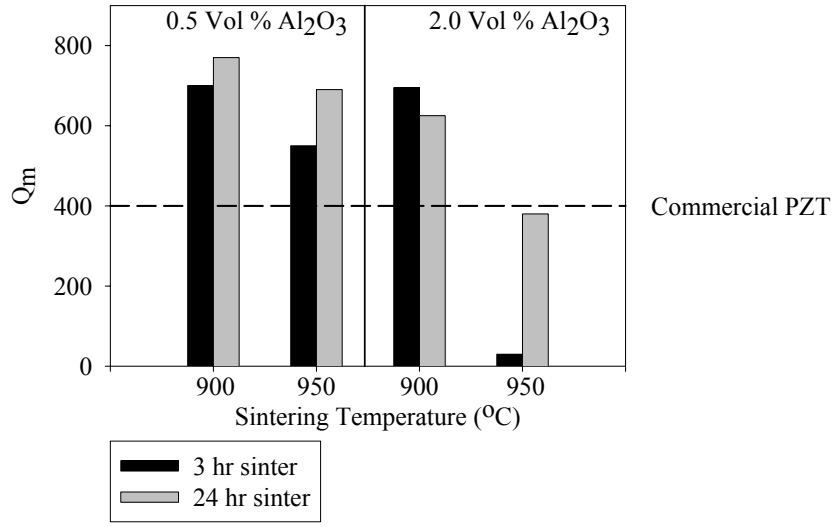

on Q_m **O_3 O_4.**

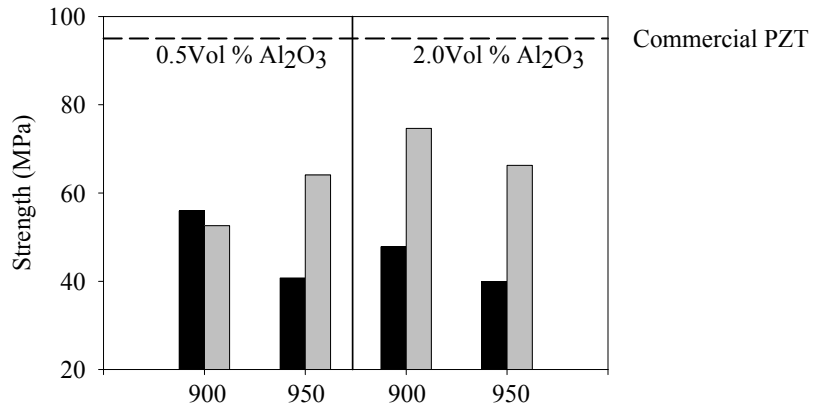

Figure 5 **$_2O_3$ on strength of PZ** **Mn_3O_4.**

sintered at 900 to 950°C. As shown in Figure 4, incorporation of the second phase Al_2O_3 reduces Q_m from this value, but, in most cases, Q_m still exceeds the manufacturer's specification. The low value for the samples sintered at 950°C for only 3 h is a result of severe distortion in the frequency response of the radial mode which may be caused by the formation of intermediate phases.

The emphasis of this work is to increase the strength of the low temperature sintered PZT-840. Commercial PZT has strength around 95 MPa but the addition of the low temperature sintering aid reduces the strength to around 40 MPa. Adding 2 vol % of the second phase Al_2O_3 does increase the strength by about 50% but only at the longer sintering time.

In order to try to understand these results, we examined the fracture surfaces and the microstructure of the sintered bodies with SEM. PZT-840 containing 3 wt % of the sintering aid annealed at 900 to 950°C has a grain size around 1.5 µm. Adding 0.5 vol %

Table 1. Properties of dispersoids in PZT-840 densified with 3 wt % of the Bi_2O_3 sintering aid and 2 vol % of nanophase Al_2O_3.

Sample	Temp.(°C)	Time (h)	Count per 1600 µm^2	Length (µm)	
				Mean	Std. Dev.
118-A	900	3	24	0.93	0.26
125-A	900	24	41	0.79	0.26
111-A	950	3	81	0.83	0.27
135-A	950	24	77	0.84	0.28

of nanophase Al_2O_3 does not affect the grain size at 900°C but at 950°C the grain size increases to greater than 2 µm. As can be seen by comparing the microstructure shown in Figure 6a with that shown in Figure 6c, increasing the concentration of Al_2O_3 to 2 vol % retards the rate of grain growth. After 3 h at 950°C the sample with 2 vol % has an average grain size of 1.7 ± 0.1 µm but the sample with 0.5 vol % has an average grain size of 2.4 ± 0.2 µm. After 24 h , however, the grain sizes are similar (2.0 ± 0.1 µm).

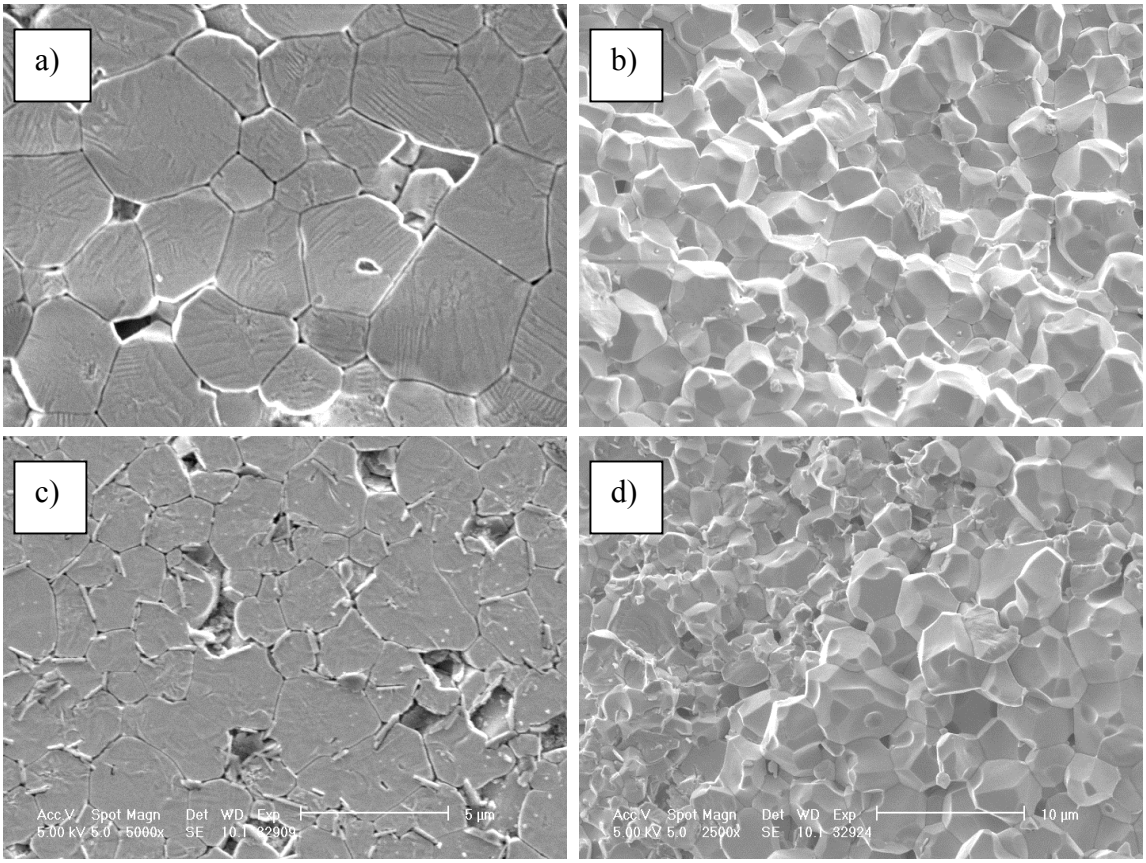

Figure 6. Microstructure (a,c 5000x) and fracture surface (b,d 2500x) of PZT-840 sintered for 3 h at 950°C with 3 wt % sintering aid and: (a,b) 0.5 vol % Al_2O_3; (c,d) 2 vol % Al_2O_3.

In the PZT containing 2 vol % nanophase Al_2O_3 there are platelets dispersed both at the grain boundaries and in the grains (Figure 6c). These dispersoids are not present in the In PZT containing 0.5 vol % Al_2O_3 (Figure 6a). The lengths of the dispersoids are about 0.8 µm regardless of the sintering time or temperature. The number of dispersoids (Table 1) is dependent on the sintering time at 900°C, but is independent of the time at 950°C. There are about twice as many in samples heated at 950°C than there are in the 900°C samples.

Tajima[1] has also doped hard PZT with Al_2O_3. After sintering at 1200°C, he also observed Al_2O_3 dispersoids at grain boundaries and in the grains. Micrometer sized dispersoids that were agglomerations of smaller particles were found in samples that contained 1 vol % Al_2O_3. In PZT with 0.5 vol % Al_2O_3 the inclusions were only a few hundred nanometers in size. Tajima studied crack growth behavior in the PZT/Al_2O_3 composites. The dispersoids slowed crack propagation either by reinforcing the grain boundaries or by acting as pins against the propagation.

The fracture mode is influenced by the amount of second phase Al_2O_3 in the ceramic. As we reported in a previous quarterly, the fracture for the base PZT is completely intergranular occurring along grain boundaries. Intergranular fracture is predominately the failure mode when the concentration of Al_2O_3 is only 0.5 vol %. However, as shown in Figure 6d, the fracture of the PZT with 2 vol % Al_2O_3 results in cleavage of the grains as well as cleavage along grain boundaries.

References

[1] Tajima, K., H. J. Hwang, and M. Sando, J. of the American Ceramic Society, **83** (2000) 651-653.

[2] Facts Sheet, American Piezo Ceramics Inc., Duck Run Road, Mackeyville, PA, USA.

Task 3 - Fabricate a test fixture for stroking the multiplayer PZT parts.

As reported in the last report, work for this task is in progress, and is being directed by Boyd Evans of ORNL

Status of Milestones

1) Fabricate and characterize several multilayer PZT stacks using low temperature PZT materials.
Status: This task has not started, but is planned for the next two reporting periods.

2). Fabricate a test fixture for stroking the multiplayer PZT parts.
Status: This task is underway with no results to report.

3). Make PZT powders with a nano-additive and characterize sintered discs for electromechanical and strength measurements.
Status: Data reported in the present report. Additional PZT materials with nano-alumina addition have been prepared. Discs will be pressed, sintered, and tested during the next reporting period.

Low-Cost Manufacturing Processes for Ceramic and Cermet Diesel Engine Components

D. E. Wittmer
Southern Illinois University, Carbondale

Objective/Scope

The purpose of this work is to investigate the potential of low-cost manufacturing processes for ceramic and cermet diesel engine components. The primary task is to develop cost effective processing, forming and sintering methodologies for cermet and ceramic formulations, used by industrial diesel engine manufacturers.

Technical Highlights

Task 1. Collaboration with industrial partner(s).

This task involves the collaboration with industrial partners to assist them in processing and sintering of their diesel engine components. Our goal is provide assistance in processing and sintering which may result in a reduction in surface reactions and part warping. Moreover, this may also provide an alternative sintering process that will allow improved throughput efficiency and manufacturing economy. Due to the proprietary nature of this task, any research data generated from this task is normally controlled by the terms of each specific confidentiality agreement. The reporting of this data and any results are the responsibility of the industrial partner(s).

Task 2. Cost Effective Processing and Sintering

This task was completed and reported in previous quarterly report.

Task 3. Economic Comparison of Materials and Processing of Cermets for Use as Diesel Engine Components

This task involves the development of an economic model for comparing both materials and processing methods for cermets targeted for use as diesel engine components. The cermet is a combination of an intermetallic and TiC; where the intermetallic can be nickel aluminide, chrome aluminide, nickel chromium. Modification of these intermetallics may be necessary to obtain the properties desired.

During this reporting period, plastisol as a binder and coconut oil, as a binder- modifier, were investigated as a means of reducing the cost of intermetallic-bonded TiC. It is believed that one of the critical steps in reducing overall costs can be achieved through reducing the manufacturing/processing costs associated with forming and sintering. Extrusion has been identified as the most cost effective means of making high aspect ratio, simple cross-section forms and low-pressure injection molding as a cost effective means of forming forms with more complex cross-sections. Such forms must be amenable to continuous sintering in order to take full advantage of potential cost reductions. This work will continue during the next reporting period.

Also during this reporting period, a proposal was made to modify the current contract to include more fully investigating the influence of high heating rates on the microstructure and properties of continuously sintered cermets. If it is possible to continuously sinter selected cermets to high density with a significantly reduced sintering cycle, it could prove to be even more cost effective. In addition, 5 different groups of wear specimens of cermets that were processed by low-pressure injection molding and continuous sintering were submitted to Peter Blau at ORNL for tribological studies.

Status of Milestones

Collaboration with Industrial Partners	On Schedule
Cost Effective Processing and Sintering of Diesel Engine Components	Completed
Economic Comparison	On Schedule

Communications/Visits/Travel

D. E. Wittmer to ORNL to meet with D. Ray Johnson and Terry Tiegs for discussions regarding contract modifications and to give technical progress report.

D. E. Wittmer spoke with Alan Weimer at Colorado School of Mines about including some of his powders in our investigations.

Problems Encountered

None

Publications and Presentations

"Low Pressure Injection Molding of Intermetallic-TiC Cermets," Jeffrey Hazelwood, Dale E. Wittmer, and Joshua Steffen (SIUC) and Terry N. Tiegs (ORNL), paper submitted to MPIF for publication and presentation at PM2TEC 2003, Las Vegas, NV, June 8-12, 2003.

Intermetallic-Bonded Cermets

P. F. Becher and S. B. Waters
Oak Ridge National Laboratory

Objective/Scope

The goal of this task is to develop materials for diesel engine applications, specifically for fuel delivery systems and wear components (e.g., valve seats and turbocharger components). This will require materials that have a minimum hardness of 11 GPa and a thermal expansion coefficient of between 10 to 15 x 10^{-6}/°C. The material should also have excellent corrosion resistance in a diesel engine environment, flexure strength in excess of 700 MPa, and fracture toughness greater than 10 MPa√m to ensure long-term reliability. The material should also be compatible with steels and not cause excessive wear of the steel counter face. The upper temperature limit for fuel delivery systems applications is 200°C, and for the other wear applications, the limit is 815°C. Finally, the total material processing costs for these advanced materials should be competitive with competing technologies such as TiN or other ceramic coatings on high-speed tool steels.

Technical Highlights

The composition of the TiC-Ni_3Al cermets influences the wear characteristics as observed in pin on disk rotating wear studies. Evidence of this is seen in cermets containing 40 vol % in which Mo or Cr_3C_2 powder was added to the TiC powder prior to attritor milling to reduce the TiC particle size. Molybdenum is employed as it has been indicated to improve the wetting of TiC by nickel during liquid phase sintering and improves the strength of the interface between the TiC and Ni [1]. Chromium additions are seen to increase the yield stress and hardness of the Ni_3Al phase to a greater extent than does Mo [2,3], but carbon is seen to much more effective [2,4]. The thought was that increasing the hardness of the Ni_3Al might improve the wear resistance. However, evaluation of cermets fabricated in this project using these additives reveal that the molybdenum addition resulted in better wear performance with regard to the wear of both the cermet pin and the steel disk materials, Figures 1 and 2. Based on the wear surface observations, it appears that pullout and fracture of the TiC grains is diminished with the Mo addition as compared to the response when the Cr_3C_2 addition was employed.

Status of Milestones

On Schedule

Communication/Visits/Travel

None

Publications

E. Rocha-Rangel, P. F. Becher and E. Lara-Curzio, "Influence of Carbon on the Interfacial Contact Angle Between Alumina and Liquid Aluminum," Surface *and Interface Analysis*, in press.

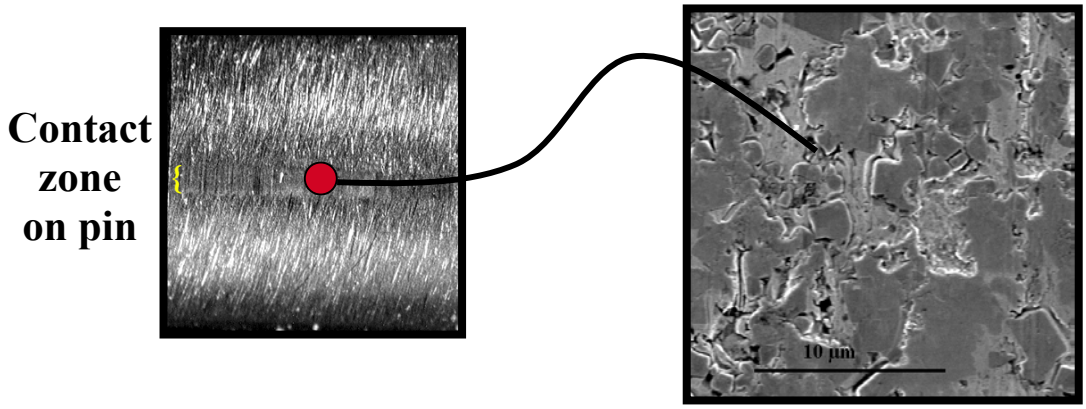

Figure 1. Contact surface of (TiC+2 wt % Mo) + 40 vol % Ni_3Al cermet pin after pin on disk (tool steel) wear test (M. Naylor, Cummins Engine). Low wear coefficients were obtained for both pin and disk materials. This is reflected by the fact that the angular TiC grains (darker gray grains, right) did not cleave and form abrasive debris.

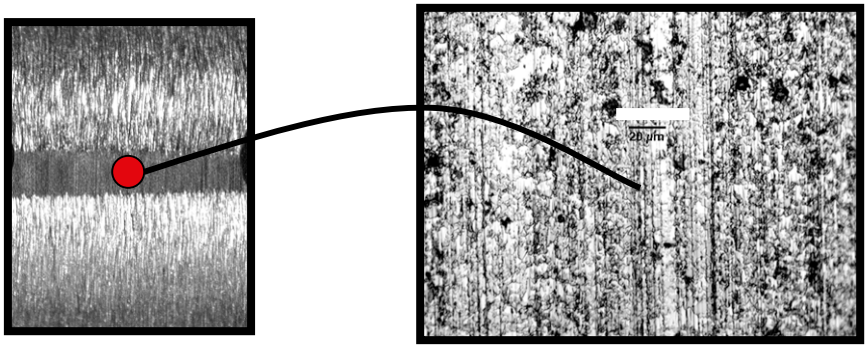

Figure 2. Wear coefficients of both pin and disk increase when Cr_3C_2 addition to TiC is substituted for Mo as reflected by the wide wear track on the pin (left) and the pull-out of TiC grains from surface evidenced by the dark pits (right).

References

1. P. Ettmayer, "Hardmetals and Cermets," pp. 145-64, Annual Review of Materials Science, Vol. 19, Annual Reviews Inc., Palo Alto, CA, 1989.
2. S. C. Huang, C. L. Briant, K.-M. Chang, A. I. Taub, and E. L. Hall, "Carbon Effects in Rapidly Solidified Ni_3Al," *J. Mater. Res*., 1(1) 60-7 (1986).
3. R. D. Rawlings and A. E. Staton-Bevan, "The Alloying Behavior and Mechanical Properties of Polycrystalline Ni3Al (γ' Phase) with Ternary Additions," *J. Mater. Sci*., 10: 505 (1975).
4. S. C. Huang, A. I. Taub, and K. M. Chang, "Boron Extended Solubility and Strengthening Potency in Rapidly Solidified Ni_3Al," *Acta Metall*., 32(10) 1703-07 (1984).

Low Cost-High Toughness Ceramics

T. N. Tiegs, F. C. Montgomery, and P. A. Menchhofer
Oak Ridge National Laboratory

Objective/Scope

Significant improvement in the reliability of structural ceramics for advanced diesel engine applications could be attained if the critical fracture toughness (K_{Ic}) were increased without strength degradation. Currently, the project is examining toughening of ceramics by incorporation of ductile intermetallic phases.

Technical Highlights

Previous studies have shown that the properties of the aluminide-bonded ceramics are attractive for diesel engine applications and consequently, development of these materials was started. At the present time, TiC-based composites with 40-60 vol % Ni_3Al are being developed because they have expansion characteristics very close to those for steel. Previously, the general property envelope has been studied and the compositions refined. Further processing studies are needed to examine lot-to-lot variation using statistically designed experiments, determine compaction behavior, assess dimensional control during sintering, identify suitable binders which will not add carbon ash during sintering, and develop a viable and cost-effective source of NiAl powder. The development effort is being done in collaboration with CoorsTek, Inc.

Large Batch Processing of TiC-Ni_3Al Composites – Several large batches of composite powder have been produced and sent to CoorsTek for injection molding testing. To date, five 3-kg mill runs were processed of a 50% TiC-Ni_3Al (with 2% Mo) composition. The different runs were blended together prior to shipping.

Alternate Precursors for Ni_3Al Formation - All previous work used a combination of Ni and NiAl for an in-situ reaction to form the Ni_3Al. Because the costs of the starting raw materials can be a significant fraction of the total cost of a component, alternative materials for fabricating the cermets are of interest. Ni and Al powders are produced in sufficient quantities to be relatively cost-effective and so tests were done to maximize their usage in the composites.

Two samples were fabricated of a 50% TiC-Ni_3Al (with 2% Mo) composition where the Ni_3Al was produced by either (1) Ni and Al powders only, or (2) Ni, Al, and NiAl powders. The amount of NiAl powder used for the latter sample was about half of what was required in a typical batch. An initial sintering run was done using the same heating rates as used previously when only Ni and NiAl were used (i.e., 10°C/min). The samples from this initial run showed severe macroscopic cracking and differential shrinkage. Typically, this behavior is a result of non-uniform heating of the compact. The most likely cause of the temperature difference was the exothermic reaction that occurs due to the reaction of the Ni and Al to form the Ni_3Al intermetallic. This exothermic reaction was known before the sintering run, but it was thought that the large fraction of TiC contained in the samples would act as a diluent to reduce the effects of the temperature rise.

A DTA analysis of the mixtures showed an endotherm at 625-640°C and an exotherm at ~645°C. The endotherm is the initial melting of the Al-Ni mixture and the exotherm indicates the reaction

to form the intermetallic. A second sintering run was performed using a reduced heating rate of ≤0.5°C/min in the critical temperature range of 620-670°C. This added about 2 hours to the total sintering run time. Unfortunately, the samples sintered at the slower heating rate also exhibited macroscopic cracking and non-uniform shrinkage similar to the initial samples. Further tests will be made where the sintering run is interrupted and the samples inspected at intermediate temperatures. This will help identify critical temperatures to reduce cracking.

Status of Milestones

On schedule.

Communications/Visits/Travel

Travel by T. N. Tiegs to Knoxville, TN, on Feb. 11, 2003, to present graduate student seminar on "Processing and Properties of TiC-Ni_3Al Composites."

Problems Encountered

None.

Publications

None.

Materials for Exhaust Aftertreatment

Paul W. Park, Alexander G. Panov, and Craig F. Habeger
Caterpillar Inc.

Objective/Scope

The objective of this effort is to develop and evaluate materials that will be utilized in aftertreatment systems for diesel engines. These materials include catalyst for NO_x abatement, filtration media for particulate abatement, and materials to improve NO_x sensing capabilities in the exhaust system. This project is part of a Caterpillar strategy to meet EPA requirements for regulated emissions in 2007 and out. This years focus is on the durability of NO_x catalysts developed for lean burn applications in the presence of sulfur, evaluation of filtration properties of sintered metal media for application in diesel particulate filters (DPF), and evaluation of current NO_x sensor technologies while developing materials to improve sensing capabilities.

Technical Highlights

Lean NOx Catalysis. A number of Fe-zeolites with different Al:Si ratios and different surface areas were prepared and their de-NO_x performance with propene was studied. The Fe-ZSM5 sample showed the best performance (42% NO, 36% NO_2), but X-ray analysis showed that there was substantial amount of individual Fe_2O_3 phase in the zeolite that can negatively impact its performance. Therefore, the preparation methods require further development to eliminate formation of non-framed iron oxides inside zeolite structure.

The study of Ga doped alumina catalyst was continued. The additional synthesis method (single step) to prepare a series of Ga/Al_2O_3 catalysts using various precursors including $Ga(NO_3)_3 \bullet 2.5H_2O$, $Ga(OPr\text{-}i)_3$ and $Ga(acac)_3$ were performed. Comparison of the Ga/aluminas prepared with incipient wetness (IW) and single-step (SS) methods leads to the following conclusions: (1) in both cases surface area and pore volume decreases as Ga content increases, but SS samples have higher surface areas and pore volume than IW samples, and (2) pore diameter for IW samples gradually decreases as Ga content increases, while pore diameter for SS samples pass the minimum at 5% Ga load. Obviously, there are Ga layers on the pore surfaces in case of IW samples, while in case of SS samples some amount of Ga is built into bulk material. SS samples may or may not have continuous Ga layer on pore surfaces. This results in different deNO_x-performance of the catalysts prepared by different methods. Incipient wetness preparation results in NO/NO_2 conversion gradually increasing (up to 66% NO, 82% NO_2) as Ga content increases up to 30%. While single-step processing results show NO/NO_2 conversion pass through a minimum (36% NO, 56% NO_2) at Ga content of 5%, then increases (up to 68% NO, 74% NO_2) and exceeds the performance of IW samples at 25% Ga load.

A new test protocol was developed to evaluate catalyst materials using liquid hydrocarbon reductants on the powder bench system. The effect of various hydrocarbons on the performance of lean-NO_x catalyst can be examined with the developed test protocol. The lean-NO_x performance of a silver alumina catalyst (prepared by AMT) and Cu- and Fe-ZSM5 catalysts were compared with various hydrocarbons. Preliminary results showed that 2 wt % silver-doped on alumina catalyst was most active and selective with ethanol (up to 97% NO_x reduction) compared to octane (69%) and propene (34%).

The development effort of a new lean-NOx catalyst formulation continued. A physical mixture of silver sulfate (2 wt % Ag) and γ-alumina was prepared and evaluated the Lean-NO_x performance of the catalyst on the powder bench. A series of silver and gallium doped alumina catalysts prepared with a co-impregnation technique were evaluated on the powder bench with propene. The silver weight percent was varied and the gallium loading was kept constant at 10%. The optimum weight percent of silver will be determined.

Catalyst formulations and a coating technique developed in AMT were applied on full size honeycomb monolith bricks (10.5 x 6 in.) for engine tests. The catalysts demonstrated 18% NO_x conversion with post injected diesel fuel of $C1/NO_x = 6$ (5% fuel penalty). The result indicated that the post-injected diesel fuel was not reformed into desirable reductants for the catalysts tested.

The installation of the Xytel multi-reactor catalyst test bench system has been 95% completed. This multi-reactor system will allow high throughput screening of catalyst materials in both powder and washcoated-core samples for various catalyst aftertreatment technologies including oxidation, ammonia-SCR, Lean-NO_x and NO_x-trap.

Diesel Particulate Trap. The goal this quarter was to specify the properties of the sintered powder materials for deep-bed filtration. A series of the sintered metal powder materials prepared earlier were evaluated for pressure drop and filtration efficiency.

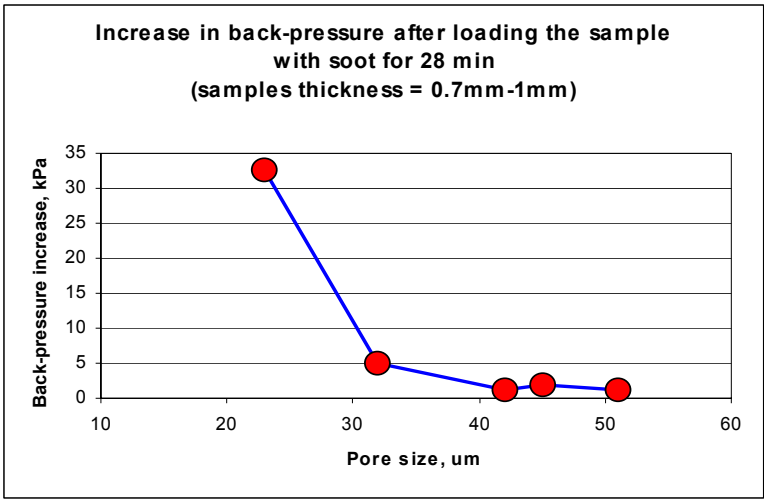

Figure 1. A demonstration of backpressure (dPfinal-dPinitial) increase for sintered metal samples. Flow velocity is 70cm/s.

Filtration efficiency varied from 38% to 88% depending on filter thickness and pore size. Pore size and thickness of the filter also affected the pressure drop as demonstrated in Figure 1. Data analysis led to the selection of the optimum pore size, filter thickness, and initial powder size for preparation of the deep-bed filtration media. New materials for catalyzed DPF applications will be prepared according to these specifications.

Sintered metal powder filters earlier produced by rolling contained defects. Defects in the form of cracks may affect the filtration efficiency. To improve the filtration media quality, a tape casting procedure was developed. Several sintered metal powder sheets were prepared with tape casting and are ready for sintering.

In addition, several sintered metal samples were obtained from an outside supplier and are pending diesel burner test.

NO_x Sensor. The reactor bench principle is to flow reaction gas over the sensor and measure the sensor response. Figure 2 shows a schematic diagram of the NO_x sensor test bench. The reaction gas is mixed in the desired proportions using the starting compressed gas cylinder concentrations and the mass flow controllers. The gas flow compositions available for this bench with the corresponding starting gas compositions are listed in Table 1. The flow rate of gas can be from 5 sccm to 500 sccm. This bench was designed to perform initial evaluation and more fundamental study. The temperature of the gas or reactor can span the range of ambient to 1000°C to evaluate the effect of temperature.

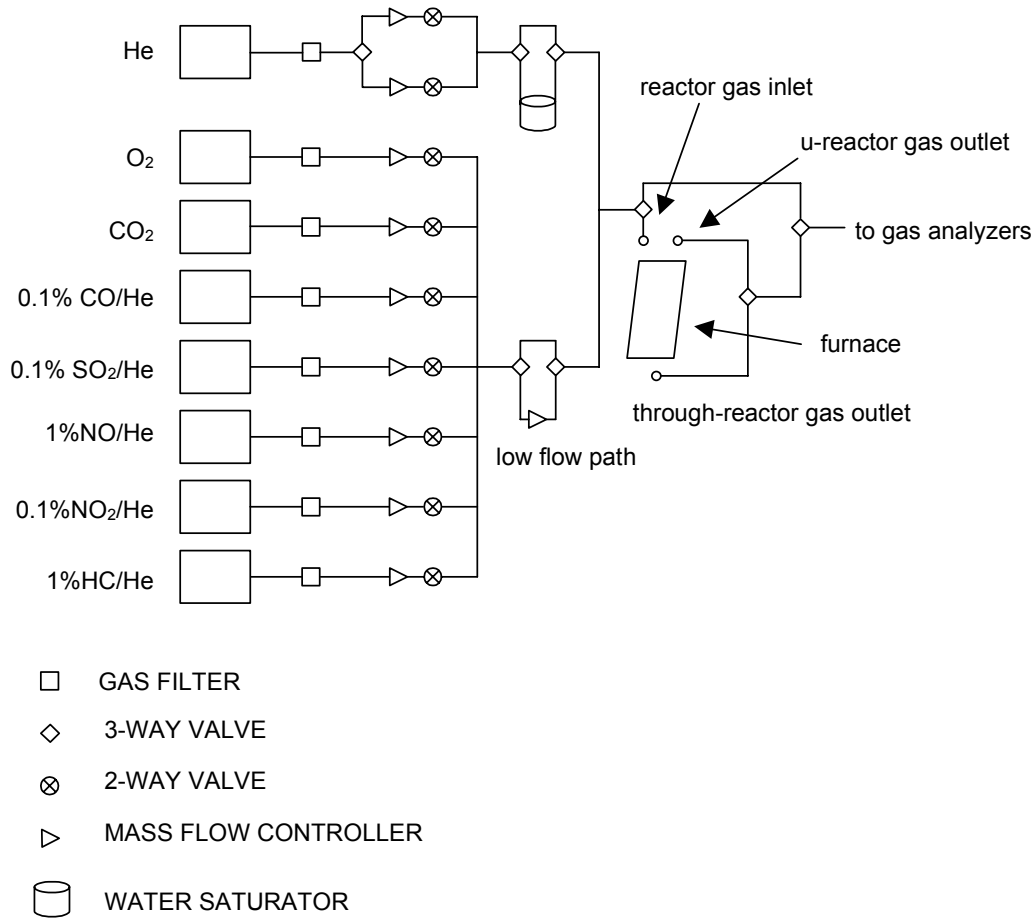

Figure 2. A schematic diagram of the NO_x sensor test bench.

Table 1. Simulated exhaust composition ranges.

Gas Constituent	Final Concentration Range	Starting Cylinder Concentration (%)
NO	5 ppm – 800 ppm	1
NO_2	1.5 ppm – 200 ppm	0.1
C_3H_6	50 ppm – 5000 ppm	1
SO_2	1.5 ppm – 200 ppm	0.1
CO	1.5 ppm – 200 ppm	0.1
CO_2	1% - 10%	100
O_2	1% - 15%	100
H_2O	1% - 10%	N/A
He	Balance	100

The test bench is almost entirely computer controlled. It was designed to versatile yet easy to use. The computer using Labview software controls the mass flow controllers and all the valving. The aspects of the test bench that are not yet computer controlled are the furnace control and the data acquisition. The graphical user interface, shown in Figure 3, of the test program is intuitive and easily operated. As can be seen from the figure the choice of each gas is available for testing. The user can adjust the flow rates by filling in the desired flow rate or toggling up the number to the preferred rate. The user can also change the flow paths by toggling between high flow/low flow, no water/water, to analyzer/to reactor, or "u" reactor/through reactor. In all cases, one toggle click will adjust all the necessary valves to alter the flow path correctly.

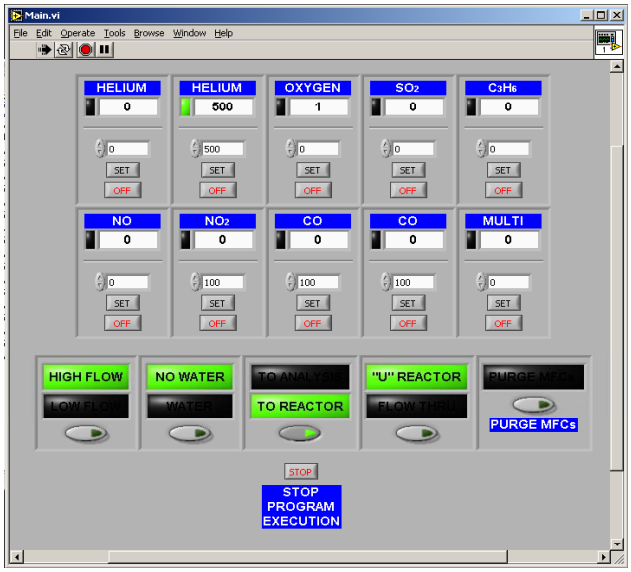

Figure 3. A picture of the NO_x sensor test bench control screen.

The focus of the current quarter was to debug the NO_x sensor bench and make certain the test fixtures were working as planned. The software was also debugged. Both the bench and the software had a few problems that are still being resolved. Once complete, the bench will be entirely controlled from the computer to allow for ease of use. The versatile configuration allows testing of both commercial production and experimental sensors.

Currently, we possess two sensors that are being developed by outside parties. We are also working on acquiring two more developmental sensors from others. All of the sensors acquired are based on the mixed potential measurement technique. Experimental electrochemical sensors have been fabricated and are being prepared for evaluation.

Future Plans

(1) Optimize layered catalyst formulation.
(2) Continue to characterize silver catalyst.
(3) Improve catalyst durability.
(4) Complete testing of the prepared 430SS sintered metal materials.
(5) Sinter and test high temperature alloy sintered metal filters.
(6) Develop a model correlating materials' properties to filtration efficiency and pressure drop.
(7) Begin evaluation of NO_x sensors.
(8) Interact with sensor developers to meet heavy-duty diesel needs.

Travel

None.

Status of FY 2003 Milestones

1) *Catalyst Formulation:* Improve catalyst deNO_x performance via dual function mechanism concept identified in the previous study (under progress)
2) *Catalyst Durability:* Improve catalyst durability for sulfur poisoning (under progress)
3) *Washcoat Technology:* Develop a controlled catalyst coating technique in order to fully demonstrate selected catalyst chemistries on a full size honeycomb monolith (under progress)
4) *NO_x Sensor:* Complete NO_x sensor bench fabrication. (complete)

Publications

Carrie Boyer, "Investigation of Silver Doped Alumina Catalysts for the Aftertreatment of Diesel Exhaust," Thesis,

Paul Park, Christie Ragle, Carrie Boyer, "Steady-State-State Engine Testing of γ-alumina Catalysts Under Plasma Assist for NO_x Control in Heavy Duty Diesel Exhaust" SAE

Development of Materials Analysis Tools for Studying NO_x Adsorber Catalysts

Roger England, Cummins Engine Company
and Thomas Watkins, Oak Ridge National Laboratory

Objective/Scope

The objective of this cooperative effort is to participate in development of NO_X control for diesel engine exhaust, with the aim of answering fundamental questions about the microscale dynamics of the NO_X conversion process. The expected result is that this improved description of mechanisms will enable industry to improve NO_X catalyst performance and durability. As the state-of-the-art evolved during the course of the CRADA, the study focused more on NO_X adsorber materials and processes. A Cummins catalyst supplier provided new catalyst materials, which are being examined with diagnostic tools developed under the CRADA. Investigations of these candidate-production materials are being implemented on both the bench and engine research scale. These investigations include the examination of unused and engine-aged catalyst samples. Investigative tools included transmission electron microscopy (TEM), X-ray diffraction (XRD), Raman Spectroscopy and infrared spectroscopy (IR).

Technical Highlights

X-ray diffraction (XRD) was employed to understand the crystalline nature of the samples. The width of a peak in an XRD pattern can be related to the crystallite size of the diffracting material. A crystallite is a region of coherent diffraction and can significantly contribute to peak broadening if smaller than 0.1 μm. Crystallite boundaries are often defects, like dislocations, which affect diffraction. If these defects are eliminated or removed, the crystallite size increases, but the overall physical particle size may not necessarily increase. Typically, the crystallite size is much less than the grain size of a material as observed on the SEM. In this context, crystallites can be thought of as sub-grains, which are very small perfect single crystals. This technique was particularly useful to monitor precious metal changes that occurred with catalyst aging. As the time at desulfation temperature increased, the Pt atoms began to sinter, forming larger crystallites (see Figure 1).

Three different spectroscopic techniques were used to characterize the adsorbed species -- Raman spectroscopy, Fourier Transform Infrared Spectroscopy (FTIR), and X-ray Photoelectron Spectroscopy (XPS). Raman spectroscopy measures the characteristic vibrational energy levels of molecules and crystals and so is very sensitive to any changes in bonding, stoichiometry and phase/symmetry. In this case, changes of the vibrations from the support material with desulfation time were monitored. Figure 2 shows the decrease in peak width and the increase in peak position of the band that occurs due to the growth of the Pt particle size. These changes in the Raman spectra have been confirmed with XRD results and are believed to be caused by energy changes of the Pt valence orbital induced by Pt-support interaction. Although Raman spectroscopy could not directly measure the Pt particle size in these samples, the changes in the support Raman spectra with Pt size were calibrated for this specific catalyst formulation and used for measuring Pt particle coarsening.

Transmission electron microscopy (TEM), Scanning Transmission Electron Microscopy (STEM) and Electron Probe Microanalysis (EPMA) techniques were employed to characterize the

microstructure of the NO_x trap catalysts. Standard TEM images of the wash coat/support particles showed two morphologies: a very fine-grained aggregate structure and a small fraction of large-grained material. High-resolution bright-field TEM images of the fresh catalyst did not clearly reveal discrete Pt catalyst particles, but associated energy-dispersive x-ray spectroscopy (EDS) results did indicate the presence of Pt. High-angle annular dark-field (ADF) images, however, showed faint bright contrast in 0.5-1.5 nm clusters of particles, which were consistent with essentially mono-layer "rafts" of Pt on the surface of the support particles ADF images on the STEM provided a facile method for imaging the particles in high contrast, and for measuring particle sizes (see Figure 3). Samples with 150, 500 and 1000 desulfation hours displayed 8, 9.5 and 10.5 nm particles, respectively. These data are consistent with XRD analysis. It should be noted that the increase in the Pt particle size, although significant, is still comparable to that observed in commercial three-way catalysts for gasoline engines. The Pt particle size distribution in current commercial three-way catalyst for gasoline engines increases from being centered at 1.3 nm to 5.7 nm after 50,000 miles of operation.

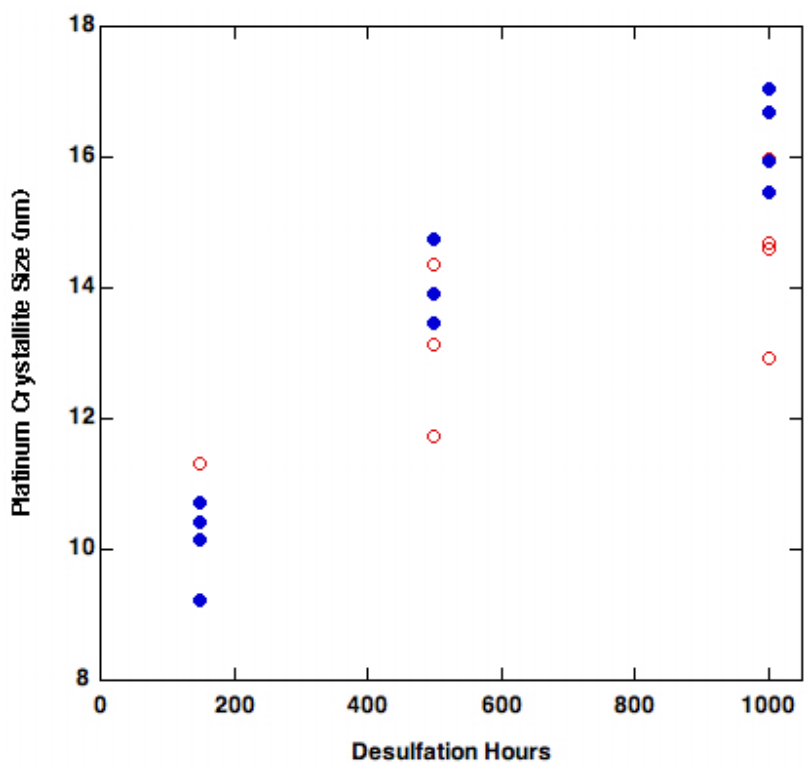

Figure 1 – Platinum crystallite size as a function of desulfation time. The red and blue symbols represent samples that contain different Pt loadings.

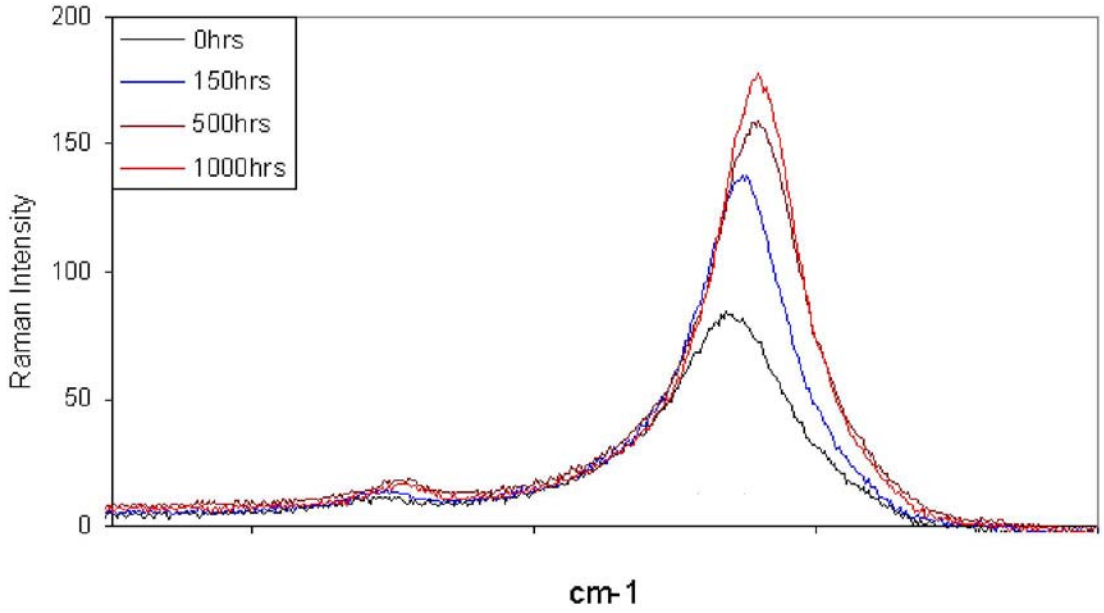

Figure 2 - Raman Spectra of the support for various desulfation times. The change in the peak width and position is caused by the increase in Pt particle size.

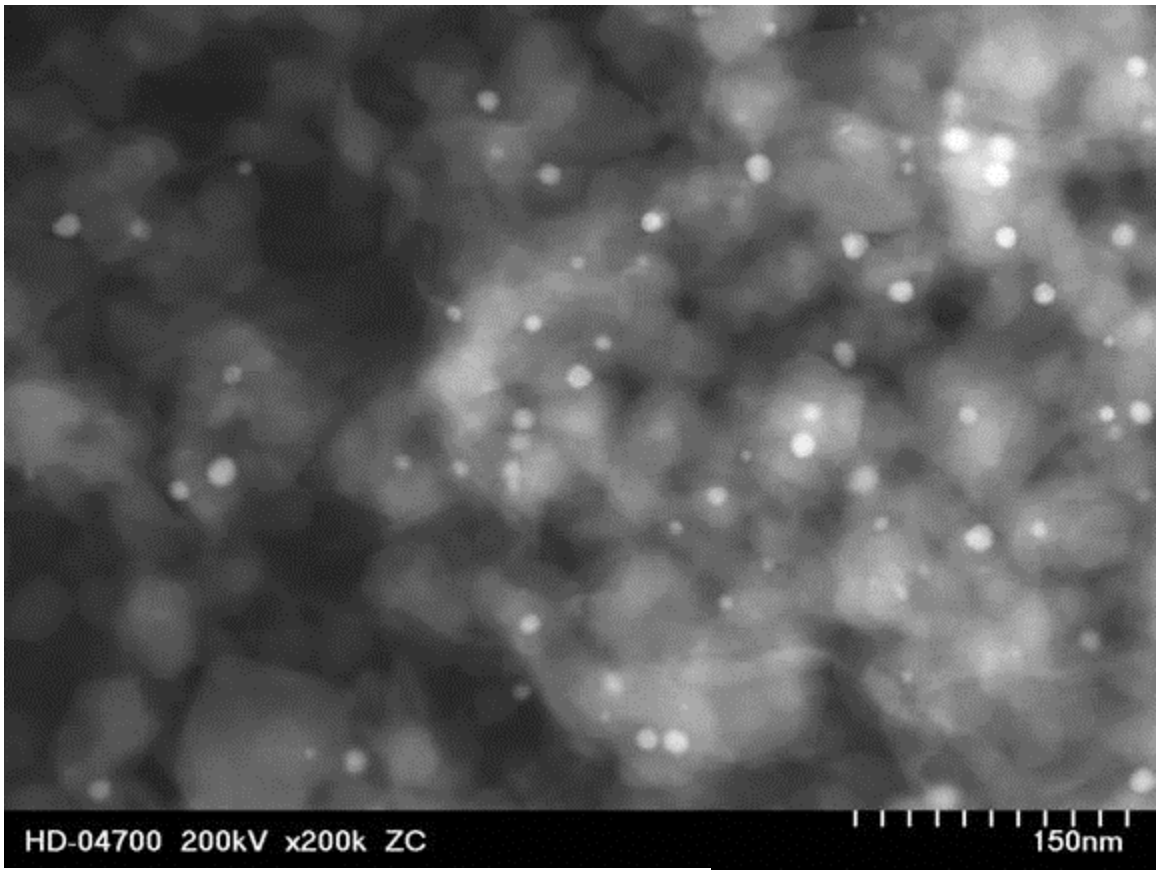

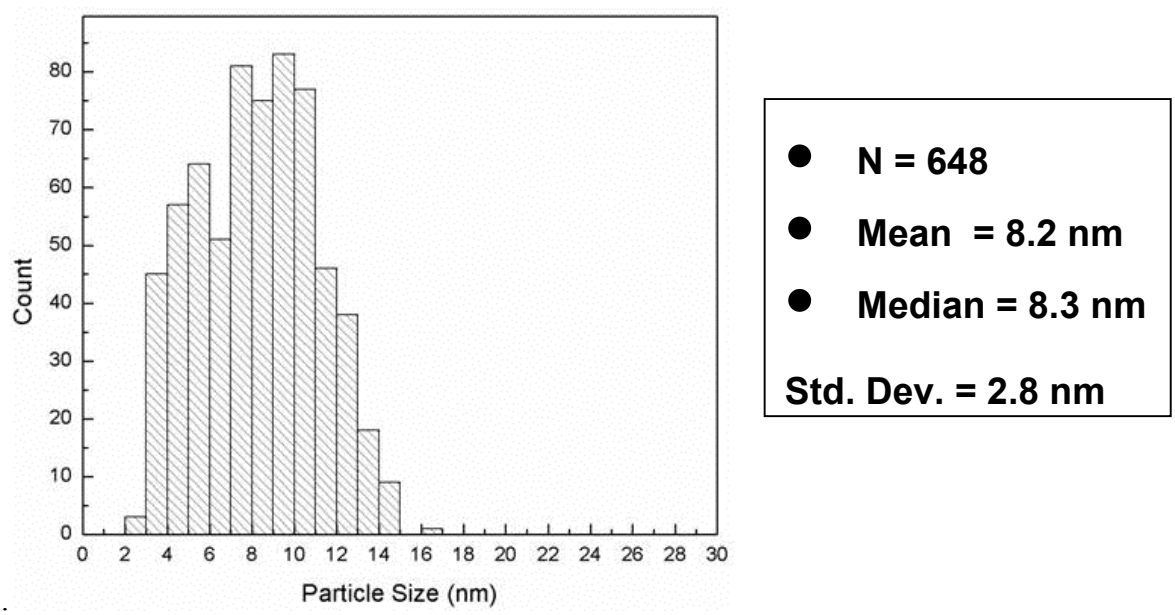

B.

Figure 3 – **A** shows ADF image from the STEM showing Pt particles in bright contrast after 150 desulfation hours. Digital processing yields distribution of Pt particles shown in **B**, with statistics as shown.

Development of NO_x Sensors for Heavy Vehicle Applications

Timothy R. Armstrong, David L. West, Fred C. Montgomery
Oak Ridge National Laboratory

CRADA No. ORNL 01-0627
with Ford Motor Company

Objective

The proposed project seeks to develop technologies and materials that will facilitate the development of NO_x and ammonia sensors. The development of low-cost, simple NO_x will facilitate the development of ultra-low NO_x emission engines, directly supporting the OHVT goals.

Technical Highlights

1. The most significant improvement has been incorporation of programmed concentration changes and automated data recording for NO and NO_2. We are now able to simultaneously record NO_x levels (determined by a Thermo Environmental Instruments TL 42C NO_x monitor), and the measured response of candidate sensing materials, while changing flow conditions.
2. ORNL designed and constructed a test stand to screen catalysts. The test cell utilizes a small quartz tube packed with catalyst. NO and NO_2 can be flowed thought the cell and the tail gas is quantified with the NO_x sensor. This test provides a rapid indication as a function of temperature of how good the catalyst is for the decomposition of NO and NO_2.
3. Past testing has indicated that mixed potential sensors are very sensitive to the oxygen concentration in the exhaust gas. To date, very few research organizations have indicated the severity of the problem. We have found large oxygen dependence in the sensor tests carried out to date. Further examination has indicated that the vast majority of the oxygen sensitivity is due to the Pt electrodes. Studies with and without Pt electrodes have shown that the oxygen dependence can be nearly eliminated by replacing Pt with a non-noble electrode.
4. Catalyst testing has been carried out on a limited number of perovskites and spinel materials. All the test data collected indicates that NO_2 gives a very large signal with all of the materials tested, while NO has little or no signal. Work is ongoing to identify and test a strong NO catalyst.

Status of Milestones

Although this project had a late kick-off, we are ahead of schedule of most of the milestones:

1. Modify current sensor test stand for operation at 800°C (delayed at request of Ford)
2. Test NGK sensor in modified test stand (delayed at request of Ford)
3. Deliver NO_x catalyst assessment and program plan to Ford (completed 6/2002)
4. Construct NO_x electrode test stand. (Completed 12/2003)
5. Deliver report on initial rest results (Completed 2/2003)
6. Design and procure screens for simplified NO_x sensor design. (Completed 12/2003)
7. Produce first simplified NO_x sensors for testing (delayed until December 2003).

Communications/Visits/Travel

We delivered a quarterly report of our activities to Ford in April 2003.

Problems Encountered
None to date.

Publications
None to date.

Microstructural Changes in NO_x Trap Materials under Lean and Rich Conditions at High Temperatures

C. K. Narula and L. F. Allard
Oak Ridge National Laboratory
and
C. Goralski and J. Li
Ford Motor Co.

Objective/Scope

NO_x traps are at the forefront of various strategies under investigation to treat NO_x from Diesel or Lean-gasoline engines [1]. NO_x traps collect engine out NO_x during lean operation and treat it during short rich operation cycles [2]. Fresh NO_x traps work very well but cannot sustain their high efficiency over the lifetime of vehicles. This is believed to be caused by aging due to high-temperature operation and sulfation-desulfation cycles necessitated by the sulfur oxides in the emissions from the oxidation of sulfur in fuel. In order to design a thermally durable NO_x trap, there is need to understand the changes in the microstructure of materials that occur during various modes of operation (lean, rich, and lean-rich cycles). This information can form the basis for selection and design of new NO_x trap materials that can resist the deterioration under normal operation.

The NO_x traps are derived from commercial three-way catalysts installed to treat emissions from engines operating at stoichiometric air-fuel ratios. As such, the basic components of NO_x traps are identical to three-way catalysts. The advance version of three-way catalyst is a two-layer system on a honeycomb substrate with the inner layer based on platinum-alumina and the outer layer on rhodium-ceria-zirconia. The NO_x traps derived from advanced three-way catalysts are identical to it with the exception of high baria content (the upper limit being close to 20%) in alumina layer. Thus, the aging can lead to intermixing of layers, crystallization of baria containing phases that are not good NO_x absorbers, and the sintering of precious metals. The first goal of the project is to determine if one or all of the microstructural changes take place and if these changes occur during lean, rich, or lean-rich cycles.

The tasks to achieve this goal are as follows:

- Complete microstructural characterization of fresh and thermally aged NO_x trap materials to determine the species formed as a result of aging.
- Complete microstructural characterization of fresh NO_x trap materials after exposure to lean conditions to determine the species formed during lean cycles.
- Complete microstructural characterization of fresh NO_x trap materials after exposure to lean conditions to determine the species formed during lean cycles.

The second goal of the project is to investigate and design new materials that can withstand NOx trap operating conditions without undergoing detrimental structural changes. The results from first goal will provide insights into changes that occur in NO_x trap materials at microstructural level upon extended exposure to NO_x trap operating conditions enabling selection and design of materials for the second goal.

Technical Highlights

We initiated the work by characterizing the microstructures of samples prepared by two methods. In the first method, a sample of Pt-alumina was impregnated with a barium compound and carefully pyrolyzed. In the second method, a sample of Pt-alumina was ball milled with a barium compound and then pyrolyzed. The samples have 2wt% Pt and 18wt% barium. The X-ray powder diffraction patterns (e.g. Fig. 1) of the samples show sharp peaks due to barium carbonate, suggesting that barium oxide component has reacted with atmospheric CO_2. The broad diffraction peaks due to microcrystalline γ-alumina can also be seen.

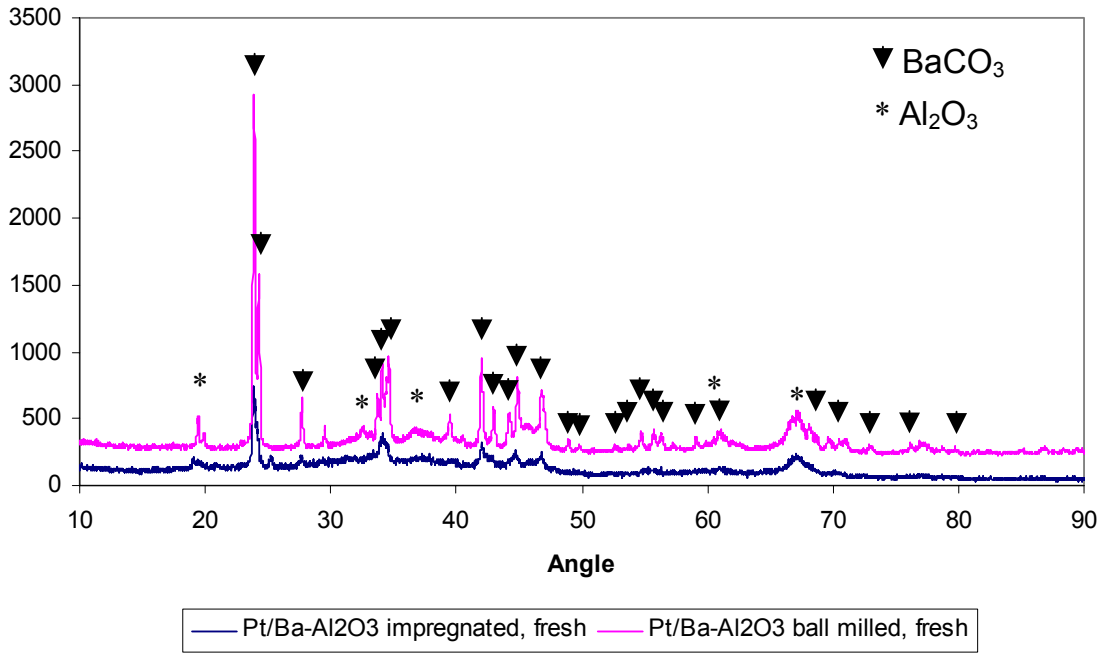

Figure 1: The X-ray Powder Diffraction Patterns of the Pt/Ba-Al_2O_3 samples.

Figure 2a shows typical morphologies of the as-impregnated barium carbonate and alumina components. The long needles show energy-dispersive X-ray spectra (Fig. 2b) consistent with $BaCO_3$ (as expected, based on XRD data), as shown in the computed spectrum for $BaCO_3$ in Fig. 2c. The Cu and Al peaks come from secondary excitation of Cu specimen grid and the adjacent alumina phase, respectively. Figure 2d shows the spectrum from the fine-grain structure, confirming the composition as alumina, with clear Pt peaks arising from the Pt loading as the catalytic species.

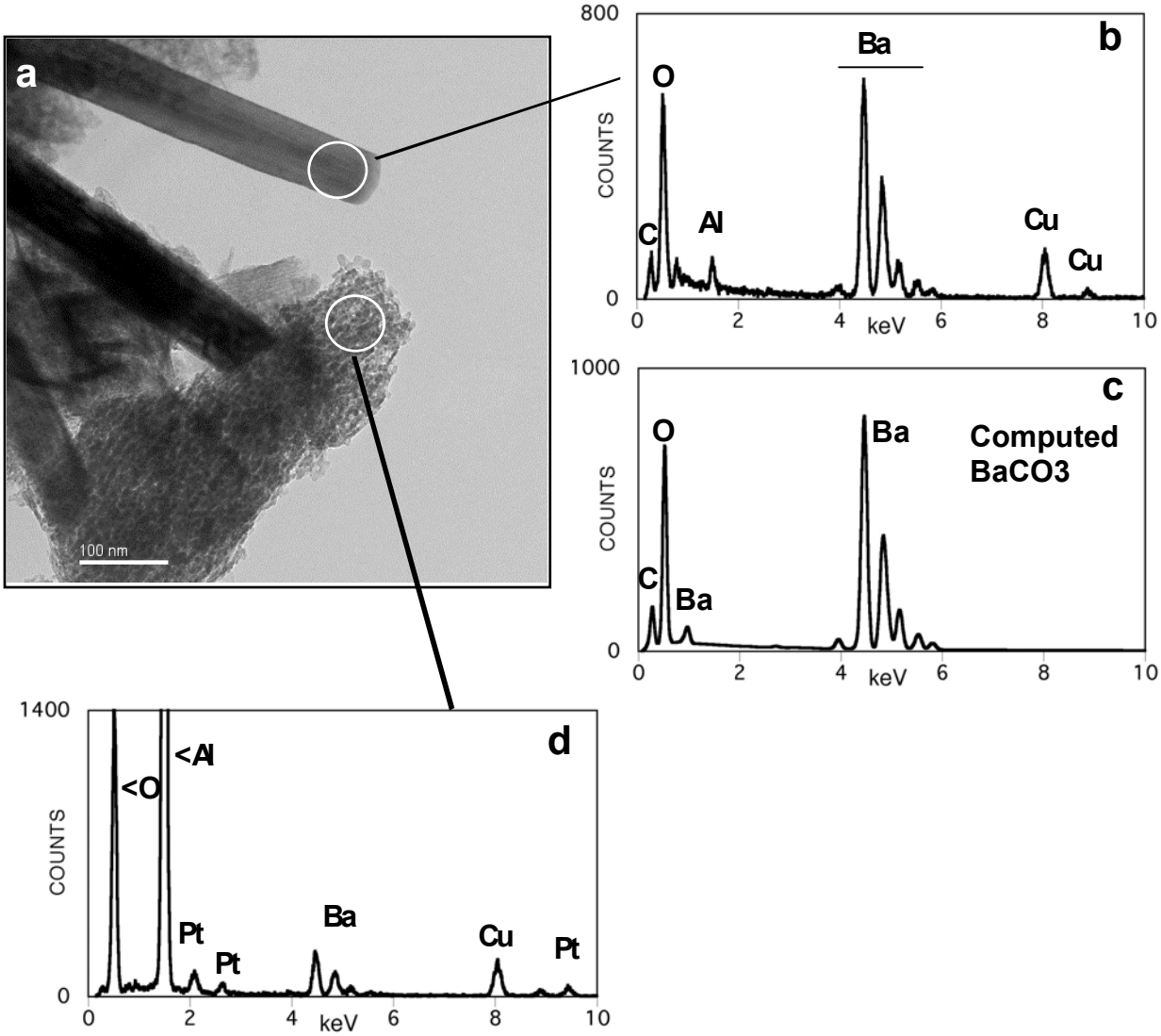

Fig. 2 Pt/Al_2O_3 catalyst as-impregnated with BaO. Needle structures are $BaCO_3$ phase, and fine structure is Pt/alumina phase. Cu results from the specimen grid.

Figure 3 is a typical micrograph of the ball-milled Pt/Al_2O_3/baria material. The carbonate needles are effectively broken up so there is a more intimate mixture of the Ba compound with the Pt/alumina material.

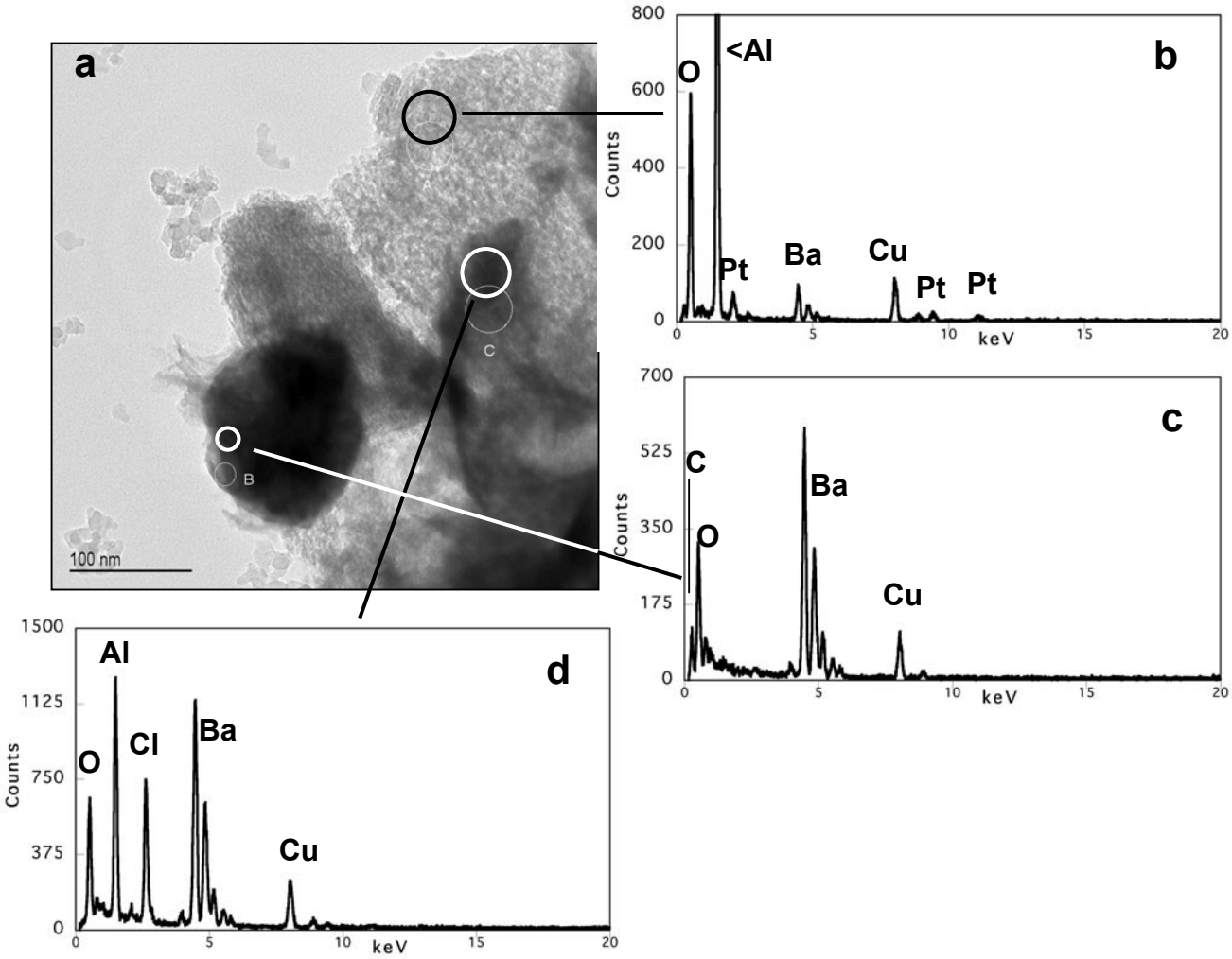

Fig. 3 Ball-milled Pt/Al_2O_3/baria catalyst showing break-up of carbonate needles to give intimate mixture of fine-structured Pt/alumina phase and barium carbonate. Cu results from specimen grid, and Cl peak in 3d is most likely from residual Cl from precursors. (Note energy scale change from Fig. 2.)

Other activities

The ex-situ reactor, available at HTML, needed upgrades for additional gases in the simulated lean and rich exhaust. The gas-flow controllers have been received and are being installed.

Communications/Visitors/Travel

We traveled to Ford Research Laboratory to work on a comprehensive joint proposal with Profs. J. Schwank, R. Laine of University of Michigan Drs. W. Schneider, C. Goralski, J. Li, and P. Schmitz of Ford Research Laboratory on Lean NO_x Trap Technology that has been submitted to DOE-BES. This proposal, entitled "A combinatorial approach to the rational design and optimization of multifunctional heterogeneous catalysts" is a result of strengthening ties with our collaborators at Ford Research Laboratory.

Problems Encountered
None

Publications
None

References
1. Miyoshi, N.; Matsumoto, S.; Katoh, K.; Tanaka, T.; Harada, J.; Takahashi, N.; Yokota, K.; Sigiura M., and Kasahra, K.; "Development of New Concept Three-Way Catalyst for Automotive Lena-Burn Engines", SAE paper 95-0809.
2. Takahashi, N.; Shinjoh, H.; Iijima, T.; Suzuki, T.; Yamazaki, K.; Yokota, K.; Suzuki, H.; Miyoshi, N.; Matsumoto, S.; Tanizawa, T.; Tateishi, S.; and Kasahara, K.; "The New Concept 3-Way Catalyst for Automotive Lean-Burn Engine: NOx Storage and Reduction Catalyst", Catalysis Today, 1996, 27, 63-69.

Lightweight Valve Train Materials

Mark J. Andrews
Caterpillar Inc.

Introduction

Valve train components in heavy-duty engines operate under high stresses and temperatures, and in severe corrosive environments. The light-duty engine market requires cost-effective reliable materials that are wear resistant and lightweight in order to achieve high power density. For both engine classes, better valve train materials need to be identified to meet market demand for high reliability and improved performance while providing the consumer lower operating costs.

Advanced ceramics and emerging intermetallic materials are highly corrosion and oxidation resistant, and possess high strength and hardness at elevated temperatures. These properties are expected to allow higher engine operating temperatures, lower wear, and enhanced reliability. In addition, the lighter weight of these materials (about 1/3 of production alloys) will lead to lower reciprocating valve train mass that could improve fuel efficiency. This research and development program is an in-depth investigation of the potential for use of these materials in aggressive engine environments.

The overall valve train effort will provide the materials, design, manufacturing, and economic information necessary to bring these new materials and technologies to commercial realization. With this information, component designs will be optimized using computer-based lifetime prediction models, and validated in rig bench tests and short- and long-term engine tests.

Program Overview

Information presented in this report is based on previous proprietary research conducted under Cooperative Agreement DE-FC05-97OR22579.

Ceramic Materials

Silicon nitride materials have been targeted for valve train materials in automotive and diesel industries since early 1980's. Silicon nitride material grades have now reached maturity, and few new material grades are being introduced. Commercial successes have been reported in both automotive and diesel valve trains, with large-scale production underway. The reported valve train applications exploit the high contact damage and wear resistance of the ceramic material.

Intermetallic Materials

Titanium aluminide based intermetallics retain their strength to elevated temperature and are highly corrosion-resistant. They are lightweight, and posses high fracture toughness. These alloys are actively being investigated for several aerospace and automotive applications.

Summary

Valve Test Rig

Impact and wear test results previously presented from the valve test rig have illustrated the removal of small Si_3N_4 particles of from the contact region. This phenomenon is demonstrated by the identification of Si_3N_4 particles found imbedded in the metallic seat insert using the EDS

on the SEM. It is presumed that since this material removal occurred over a short 100-hour test period, that it might lead to early valve failure. To better understand this phenomenon, a study was initiated in the present reporting period to examine the contact stresses between the valve and the seat insert during the seating event. This study is being conducted by Surface Engineering staff members of AMT and uses an in-house developed software with finite element modeling to estimate stresses at and below the contact surface of the valve. Results of this study have not been analyzed and are anticipated in the 2nd quarter of 2003.

Machining Study

The surface finish as a function of material performance will be assessed for silicon nitride and titanium aluminide materials under Caterpillar's Alliance for Innovative Manufacturing (AIM) program located in TC-K. The program plans to use a Thielenhaus continuous abrasive belt machine and machine test specimens having variations on the surface finish. The fracture strength of the machined test specimens will assess the materials performance.

Silicon Nitride Valve Blanks

The 50 silicon nitride valve blanks fabricated by Kyocera were examined using a coordinate measuring machine. The straightness of the valve stem and its orientation with the valve head at the face are required in order to prepare final print specifications for machining. The center of the valve head was compared to the center of the valve along the stem. Many of the valves measured a small (compliant) distance between the centers, while a few valves measured a (noncompliant) distance as much as 7 mm between the centers (see Figure 1). Kyocera was notified of this finding and will replace any valve blanks at no cost to Caterpillar that cannot be machined to print specifications.

Caterpillar has ordered and received 220 four-point flexure test specimens for strength and fatigue evaluation and has sent 120 of them to Dr. H. T. Lin of ORNL to perform the strength tests.

Life Prediction of Ceramic Engine Valves

Finite element analyses of prototype silicon nitride engine valves examined the keeper lock that connects the return spring to the valve stem. Failures in this region have been reported in the literature and have also been observed at AMT. The analyses assumed an engine operating at 1.5 times the normal rpm, and estimated stresses during the seating event. Both 2D and 3D analyses were conducted using the same established boundary conditions and each model estimated the maximum principle tensile stress in the valve stem notch at 70-90 MPa. This stress level is below the fracture strength of the Si_3N_4 valve stem; however optimization of this valve feature will be made in order to examine notch designs that potentially reduce the maximum principal tensile stress.

Design of Silicon Nitride Engine Valves

A review of the prototype silicon nitride valve design was conducted at LEC. Alterations to the valve design were adopted and additional valve boundary conditions were discussed. A second meeting will be scheduled with LEC and MEC once the final print specifications are completed.

Intermetallic Materials Research

The wear characterization for different combinations of TiAl and seat insert materials was completed. Optical interferometry was used to measure the volume of material removed from the surfaces in contact. Ball-on-flat reciprocating sliding wear from room temperature to 600°C was conducted as described in previous reports. A valve-seat insert material pair currently used for high temperature applications was also evaluated for establishing a comparative baseline for. This pair consists of Pyromet 31 (P31) and the cobalt-based alloy J3, used for the valve and the seat-insert respectively. A plot comparing the wear for the different material combinations is shown in Figure 2. The combination of TiAl with J3 shows lower amounts of wear on both surfaces as compared to the currently used P31/J3 combination. Based on these results the seat-insert material J3 will be used for future engine testing of TiAl valves.

Tensile testing of TiAl at high temperatures was conducted in collaboration with Dr. H.T. Lin at ORNL. The tensile specimens were exposed to oil-ash at 750°C for 48 hours to induce corrosive media typically observed on the surface of engine valves. A tensile specimen after exposure to oil ash media is illustrated in Figure 3. After the oil-ash exposure the specimens were tested in tension and the strengths were compared with results obtained for pristine specimens as shown in Figure 4. Only a minor decrease in strength at low temperatures was observed as a result of corrosion. The difference in strength for the exposed and pristine test specimens was observed to decrease with increasing test temperature and likely due to surface healing by oxidation.

The effects on joint strength and material flow by using different combinations of friction welding parameters are being analyzed. The material flow is characterized by the upset, which is the reduction in length resulting from the deformation and flashing of material during the friction welding operation. Significant changes in the deformation behavior were observed by changing rotational speeds, while maintaining constant friction and forging pressures. Upsets are shown for 1200RPM and 3600RPM in Figure 5 with friction and forging pressures of 59 and 98MPa respectively. At 1200RPM the upset increases at an approximate constant rate during the friction stage. The friction upset is initially larger at 3600RPM, after 2 seconds the rate of upset decreases. Higher joint strengths were measured for specimens presenting the inflection in the upset-time curve. The cause for this effect and the impact on the quality of the weld is being investigated.

ANL

None

Presentations

Mark J. Andrews and Jesus Chapa-Cabrera made program review presentations to the ORNL and DOE staff in February 2003.

Future Work

Additional finite element modeling will be made and will focus on optimizing the valve keeper notch, and with establishing a complete valve load cycle for fatigue analyses. Life prediction codes will then estimate the probability of failure for many of the finite element models developed. A final design will be agreed upon that includes members from LEC, CTO, MEC and Engine Research.

Final print specifications and solicitations for machining the Si_3N_4 valves will be sent out and a vendor(s) will be chosen. Valves that have been tested in the bench test will be sent to ANL for NDE.

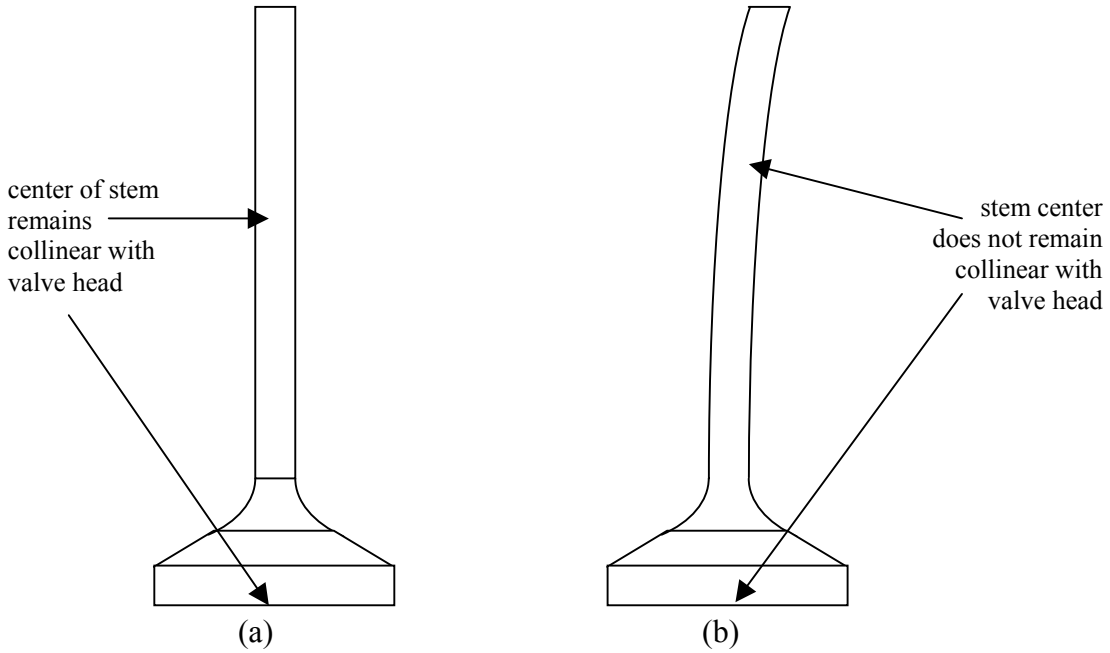

Figure 1. Illustration of the measurements results from the as-received Kyocera valve blanks. In (a) the center of the valve head remains collinear with the valve stem while in (b) the centers of the valve stem and head are not collinear.

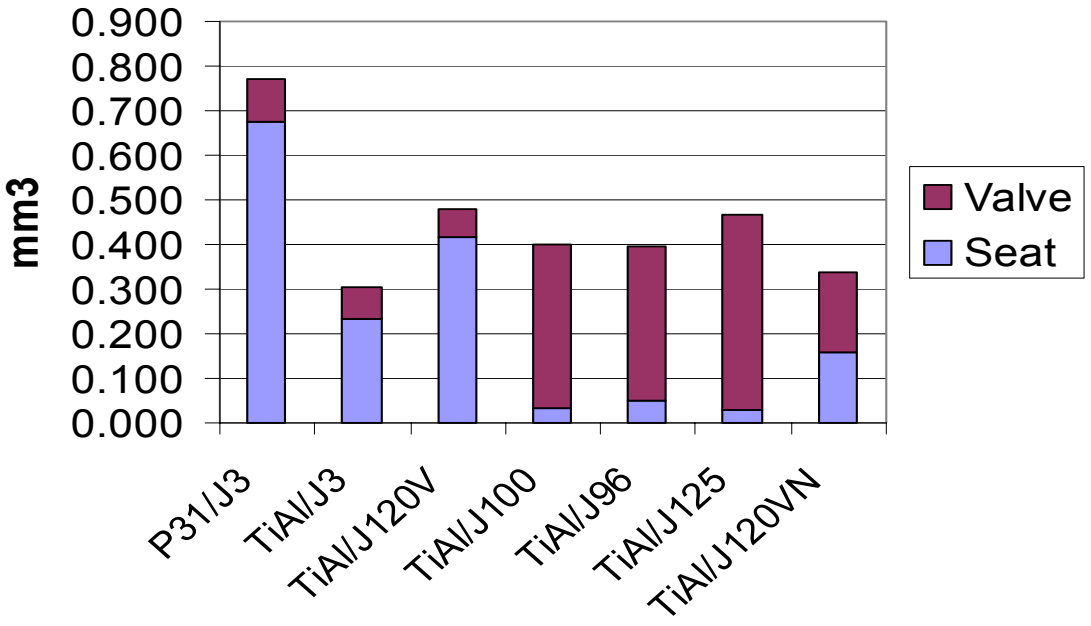

Figure 2. Volume removed after high temperature reciprocating wear testing for different valve / seat insert material pair combinations.

Figure 3 Oil-ash TiAl tensile specimen.

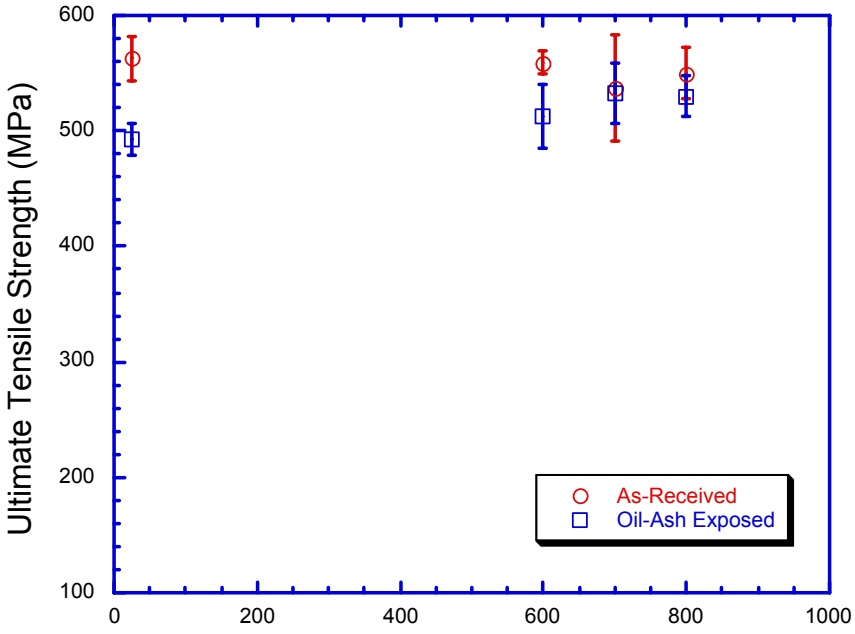

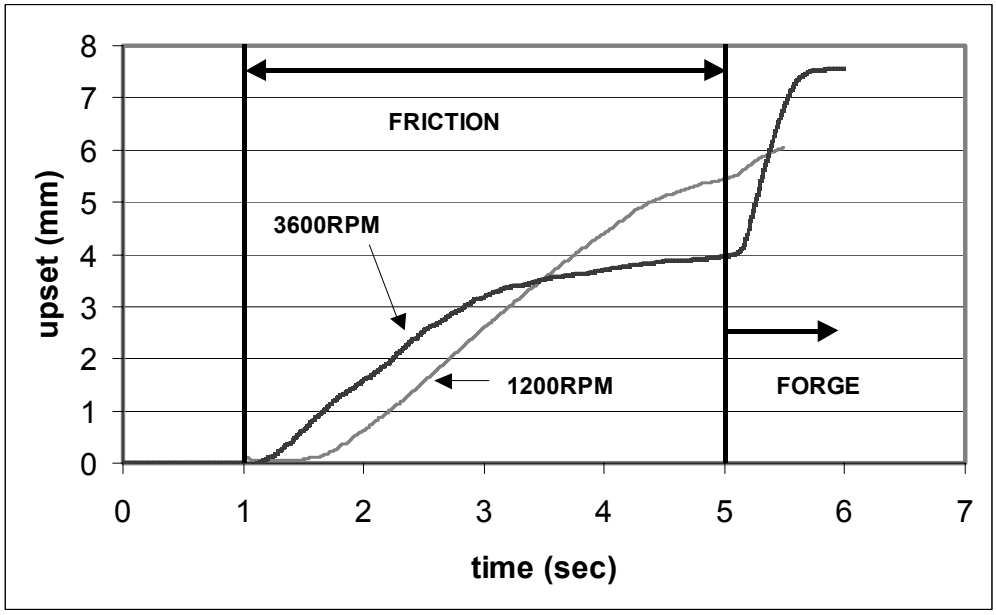

Figure 5. Effect of rotational speed on the axial upset during the friction welding operation

Thick Thermal Barrier Coatings (TTBCs) for Low Emission, High Efficiency Diesel Engine Components

M. Brad Beardsley and Jesus G. Chapa-Cabrera
Caterpillar Inc.

Objective/Scope

Engine testing of thermal sprayed coatings has demonstrated their use as thermal barriers and wear coatings can reduce fuel consumption, reduce wear and reduce component temperatures. The durability of thermal sprayed coatings, particularly thermal barrier coatings, remains as the major technical challenge to their implementation in new engine designs. New approaches to coating design and fabrication will be developed to aid in overcoming this technical hurdle. New laser technology of surface dimpling, cleaning and laser assisted spraying will be applied to enhance adherence and increase coating strength. Refinements of current seal coating technologies will be developed to further enhance the durability of the coating structure. New quasicrystalline materials will be evaluated as thermal barrier coatings as well as wear coatings for ring and liner applications and as low friction coatings for camshafts and crankshafts. Plasma spraying, D-Gun and HVOF processing will be used to develop these new coatings.

Technical Highlights

Initial spraying for coatings to be laser assisted deposited have been done. A NiCrAlY bond coating material has been chosen to spray initially and parameters have been developed for the as-sprayed material. Spray equipment has been shipped to the laser area and will be setup for the laser assisted deposition trials in the next quarter.

Quasicrystal coatings have been sprayed using the $Al_{71}Co_{13}Fe_8Cr_8$ material with both plasma and HVOF processing. The deposition efficiencies of the spray processes are show in Table 1 and 2. The material has very good deposition efficiency over the range of plasma spray parameters evaluated. This is similar to a metal coating where as a ceramic coating of zirconia would show a wider variability and lower deposition efficiency. In HVOF spraying, the quasicrystal material behaves more like a carbide with low efficiency. These differences reflect the materials higher ductility at the high temperatures of the plasma spray verses the lower HVOF spraying temperatures. Further optimization of the plasma and HVOF processing is under way as well as measurement of the thermal conductivity of the deposits.

Future Plans

Laser-assisted deposition trials will be performed with both NiCrAlY material and a NiCrAlY + zirconia grading material and microstructure on the deposits compared to the as-sprayed coatings. Quasicrystal coating will be evaluated for thermal conductivity and strength. Mechanical property testing of the phosphate-bonded coatings is planned for next quarter as well as thermal rig testing of the coatings.

Travel

M. Brad Beardsley and Jesus Chapa-Cabrera traveled to the University of Illinois to meet with Dr. Darrell Socie to discuss mechanical property testing of the new phosphate bonded materials.

Table 1. Plasma Processing Variables and Resulting Deposition Efficiencies for Quasicrystal TBC Material

Run No.	PGF, FMR	Amps	Volts	CGF, FMR	SO	%Deposition Efficiency
1	64	350	69.2	47	75	71
2	64	350	71.2	55	75	68
3	64	350	72	62	125	60
2A	85	350	71.5	47	75	71
4	106	350	69.5	47	100	79
5	106	350	68.4	55	125	71
6	106	350	69.9	55	100	68
7	106	350	69.2	62	125	64
14	64	450	74.4	47	125	79
15	85	450	74	62	75	67
13	106	450	73.5	55	125	69
16	64	550	73.5	47	125	74
17	64	550	73.2	55	75	70
18	64	550	72.8	62	125	67
8	106	550	72.2	47	125	84
9	106	550	72.1	47	75	81
10	106	550	72	47	125	84
11	106	550	71.8	55	75	72

Table 2. HVOF Processing Variables and Resulting Deposition Efficiencies for Quasicrystal TBC Material

Fuel/Oxygen Ratio	Total Gas Flow, SCFH	Standoff, mm	Air Flow, FMR	Deposition Efficiency, %
4.1	918	260	25	34.1
4.2	1430	300	42	33
4.2	1430	220	42	28.1
3.1	1298	230	38	32.2
3.7	1414	230	42	27.8
2.3	1303	300	48	19
3.7	1044	260	30	38.9
4.2	1430	220	42	30.7
2.3	1462	300	53	13.1
4.2	1319	300	39	36.5
4.2	1188	300	29	44.1
4.3	1428	230	44	28.9
3.7	1414	230	42	31.4
4.2	1319	220	39	31.5
3.7	1414	300	42	34.1
2.3	1303	220	48	11.3

Status of FY 2003 Milestones

321. Determine the effect on TTBC bond strength due to laser micro-dimpling of the substrate surface prior to coating. **(July 31, 2003)**

Estimate of the processing times has been done to determine the feasibility of the processing.

322. Determine the effect on TTBC coating strength and permeability due to laser shock peening after coating application. **(July 31, 2003)**

No progress to report.

323. Determine the effect on the hardness and microstructure of the TTBC due to laser assisted plasma deposition. **(July 1, 2003)**

Initial spraying has been done. A consulting contract with Fraunhofer USA has been initiated to aid Caterpillar efforts in this area.

324. Incorporate torsional fatigue testing results into life models. **(Completed May 29, 2002)**

No progress to report

325. Develop FEA models to aid in the design of life prediction tools for the TTBC system. **(December 1, 2003)**

No progress to report.

324. Evaluate the microstructure of the ceramic TTBC material using varying laser power.

No progress to report.

Publications

None this period.

Processing and Characterization of Structural and Functional Materials for Heavy Vehicle Applications

J. Sankar, Z. Xu, and S. Yarmolenko
North Carolina A & T State University
and
J. Lua
Anteon Corporation

Objective/Scope

Continue to investigate the combustion chemical vapor deposition technique of fully stabilized zirconia (YSZ) thin films for solid oxide fuel cells.

Task

Investigate the microstructural evolution in the early stage of YSZ thin film deposition.

Technical Highlights

In the previous reports, the parametric studies of YSZ thin film deposition by the liquid fuel combustion chemical vapor deposition technique were presented. When YSZ is used as an electrolyte in solid oxide fuel cells, the microstructural characteristics of the thin films has played an important role in controlling efficiency and reliability of the fuel cell. Experimental studies have shown that both the grain size and the film texture highly depend on various fabrication and processing parameters. To explore an optimal processing technique for maximizing the performance and durability of the fuel cell, a stochastic grain growth model is developed by implementing Thompson's grain evolution law into a probabilistic computational framework. The resulting stochastic grain size evolution model can be used to trace both the microstructure and texture subjected to a given processing condition.

Results and Discussion

Effect of Substrate Temperature on the Nucleation Density

The temperature of the substrate is an important factor that controls the nucleation density defined as the number of aggregates created per unit area. To be able to use the image analysis software (Image Pro) for computing the nucleation density at different temperatures, the nucleation time of the YSZ particles was set for 60 seconds at temperatures of 800°C, 900°C, 1000°C, 1100°C, and 1200°C subjected to the total-metal concentration of 1.25E-03 *M*. Because of invisible sizes of aggregates after 60 seconds, the film was processed subsequently for another 240 seconds under dilute total-metal concentration of 5.5E-04 *M*. The purpose of using the dilute concentration during the nuclei growth stage was to avoid regeneration of new aggregates. The final distribution of aggregates after 1-minute nucleation and 4-minute

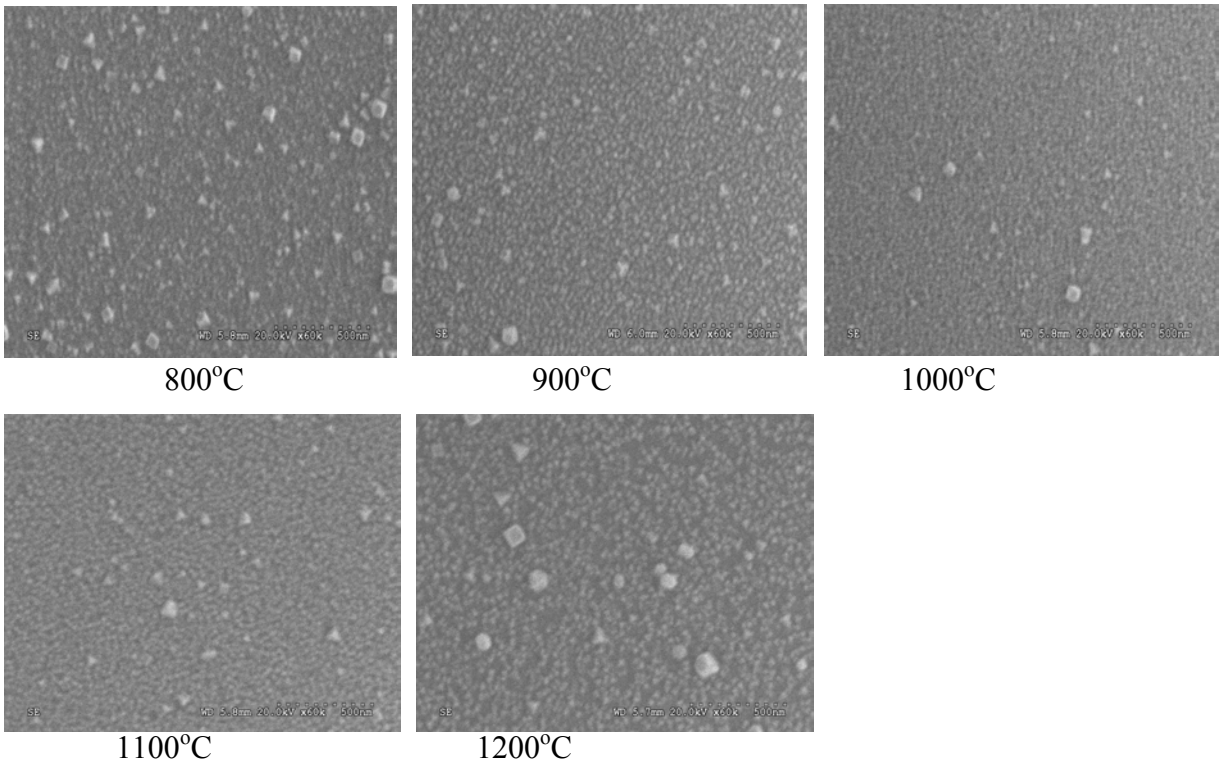

Figure 1. Distribution of Aggregates at Various Nucleation Temperature

growth is shown in Figure 1. Using the image analysis software (Image Pro), the density of aggregates was analyzed and is listed in Table 1 for different nucleation temperatures. As shown in Table 1, the density of aggregates drops as the temperature increases which is consistent with Thompson's model prediction.

Table 1. Densities of Aggregates at 5 Nucleation Temperatures

Nucleation Temperature(°C)	800	900	1000	1100	1200
Density of nucleation ($x10^{10}/cm^2$)	12.5	8.38	7.92	6.71	2.96

<u>Effect of Processing Time on Grain Size Evolution</u>

To grasp the physics of the evolution process of the YSZ thin film, the grain sizes at various stages of the processing time were measured for statistical post-processing. The YSZ film deposited on SiO_2/Si(100) substrates at 1200°C with the total-metal-concentration of 1.25E-03 *M* is shown in Fig. 3 at different stages of the processing time. As shown in Fig. 2, the average size of grains increases with the processing time. To quantitatively characterize the evolution process of grain growth, the statistical distributions of grain size at processing times of 180 sec. and 300 sec. are shown Fig. 3.

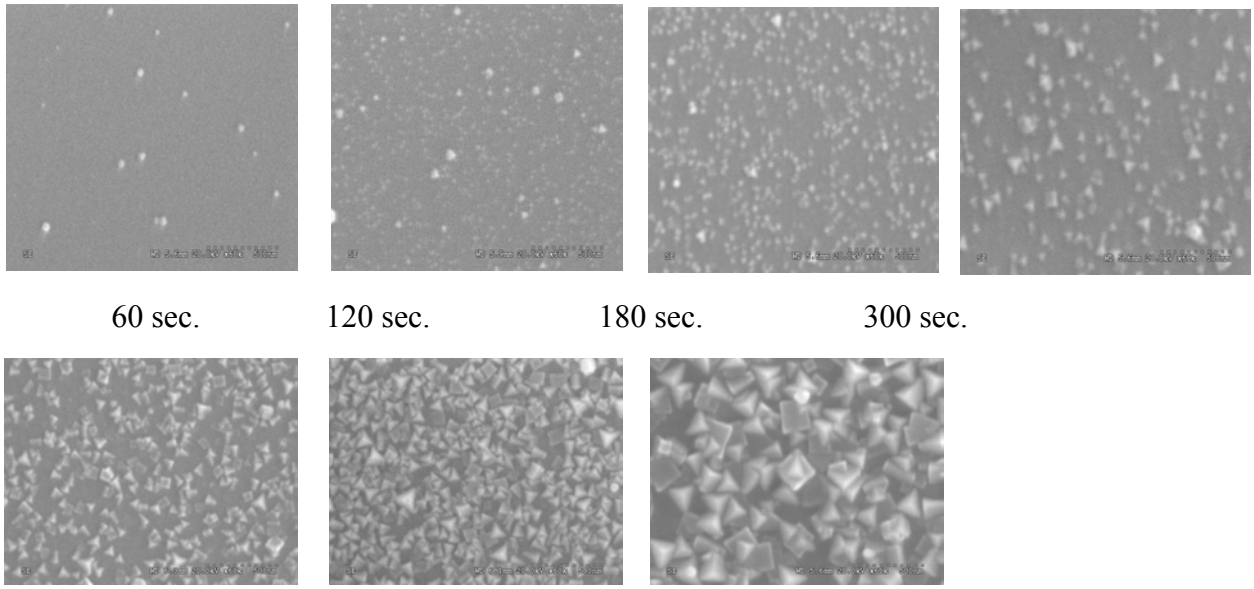

Figure 2. Display of Grain Size Distributions at Various Stages of the Processing Time

To demonstrate the validity of the lognormal approximation for normal grain growth, an equivalent lognormal distribution is determined using the sample mean and the sample standard deviation. The sample mean and the sample standard deviation of random grain size at the processing time of 180 sec. are 43.62 nm and 12.22nm, respectively. After seven more minutes, the sample mean and the same standard deviation become 67.79 nm and 15.38 nm, respectively.

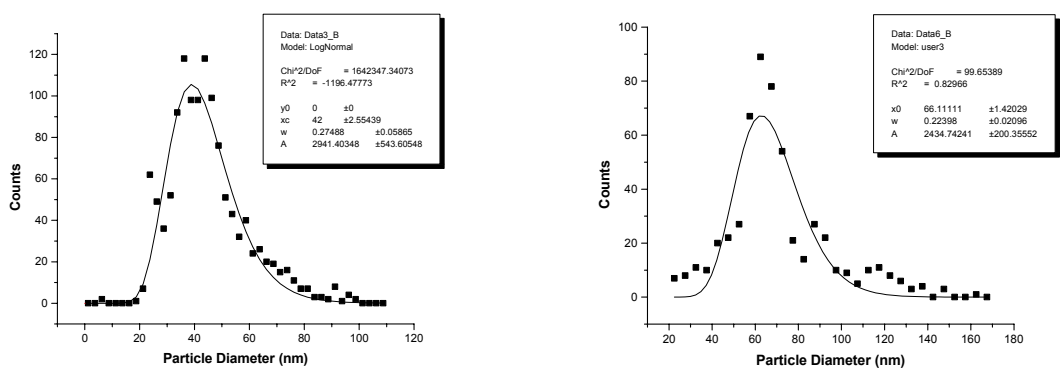

Processing time 180 sec. Processing time 300 sec.

Figure 3. Comparison of Statistical Distributions of Grain Size at Processing Times of 180 sec. and 300 sec.

<u>Development Of Stochastic Grain Growth Model</u>

In order to further explore the effects of system parameters on the evolution process of grain growth, Thomson's model for grain growth in thin films was employed. Since the lognormal

model shown in Fig. 3 does not provide an accurate statistical representation of the grain size distribution, the assumption of lognormal distribution is removed in the numerical simulation model. Using the grain growth kinetics and continuity equation, the stochastic evolution of grain size is governed by

$$\frac{\partial \phi(r,t)}{\partial t} = -\frac{\partial}{\partial r}\left[\phi \frac{\partial r}{\partial t}\right] = -\frac{\partial}{\partial r}\left\{\frac{\phi\, M \bar{\gamma}_{gb}}{2}\left(\frac{1}{r^*} - \frac{1}{r}\right)\right\} \tag{1}$$

where $\phi(r.t)$ is the probability density function of grain radius r at time t, r^* is a critical radius above which a grain will grow and below which a grain with shrink, and $\bar{\gamma}_{gb}$ is the average grain boundary energy per unit area of grain boundary. In Equation (1), M is defined by

$$M = M_0 \exp\left(\frac{-Q}{kT}\right) \tag{2}$$

where M_0 is a weakly temperature-dependent constant, Q is the activation energy, k is the Boltzman constant, and T is the temperature. To solve the above initial-boundary value problem, the following initial and boundary conditions have to specified, namely,

$$\phi(r,0) = \phi_0(r) \text{ (initial condition); } \phi(0,t) = \phi(\infty,t) = 0 \text{ (boundary condition)} \tag{3}$$

Given the initial distribution ϕ_0 measured from an experiment and other system parameters, the statistical distribution of grain size at an arbitrary time t can be determined by using Eqs. (1)-(3).

Status of Milestones

On Schedule

Communications/Visitors/Travel

None

Problems Encountered

None

Publications

1. "Deposition of YSZ Thin Films by Liquid Fuel Combustion Chemical vapor deposition", paper IMECE2002-34368 in *Processing, Characterization And Modeling Of Novel Nanoengineered And Surface Engineered Materials*, 2002 ASME International Mechanical Engineering Congress & Exposition (IMECE2002), CD-ROM, Vol. 3.
2. "Preparation and properties of YSZ electrolyte thin films via liquid fuel combustion chemical vapor deposition", *Ceram Eng Sci Proc.* Vol. 23. p. 711-718.
3. "Towards optimal processing of yttria stabilized zirconia thin films by stochastic simulation of grain growth", *Ceram Eng Sci Proc.* Vol. 23. p. 719-724.
4. "Synthesis of Yttria Stabilized Zirconia Thin Films Using combustion Chemical vapor Deposition, Part-A", ICCE/9, Edited by David Hui, July 1-6, 2002, San Diego, California, pp. 861-862.

5. “Synthesis of Yttria Stabilized Zirconia Thin Films Using combustion Chemical vapor Deposition, Part-B”, ICCE/9, Edited by David Hui, July 1-6, 2002, San Diego, California, pp. 863-864.
6. “Stochastic Evaluation Model For Grain Growth in YSZ Films With Column Microstructures”, ICCE/9, Edited by David Hui, July 1-6, 2002, San Diego, California, pp. 493-494.

NDE Development for Ceramic Valves for Diesel Engines

J. G. Sun and W. A. Ellingson,
Argonne National Laboratory
and
M. J. Andrews
Caterpillar, Inc.

Objective/Scope

Emission reduction in diesel engines designated to burn fuels from several sources has lead to the need to assess ceramic valves to reduce corrosion and emission. The objective of this work is to evaluate several nondestructive evaluation (NDE) methods to detect defect/damage in structural ceramic valves for diesel engines. One primary NDE method to be addressed is elastic optical scattering. The end target is to demonstrate that NDE data can be correlated to material damage as well as used to predict material microstructural and mechanical properties. There are three tasks to be carried out: (1) Characterize subsurface defects and machining damage in flexure-bar specimens of NT551 and SN235 silicon nitrides to be used as valve materials. Laser-scattering studies will be conducted at various wavelengths using a He-Ne laser and a tunable-wavelength solid-state laser to optimize detection sensitivity. NDE studies will be coupled with examination of surface/subsurface microstructure and fracture surface to determine defect/damage depth and fracture origin. NDE data will also be correlated with mechanical properties. (2) Assess and evaluate subsurface damage in ceramic valves to be run in bench test and in a single-cylinder-engine test. All valves will be examined at ANL prior to test, during periodic scheduled shut downs, and at the end of the planned test runs. (3) Evaluate healing of subsurface damage by laser glazing on machined surfaces of GS44 ceramics. ANL will perform laser-scattering characterization on machining surfaces at before and after glazing treatment. NDE data will be correlated with glazing parameters and mechanical properties.

Technical Highlights

Work during this period (January-March 2003) focused on correlating laser-scattering NDE data with photomicrographs to identify detected subsurface flaws in 100-hour bench-tested Si_3N_4 ceramic valves.

1. Elastic Optical Scattering NDE for Machining Damage
   No activity in this period.
2. Laser-Scattering Characterization of Si_3N_4 Valves

During this period we continued processing and correlating laser-scattering NDE data with photomicrographs to identify detected subsurface flaws in two 100-hour bench-tested NT551 valves: 273 and 277. The contact surface of the valve is 4-mm wide with an angle of 30 degree as illustrated in Fig. 1. Dr. M. J. Andrews observed two wear scars along the entire circumference of the contact surfaces on both metallic seat inserts and ceramic valves, and with ceramic particles imbedded within the scar areas of seat inserts (M. J. Andrews, "Lightweight Valve Train Materials," Oct.-Dec. 2002 quarterly report for this program).

Figure 2 shows laser-scattering scan images of valves 273 and 277. The scanned region (valve head) is illustrated in Fig. 1. The scan resolution along the axial-length direction was 20 μm, and the resolution along the circumferential direction was 22 μm at "top" and 4 μm at "bottom"

because of the change of diameter. The wear scars on the contact surface of valve 273 were not detected, but they were detected for valve 277 with reduced optical-scattering intensity. The NDE image data in Fig. 2 indicate no apparent subsurface damage due to bench test (except wear on contact surface) and any large-scale subsurface flaws (say, >0.2 mm). Most of the flaws (appearing as high optical-scattering spots in the images) are within 50 μm in size, and they are likely high-porosity spots or small voids. However, a few noticeable flaws are observed along the top edge of the valve contact surface, and these surface regions are closely examined with an optical microscope.

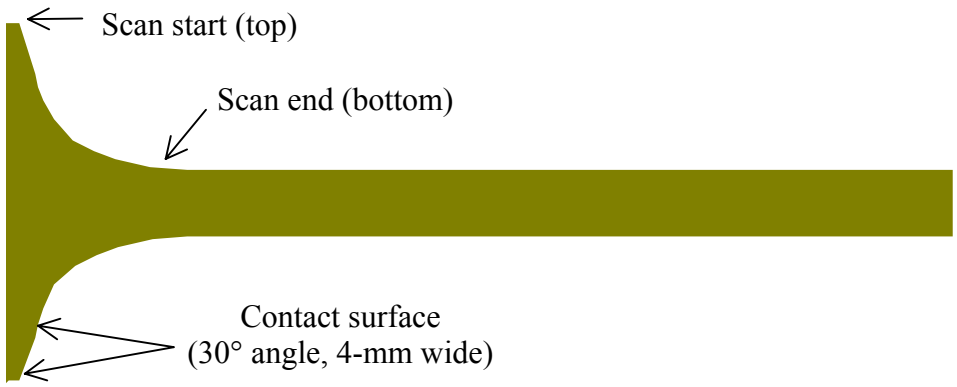

Fig. 1. Diagram of a NT551 valve showing contact surface and laser-scattering scanned region (drawing not in scale).

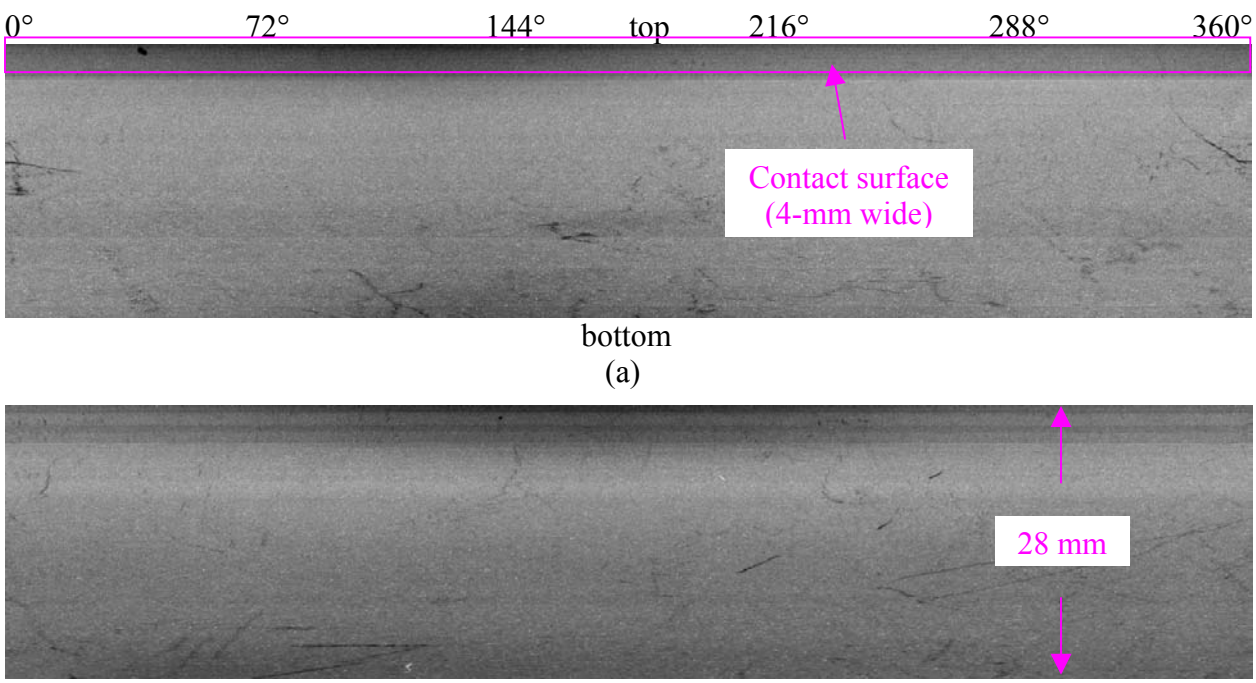

Fig. 2. Laser-scattering images of valve-head section of (a) valve 273 and (b) valve 277.

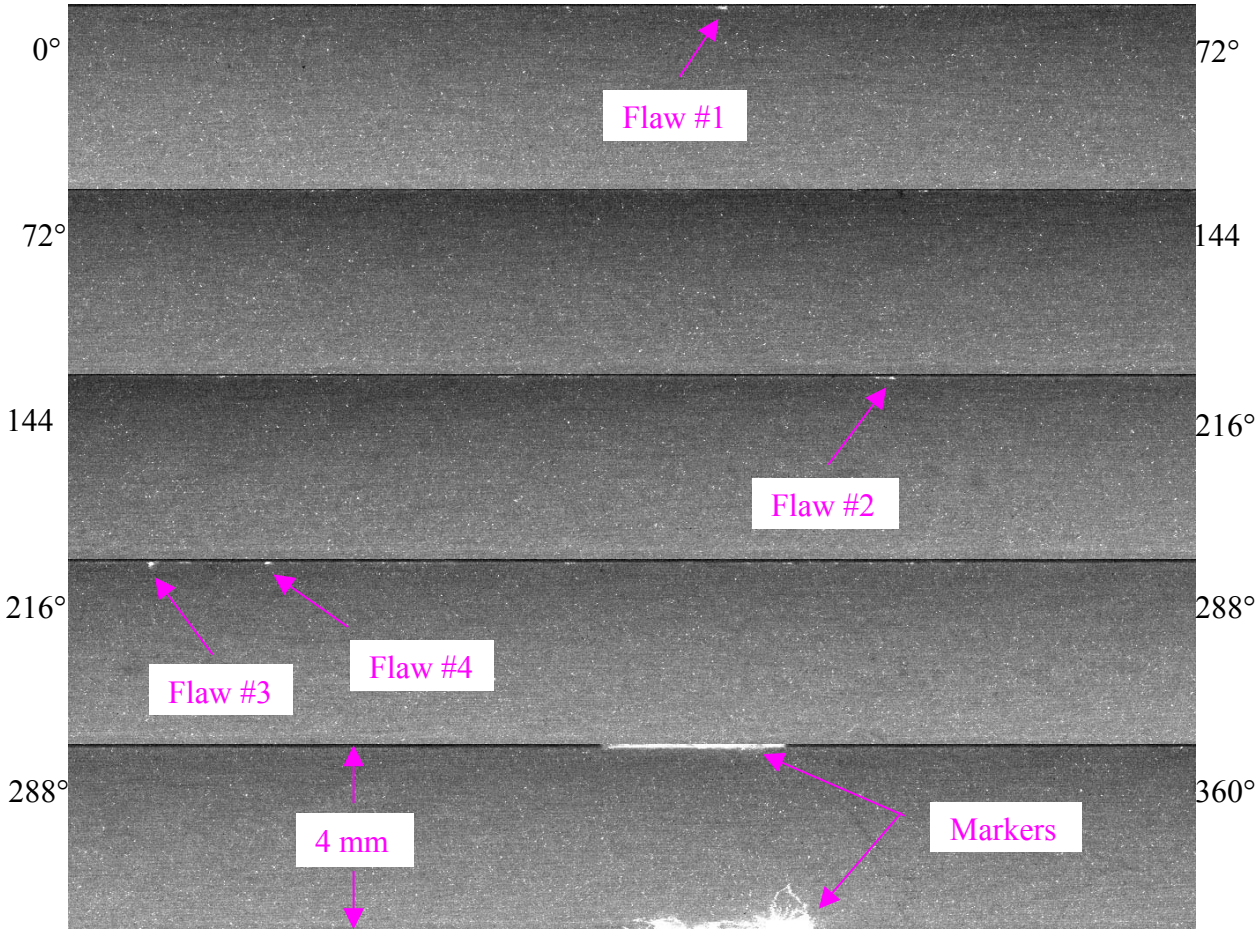

Fig. 3. Laser-scattering image of the contact surface of valve 273; 4 flaws (high optical-scattering spots) at the top edge are indicated.

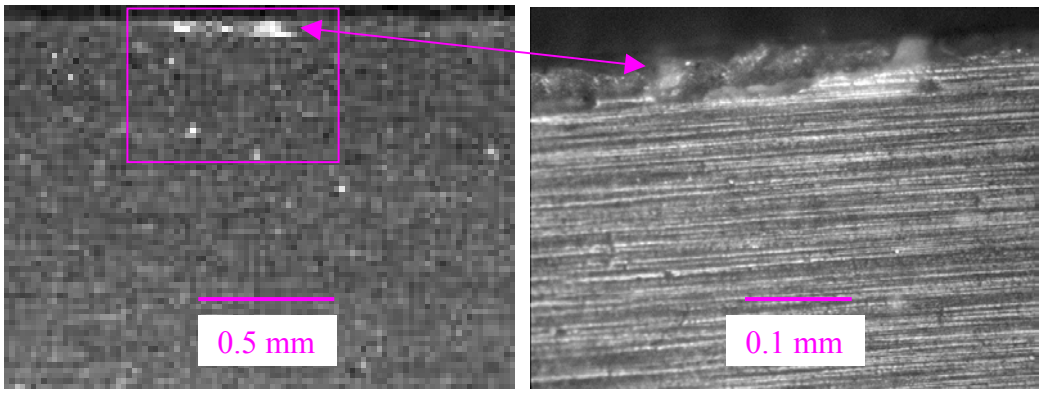

(a) (b)

Fig. 4. (a) Detailed laser-scattering image and (b) photomicrograph at 200X magnification for the surface area of Flaw #2 as indicated in Fig. 3.

Figure 3 shows the detailed laser-scattering image of the contact surface of valve 273. Four subsurface flaws (high optical-scattering spots) along the top edge are indicated in the figure. By correlating the NDE data with photomicrographs, two types of defects can be identified. The first type of defect is shown in Fig. 4 for Flaw #2. It represents material damage, possibly

microchips, under or around a large recessed area at the edge where material has been chipped off. The second type of defect is shown in Fig. 5 for Flaw #3. The detected flaw is clearly seen from the photomicrograph as a piece of chip still partially bonded at the edge. The Flaw #1 is identified as the first type (Fig. 4) and the Flaw #4 as the second type (Fig. 5). These flaws were likely generated during machining. However, the effect of the flaws on valve performance (e.g., will they serve as fracture origin or will the chips come off the valve) can only be determined if the valve is further tested to or near its failure.

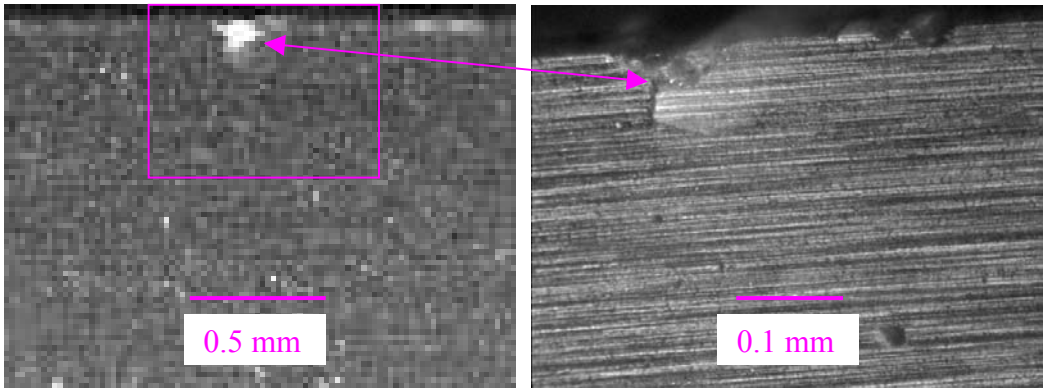

(a) (b)

Fig. 5. (a) Detailed laser-scattering image and (b) photomicrograph at 200X magnification for the surface area of Flaw #3 as indicated in Fig. 3.

Figure 6 shows the detailed laser-scattering image of the contact surface of valve 277. Two subsurface flaws (high optical-scattering spots) at the top edge and two wear scars are detected and indicated in the figure. The detected Flaw #1 is identified as the second type of defect similar to that in Fig. 5 and the Flaw #2 as the first type similar to that in Fig. 4. The two wear scars, pictured in Dr. Andrews' last quarterly report, are clearly detected with lower optical-scattering intensities. Because subsurface damage, if any, would appear with stronger subsurface optical scattering in this NDE measurement, a reduction in detected subsurface-scatter intensity indicates increased roughness on the wear surface.

Figure 7a-b show photomicrographs of the outer wear scar at 400X magnification for valves 273 and 277, respectively. It is apparent that the wear smoothed out shallow machining marks, but the combined effect of wear and impact also caused loss of surface materials. The wear surface of valve 277 becomes rougher than that of valve 273.

Status of Milestones

Current ANL milestones are on schedule.

Communications/Visits/Travel

None this period.

Problems Encountered

None this period.

Publications

None this period.

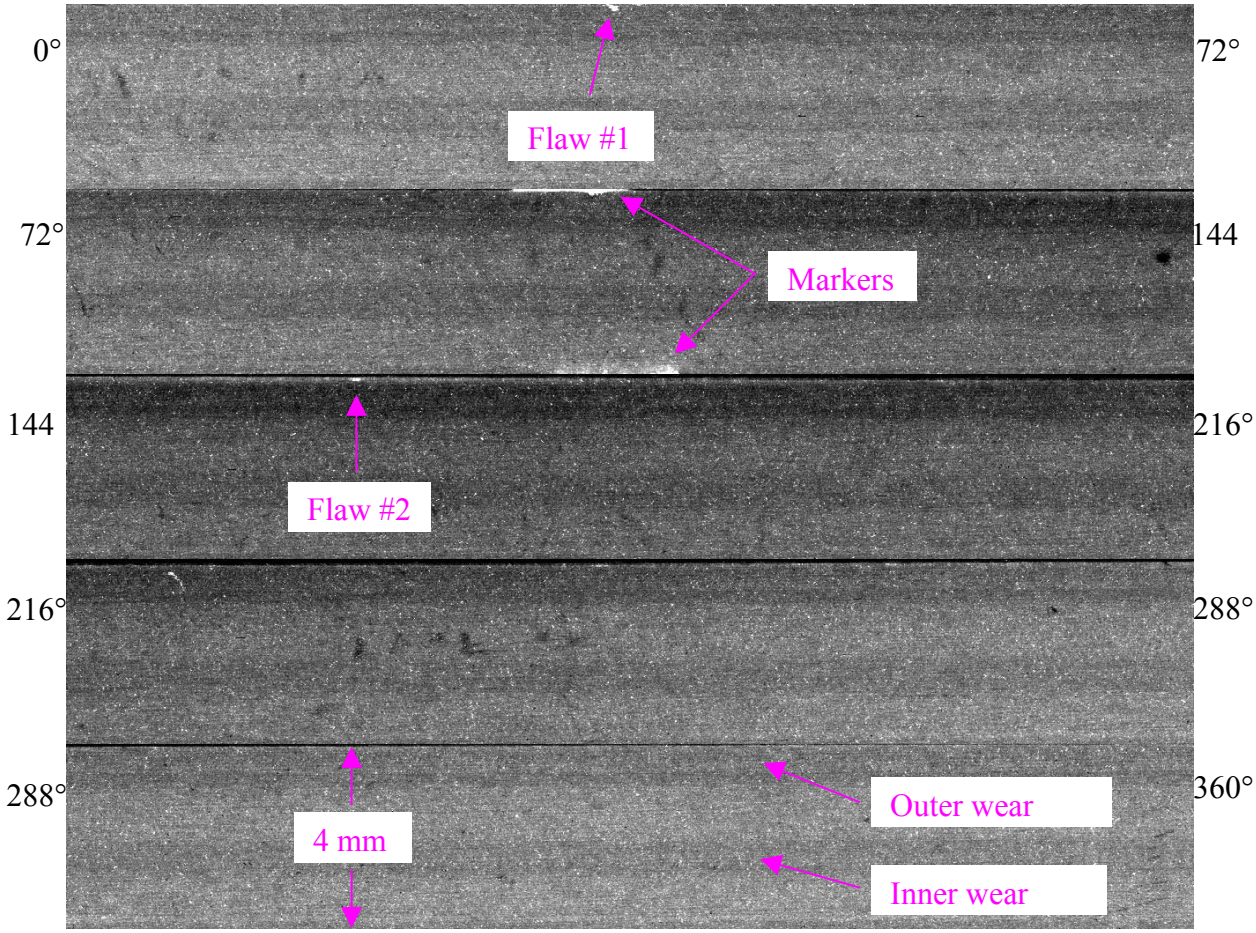

Fig. 6. Laser-scattering image of the contact surface of valve 277; 2 flaws (high optical-scattering spots) at the top edge and 2 wear scars along the entire circumference are indicated.

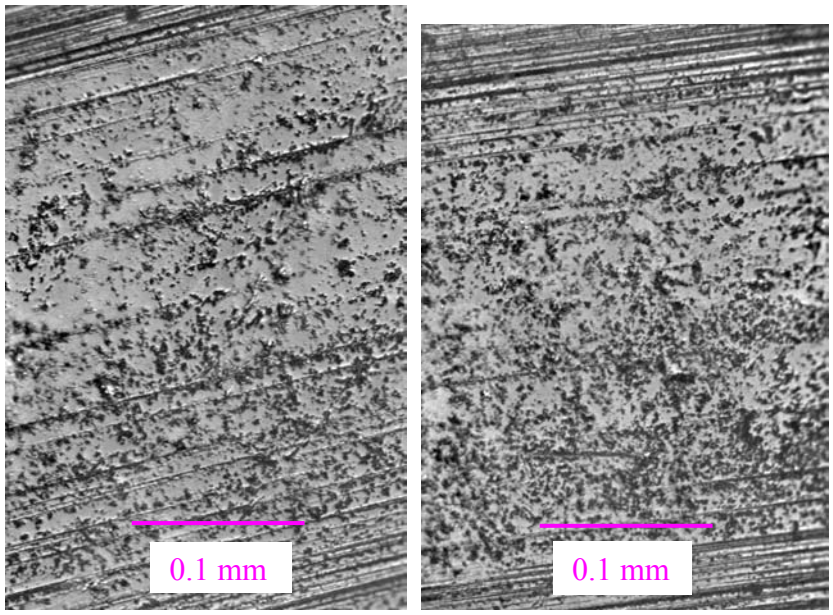

(a) (b)

Fig. 7. Photomicrographs of the outer wear scar (see Fig. 6) at 400X magnification for (a) valve 273 and (b) valve 277.

Durability of Diesel Engine Component Materials

Peter J. Blau
Oak Ridge National Laboratory

John Truhan
University of Tennessee, Knoxville, TN

Jun Qu
ORISE Post-Doctoral Fellow

Objective/Scope

The objective of this effort is to enable the development of more durable, low-friction moving parts in diesel engines for heavy vehicle propulsion systems by conducting friction, lubrication, and wear analyses of advanced materials, surface treatments, and coatings. The scope of materials and coatings is broad and includes any metallic alloy, intermetallic compound, ceramic, or composite material which is likely to be best-suited for the given application. Parts of current interest include scuffing-critical components, like fuel injector plungers and EGR waste gate components. Bench-scale simulations of the rubbing conditions in diesel engine environments are used to study the accumulation of surface damage, and to correlate this behavior with the properties and compositions of the surface species. The effects of mechanical, thermal, and chemical factors on scuffing and reciprocating sliding wear are being determined. Results will be used to refine material selection methodology and to suggest materials for durability-critical engine components.

Technical Highlights

Progress has been made in two areas of this project: (a) methodology to detect of the early stages of scuffing, and the (b) characterization and testing of cermet materials for scuffing-critical applications. These are complementary areas since the development of (a) enables (b).

Localized Scuffing Detection of the Onset of Scuffing in Laboratory Tests.

The current report describes reciprocating, pin-on-twin pin tests conducted using 50 N load, 5 Hz reciprocating frequency, 10 mm stroke, and in low sulfur Jet A aviation fuel. The two friction coefficient-time traces shown in Fig. 1 compare the frictional behavior of self-mated, E52100 bearing steel specimens in annealed and hardened conditions. Even though there were indications of scuffing on the wear scar on one of the hardened steel test pins, no obvious changes were observed on its friction trace (Fig. 1). The inability of chart recorder records to detect the subtle precursors to scuffing suggests that more detailed information was needed. Therefore, a LabView-based digital data acquisition system was used to capture the friction response instead. The sampling rate was set to 100 readings/cycle (500 readings/s).

Friction traces for individual cycles of oscillation were sampled at a series of sliding intervals up to 60 m for both the annealed [Fig 2 (a)] and hardened [Fig. 2 (b)] bearing steel. Note that the friction coefficient is not really negative, but merely reflects the sliding direction during oscillation. The difference between the friction force profiles captured at each sliding distance and that of the first cycle is shown by the thicker line, which lies close the horizontal mid-line in Fig. 2. That difference seems to be a good indicator for detecting the onset of localized scuffing.

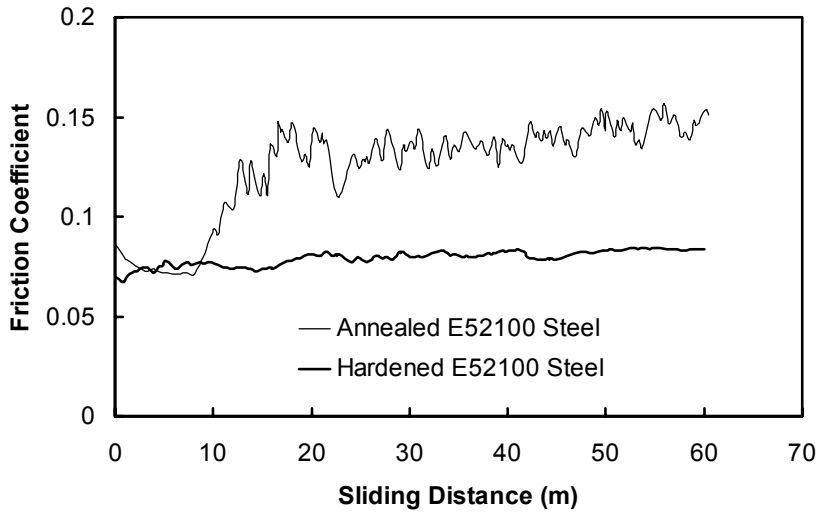

Figure 1. Chart recorder friction traces of annealed and hardened E52100 steel.

In the current work, the sinusoidally-oscillating sliding velocity varied between 0 (at the stroke ends) and 0.157 m/s (at the stroke midpoint). Since the friction coefficient was in the range of 0.05 ~ 0.2, the tribosystem was effectively operating in either the mixed or boundary lubrication regime. According to the basic concepts of liquid lubrication developed by Stribeck [1,2], a lower velocity causes a thinner lubrication film to form and gives a higher friction coefficient that makes scuffing more likely. The data in Fig. 2 follow this Stribeck-like trend. For both annealed and hardened steel, the friction coefficient began to increase at the stroke ends (after sliding 12 m for annealed steel and 18 m for hardened steel). This change indicated the onset of localized scuffing at the stroke ends, and has been verified by scanning electron microscopy.

Although the hardened steel did not resist scuffing too much longer than the annealed steel, its surface damage propagation process was far slower. As shown in Fig. 2(a), the friction coefficient for the self-mated annealed steel soared as soon as localized scuffing occurred. The whole contact length quickly scuffed and the average friction coefficient reached a higher level after sliding 6 m more. However, the friction coefficient of hardened steel grew so slowly that the increase in the friction coefficient was not as noticeable as the change portrayed in Fig. 1.

The effects of load, reciprocating frequency, and lubricant on scuffing initiation and propagation are currently under study and will be discussed in the next quarterly report. A full-length research paper describing the details of these experiments, our observations, and the use of differential friction trace approach to scuffing analysis is being prepared.

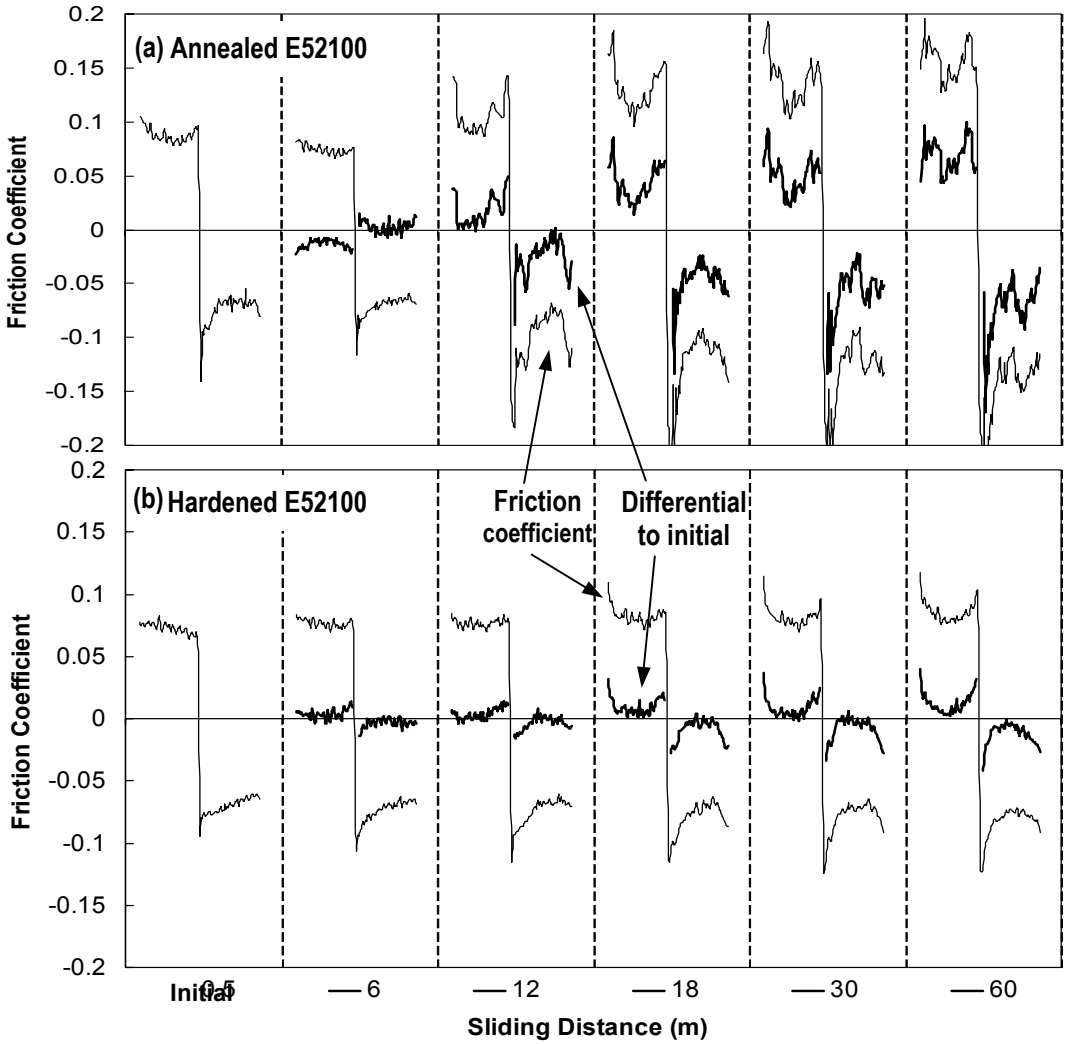

Figure 2. Comparison of the frictional responses of the two steel couples, including within the plot a line that represents the difference between each recorded profile and the initial profile.

Cermets for Fuel Injector Plunger Scuffing.

During this quarter, two new, intermetallic composite materials (cermets) based on Ni_3Al and TiC were obtained. One, designated C-10, was obtained from T. N. Tiegs, ORNL. Called C-10, it was developed under DOE, Heavy Vehicle Program, funding and has a TiC content of 50 vol %. The second cermet, containing 40 vol % TiC in Ni_3Al, was processed by D. Wittmer and his students at Southern Illinois University. Several processing routes were employed, as described by Wittmer in recent quarterly reports. Cermets prepared by two processing conditions were initially examined. One was vacuum, low-pressure hot isostatic pressed (V-LPHIP) at 1450°C, and another more porous version was conventionally sintered (CS) at 1400°C. The C-10 materials were machined for wear testing by E. Shelton, ORNL, a specialist in the preparation of non-conventional, hard materials.

Preliminary characterization of the cermets included optical metallography, Vickers micro-indentation hardness testing, and scratch testing. Microcracking around Vickers indentations (see Fig. 3) revealed the propensity for microfracture both between and within the TiC particles.

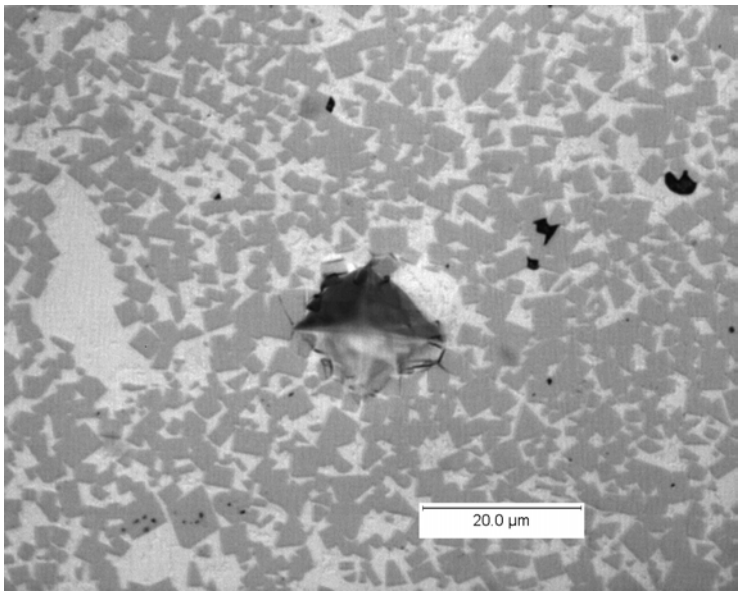

Figure 3. Microfracture and deformation associated with a 200 gr-f Vickers microindentation in the SIU V-LPHIP cermet.

Scratch hardness tests were conducted in accordance with the new standard ASTM G-171 "Standard Test Method for Scratch Hardness Number Using a Diamond Stylus," which ORNL helped to develop. The scratch hardness number (HS) is calculated from the average scratch width at a given load. Results of the hardness and scratch tests are summarized in Table 1.

Table 1. Vickers Microindentation Hardness (HV) and Scratch Hardness (HS)

Material Designation	**Normal Force (gr)**	**HV (GPa)**	**HS (GPa)**
C-10	200	8.8	9.2
	300		12.2
	400		11.9
	500		10.0
V-LPHIP (1450° C)	200	10.5	15.4
	300		10.9
	400		12.1
	500		12.7
CS (1400° C)	200	8.0	

A test matrix is currently being designed to enable comparison of the on-set of scuffing behavior of these new cermets to that of the previously tested bearing steel combinations.

Future Plans

1. Conduct scuffing experiments on candidate materials, including cermets developed under the Propulsion Materials Program and commercial fuel injector plungers coated with TiN.

2. Conduct tests on a new contact configuration, flat on flat, which is designed to better simulate the stresses and type of damage seen in actual plunger components.

Travel

From 3/30/03 to 4/3/03, P.J. Blau, J. Truhan, and J. Qu, attended and presented a poster at the 14th International Conference on Wear of Materials in Washington D.C.

Status of Milestones

1) Evaluate and report on the usefulness of scanning acoustic microscopy for characterizing the extent of subsurface damage arising from high-temperature scuffing. (March 31, 2003 – report in preparation.)

2) Report on the effects of sulfur in the fuel on the scuffing behavior of current and future candidate fuel injection system materials (September 30, 2003).

Publications

1) J. Qu, J. Truhan, P.J. Blau, and R. Ott, 2003, "The Development of a Pin-on-Twin Scuffing Test to Evaluate Materials for Heavy Duty Diesel Fuel Injectors," *Lubrication Engineering* (submitted).

2) J. Qu, J. Truhan, P.J. Blau, and R. Ott, 2003, "A Scuffing Test for Heavy Duty Diesel Fuel Injector Materials," poster presentation at the 14th International Conference on Wear of Materials, Washington D.C., Mar. 30 – Apr. 3, 2003.

Numbered References

(1) R. Stribeck (1902) "Die Wesentlichen Eigneschaften der Gleit- und Rollenlager," *Z. Verein. Deut. Ing.*, 46 (38), pp. 1341-1348; (39) 1463-1470.

(2) P. J. Blau (1995) *Friction Science and Technology*, Marcel Dekker, Inc.

(3) J. Qu, J. Truhan, P.J. Blau, and R. Ott (2003) "A Scuffing Test for Heavy Duty Diesel Fuel Injector Materials," Poster No. 41, 14th International Conference on Wear of Materials, Washington D.C., Mar. 30 – Apr. 3, 2003.

Life Prediction of Diesel Engine Components

H. T. Lin, T. P. Kirkland, A. A. Wereszczak, M. K. Ferber
Oak Ridge National laboratory
and
M. J. Andrews
Caterpillar Inc.

Objective/Scope

The valid prediction of mechanical reliability and service life is a prerequisite for the successful implementation of structural ceramics and advanced intermetallic alloys as internal combustion engine components. There are three primary goals of this research project which contribute toward that implementation: the generation of mechanical engineering data from ambient to high temperatures of candidate structural ceramics and intermetallic alloys; the microstructural characterization of failure phenomena in these ceramics and alloys and components fabricated from them; and the application and verification of probabilistic life prediction methods using diesel engine components as test cases. For all three stages, results are provided to both the material suppliers and component end-users.

The systematic study of candidate structural ceramics (primarily silicon nitride) for internal combustion engine components is undertaken as a function of temperature (< 1200°C), environment, time, and machining conditions. Properties such as strength and fatigue will be characterized via flexure and rotary bend testing.

The second goal of the program is to characterize the evolution and role of damage mechanisms, and changes in microstructure linked to the ceramic's mechanical performance, at representative engine component service conditions. These will be examined using several analytical techniques including optical and scanning electron microscopy. Specifically, several microstructural aspects of failure will be characterized:

(1) strength-limiting flaw-type identification;
(2) edge, surface, and volume effects on strength and fatigue size-scaling
(3) changes in failure mechanism as a function of temperature;
(4) the nature of slow crack growth; and
(5) what role residual stresses may have in these processes.

Lastly, numerical probabilistic models (i.e., life prediction codes) will be used in conjunction with the generated strength and fatigue data to predict the failure probability and reliability of complex-shaped components subjected to mechanical loading, such as a silicon nitride diesel engine valve. The predicted results will then be compared to actual component performance measured experimentally or from field service data. As a consequence of these efforts, the data generated in this program will not only provide a critically needed base for component utilization in internal combustion engines, but will also facilitate the maturation of candidate ceramic materials and a design algorithm for ceramic components subjected to mechanical loading in general.

Technical Highlights

Studies of dynamic fatigue behavior in four-point bending for a commercial grade silicon nitride (SN147-31N, Ceradyne Advanced Ceramic Operation, Inc., CA) were continued during this reporting period. This is part of the program efforts extending the database generation to other potential candidate silicon nitride ceramics especially manufactured by the domestic material suppliers. The database generated will be used for life prediction for exhaust valve components and be compared to those previously generated for Kyocera SN235 and SN235P silicon nitride. Note that Kyocera silicon nitride has been down-selected for valve component applications by Caterpillar. The SN147-31N silicon nitride bend bars were transversely machined based per ASTM C116 standard. The data generated for specimens transversely machined will be more representative for the case of exhaust valve components. The dynamic fatigue tests were carried out at 20 and 850°C and at stressing rate of 30 and 0.003 MPa/s in air per ASTM C1465.

Results of dynamic fatigue tests at 20 and 850°C showed that the SN147-31N transversely machined exhibited inert characteristic strengths, which were about 14-19% lower than those obtained for the longitudinally machined specimens (Table 1, and Fig. 1 and 2), similar to results reported for the cases of SN235 and SN235P silicon nitride. Also, SN147-31N revealed comparable strength values to SN235P under the same test conditions. In addition, there were minor differences in Weibull moduli between longitudinally and transversely machined SN147-31N specimens. The obtained Weibull moduli were also comparable to those reported for SN235 and SN235P under the same test conditions. On the other hand, the strength versus stressing rate curves showed that the SN147-31N exhibited high fatigue exponents (N ~ 132 and 343) at 850°C, independent upon the machining orientation (Fig. 3). However, a permanent curvature was observed for those SN147-31N bend bars after testing at 850°C and 0.003 MPa/s, indicative of onset of slow crack growth and/or creep process presumably due to the softening of secondary glassy phase. Therefore, dynamic fatigue results suggest that the application limit of SN147-31N silicon nitride will be < 800°C in air. A different grade of silicon nitride, i.e., SN147-31E, also manufactured by Ceradyne with a crystalline secondary phase has been acquired for the mechanical properties evaluation under the same test matrix. It is anticipated that SN147-31E would exhibit a higher temperature mechanical reliability than SN147-31N due to the presence of crystalline secondary phase.

Evaluation of mechanical properties of a Ni_3Al alloy, fabricated via extrusion process, after 1000h exposure to a diesel engine exhaust gas environment at 850°C was completed during this reporting period. The Ni_3Al alloy has been considered as one of the candidate advanced intermetallic alloys for exhaust valve applications. The room temperature results showed that the Ni_3Al alloy exhibited no strength degradation after 1000h exposure, indicative of excellent mechanical reliability in exhaust gas environment (Fig. 4). SEM examination of fracture surfaces of exposed bend bars showed the presence of Al_2O_3 oxide scale (~ 10 μm thick) on the surface due to the oxidation of Ni_3Al (Fig. 5). However, EDAX analysis showed no elements from exhaust gas was detected in the bulk region right underneath the oxide scale, suggestive of good long-term chemical stability. Study of effect of long-term oil immersion test at 850°C in air will be also carried out to further confirm the mechanical reliability and chemical stability of Ni_3Al alloy

<u>Status of Milestones</u>

Milestone: "Complete testing and analysis of prototype silicon nitride valves after bench rig testing" was on schedule.

Communications / Visitors / Travel

Update of the status of modification of rotary bending fatigue test rig for testing TiAl alloy was held with Jesus Chapa-Cabrera at Caterpillar

Received tensile test specimens of as-machined TiAl alloy from Jesus Chapa-Cabrera at Caterpillar for mechanical properties evaluation.

Update of the dynamic fatigue test results of Ceradyne SN147-31N silicon nitride with M. J. Andrews at Caterpillar.

Update of the room temperature test results of Ni_3Al alloy with M. J. Andrews at Caterpillar.

Problems Encountered

None.

Publications

None.

References

[1] H. T. Lin, T. P. Kirkland, M. K. Ferber, and M. J. Andrews, "Life Prediction of Diesel Engine Components," Heavy Vehicle Propulsion System Materials Program Bimonthly Technical Progress Report to DOE Office of Transportation Technologies, Jan. – March 2001.

Table 1. Summary of uncensored Weibull and strength distributions for Ceradyne SN147-31N silicon nitride specimens transversely machined per ASTM C1161. Data of Kyocera SN235/SN235P also machined transversely and SN147-31N machined longitudinally are used for reference.

Material	# of Spmns. Tested	Stressing Rate (MPa/s)	Temp. (°C)	Uncens. Weibull Modulus	± 95% Uncens. Weibull Modulus	Uncens. Chrctstic Strength (MPa)	± 95% Uncens. Chrctstic Strength (MPa)
SN235	15	30	20	23.8	15.4, 33.9	901	879, 923
SN235P	15	30	20	38.1	24.0 55.8	666	656, 676
SN147-31N*	15	30	20	21.73	14.07. 31.09	836	814, 858
SN147-31N*	15	0.003	20	20.70	13.38, 29.67	694	675, 713
SN147-31N	15	30	20	13.76	8.96, 19.59	677	649, 705
SN235	15	30	850	26.7	18.0, 36.7	777	760, 793
SN235P	15	30	850	19.3	12.5, 27.6	631	612, 649
SN147-31N*	15	30	850	20.35	13.58, 28.20	777	755, 799
SN147-31N	15	30	850	18.26	11.67, 26.47	639	619, 659
SN235	14	0.003	850	18.5	11.8, 26.8	744	720, 767
SN235P	15	0.003	850	18.2	11.5, 26.8	594	575, 612
SN147-31N*	15	0.003	850	16.19	10.57, 23.02	732	706, 757
SN147-31N	15	0.003	850	19.95	12.83, 28.63	620	602, 638

* Specimens were longitudinally machined.

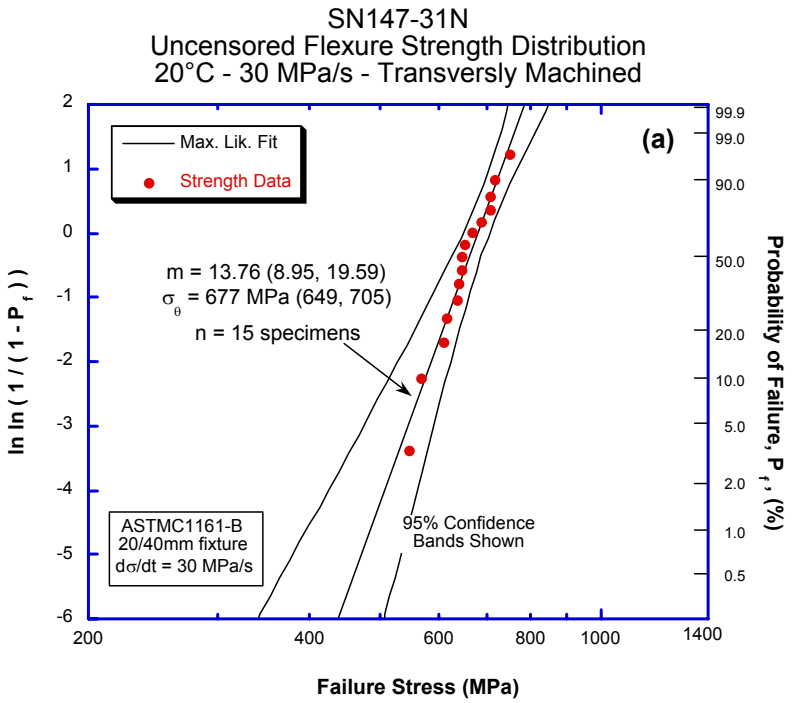

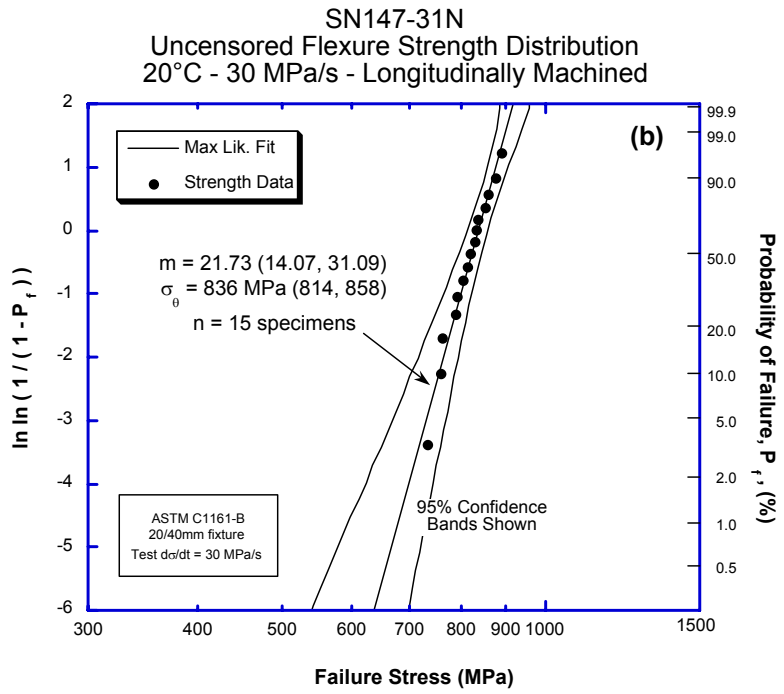

Figure 1. Strength distribution of Ceradyne SN147-31N transversely machined and tested at 20°C and at 30 MPa/s. Note that the result of SN147-31N longitudinally machined is used as a reference.

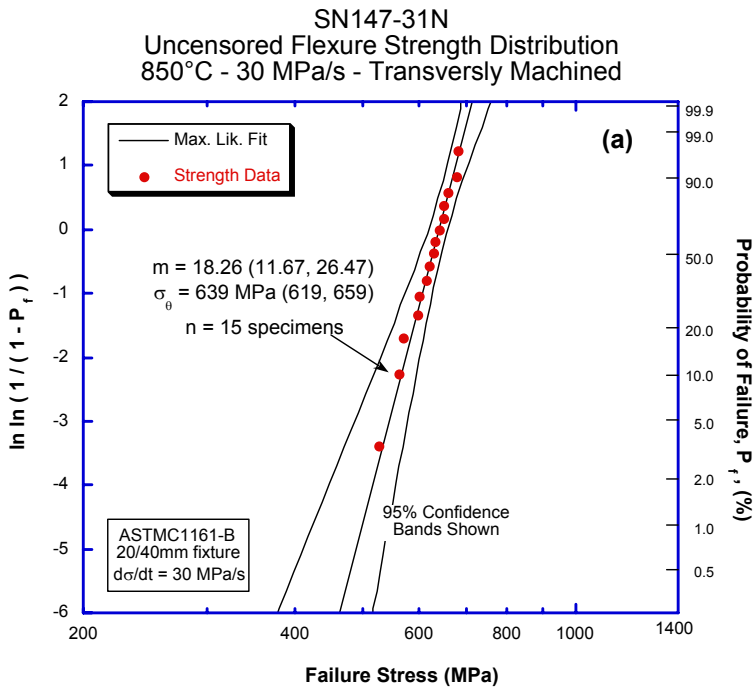

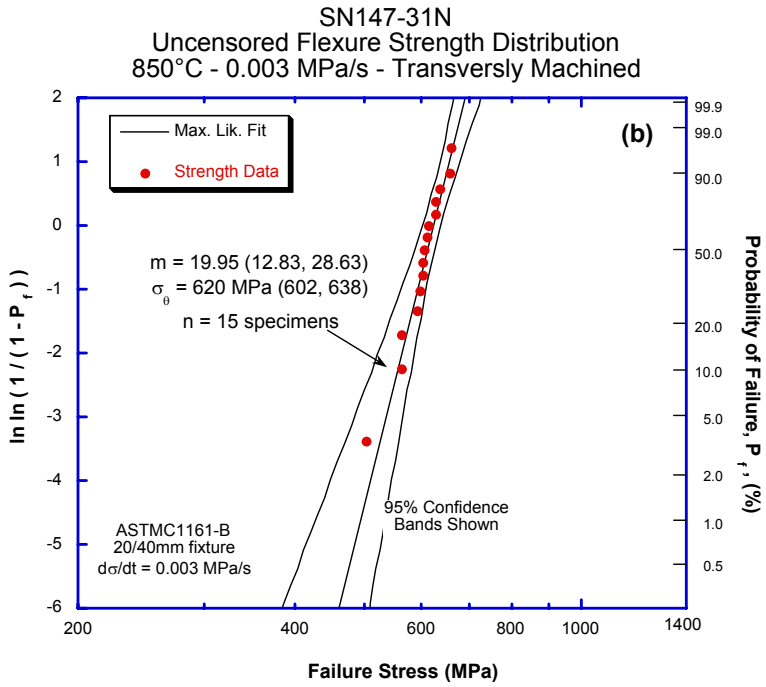

Figure 2. Strength distribution of Ceradyne SN147-31N transversely machined and tested at 850°C and at (a) 30 MPa/s and (b) 0.003 MPa/s.

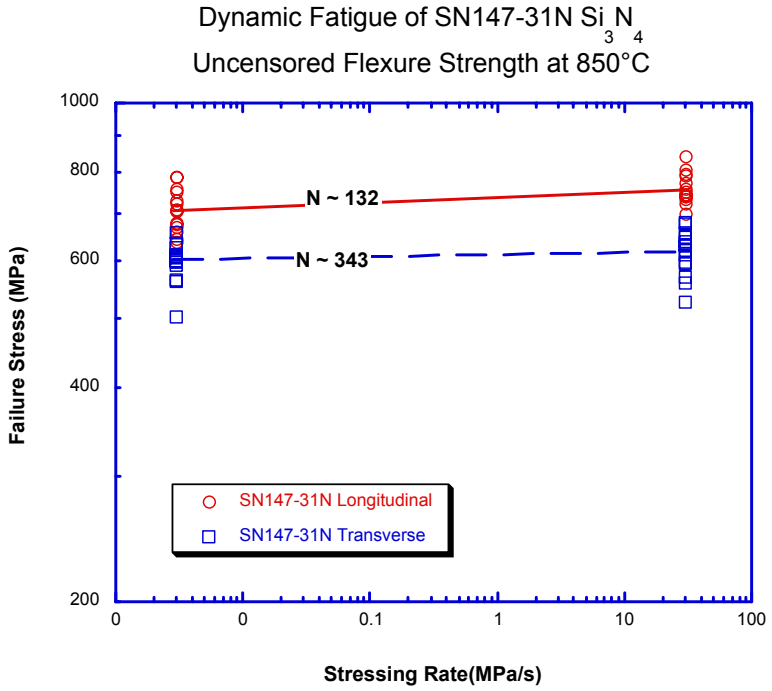

Figure 3. Strength versus stressing rate curves of SN147-31N silicon nitride transversely machined. Data from specimens longitudinally machined are used for reference.

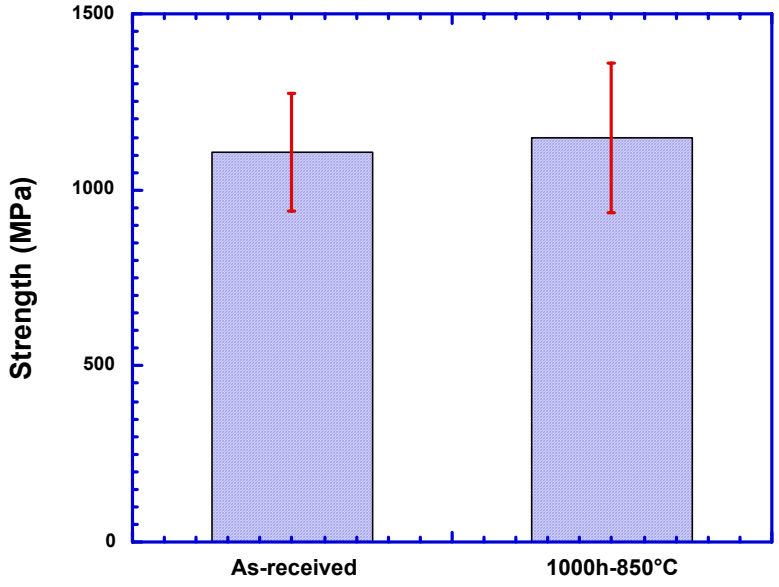

Figure 4. Flexural strength of Ni_3Al alloy in an as-received and after 1000 h exposure condition.

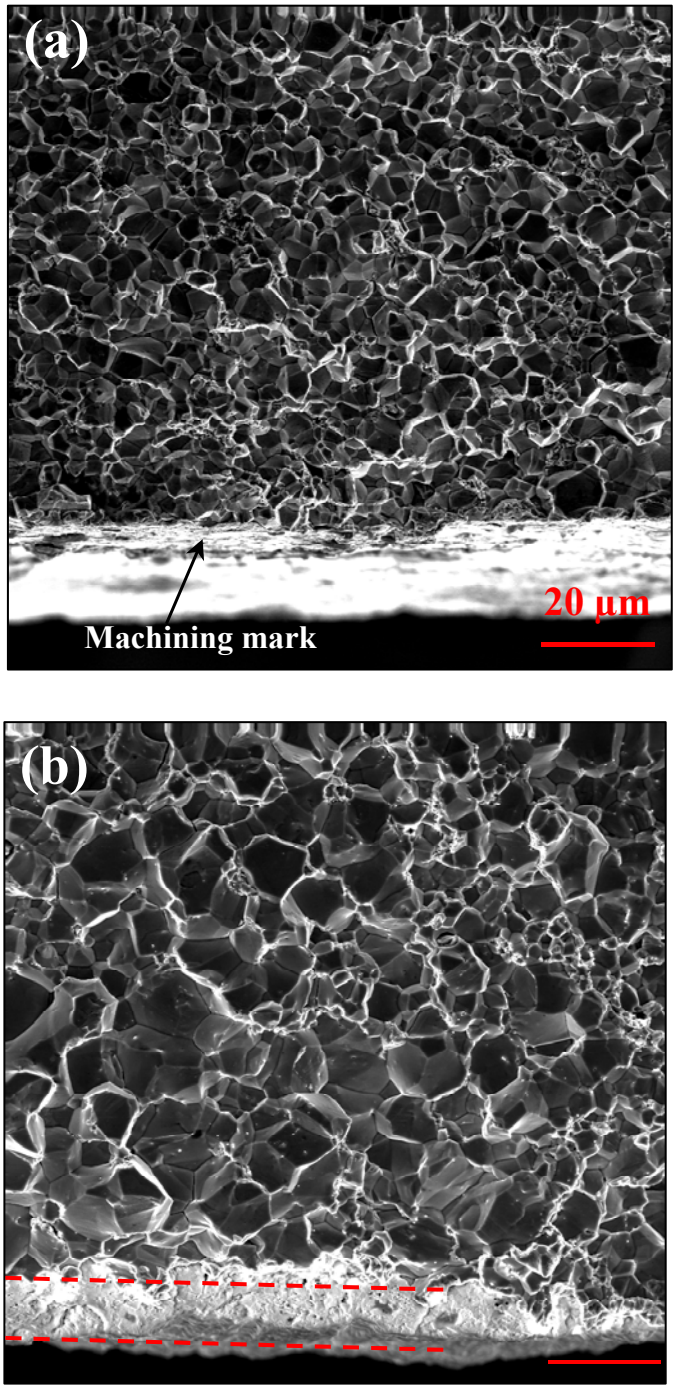

Figure 5. Scanning electron microscopy of fracture surfaces of Ni_3Al alloy before (a) and after (b) 1000 h exposure to exhaust gas at 850°C.

Diesel Exhaust Filter Temperature Measurement and Cost-Effective Machining of Titanium Alloys

Albert Shih
University of Michigan

Objective/Scope

The objective of this research is to develop infrared-based techniques for temperature measurement in diesel exhaust after-treatment filters and to investigate cost-effective machining and joining methods for titanium alloys.

Technical Highlights

1. Overview of Diesel Exhaust Aftertreatment Temperature Measurement

Extensive efforts have been spent this quarter in exploring the capability of low temperature measurement using the PbS/PbSe two-color sensor system. The temperature measurement system, as mentioned in the previous quarterly reports, consisting of the 45° angled sapphire fiber, the PbS/PbSe two color sensor and the data-acquisition system, was set up to be calibrated against a self-made blackbody in low temperature range from 80 to 400°C. The sensor output was used to evaluate the calibration and temperature measurement results. This quarterly report covers temperature measurement strategy, the system calibration and experimental results in a diesel particulate filter. The schematic of the temperature measurement system is shown in Figure 1.

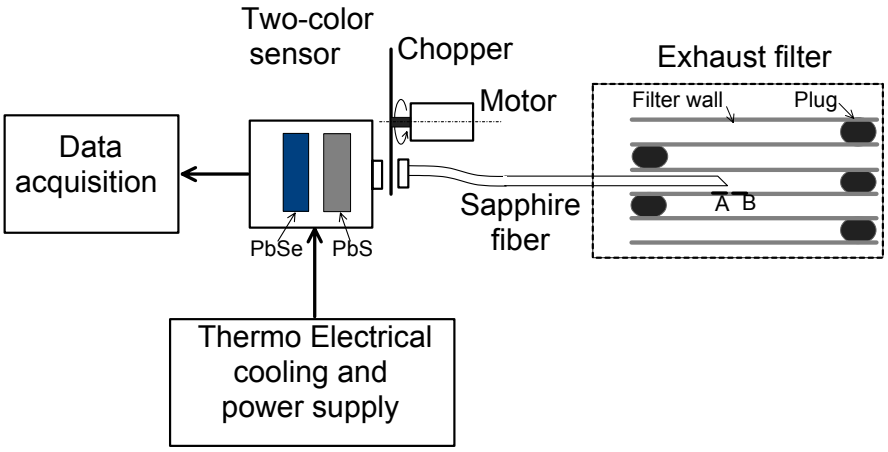

Figure 1. Schematic of the fiber optic temperature measurement system for diesel exhaust aftertreatment filters using a PbS-PbSe two color infrared detector.

Due to the rapid advancement of catalyst, material, and regeneration technologies for diesel exhaust aftertreatment filters, the focus on the temperature profile has been moved from 400 ~ 800°C range down to 100 ~400°C range. The engine turbo out exhaust temperature can vary from 100 to 550°C, depending on engine operating conditions. The exhaust temperature ranging from about 250 to 350°C covers a great number of operating conditions [1]. In light duty applications, for example, the average exhaust temperature during operation of a city bus can be under 200°C [2]. In dense traffic condition of a city bus only 150 ~ 200°C are attained, and

similar situations of low load duty cycles exist in most other applications [1]. The goal of this research is to develop a non-contact temperature measurement method that can cover a wide range of diesel engine operations, from the low-temperature at engine start-up to the high temperature during regeneration.

Newly developed catalytic technology has decreased the regeneration temperature. Catalysts may be applied through catalytic filter coatings, fuel born additives or injection of catalytic and/or reactive species in the exhaust [3]. The advanced filter catalyst technology can lower levels of soot ignition temperature to about 250 to 350°C [2]. The exact temperature for regeneration is not known. This becomes an objective of this research to accurately predict the incipient temperature and duration of chemical reaction during regeneration. The temperature profile within the diesel particulate filter is also of special interest to study the chemical kinetics of the storage and regeneration processes. Using the multi-sensor system, the distribution of temperature in the filter can be measured.

2. Temperature measurement strategy

A wall flow diesel exhaust treatment filter is typically made of porous ceramic material and comprised of parallel channels in which alternate channels are plugged on the entrance face of the filter and the adjacent channels are plugged on the exit face of the filter. As shown in Fig. 1, the filter channels are narrow and deep to increase the specific surface. The length/width ratio of a channel in the filter can be as high as 32. In addition, the diffuse filter wall surface can be characterized when considering the filter material structure and manufacturing process. Though the temperature gradient may occur across the channel depth, the close-to-unity emissivity surface property (blackbody assumption) in the channel cavity can be practically applied with reasonable accuracy. Using this assumption, one-color thermometry method can be used for the temperature measurement.

The optical fiber will work in a strenuous operating condition in the filter with different levels of exhaust gas flow through under different engine operating conditions. Varying amounts of diesel exhaust soot may obscure the fiber's field of view. The filter surface condition also varies due to the different levels of loading of soot and NO_x. In this case, the two-color thermometry method is less affected by the changing conditions and will provide a better accuracy of the target temperature as long as the effect in both wavelength regions is roughly about the same.

Both one-color and two-color thermometry methods are investigated in this study for temperature measurement in diesel exhaust filters.

3. System calibration

As shown in Figure 2, the fiber optic system was first calibrated to a blackbody source in the temperature ranging from 80 to 400°C. The blackbody used in the calibration test is composed of an oxidized Inconel tube, heating wires, feedback thermocouples, and insulations. The Inconel tube was heated in three regions by the resistance heating wire. Inside the Inconel tube, the temperature is measured at three locations using the type K thermocouples. The measured temperature is the feedback to three PID controllers, which are used to control the three heating zones to maintain a uniform temperature inside the tube cavity. The intrinsic emissivity of the oxidized Inconel wall is taken as 0.828, as given in the NIST emittance standard [4]. This

resulted in a calculated cavity emissivity of 0.997. The calculation also showed that the integrating effect of the cavity minimizes any error associated with an initial incorrect assumption of the wall emissivity [5].

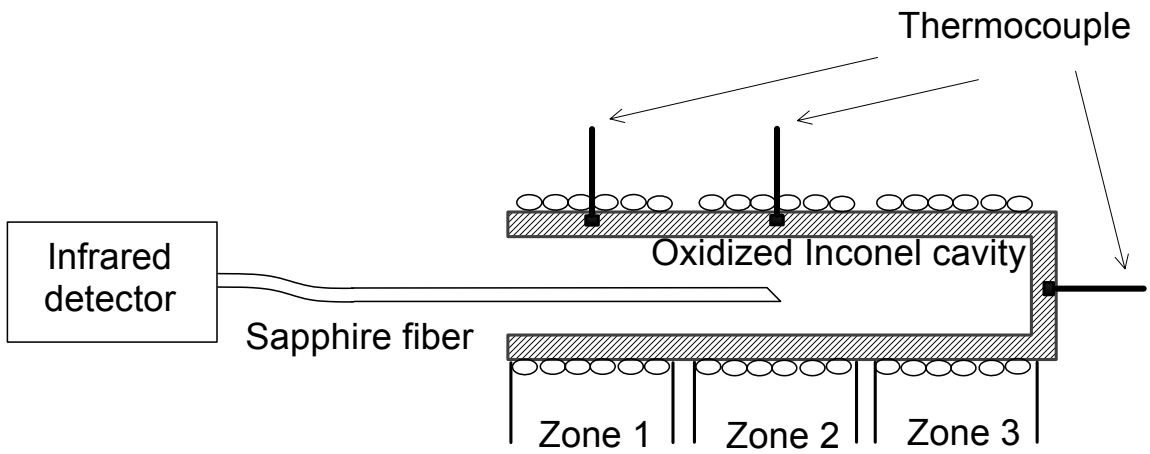

Figure 2. Schematic of calibration of the sapphire fiber and infrared detect system using the blackbody Inconel cavity.

The output signal of the PbS detector was selected as a one-color thermometer output, since the PbS output signal is stronger and the operating wavelength is shorter than that of PbSe. The ratio of the outputs from both the PbS and the PbSe detectors was considered as a two-color thermometer output. After the calibration data was obtained, a polynomial curve was used to fit the data for each output. Results of measurement points and calibration curves are shown in Figure 3. The lowest temperature used in calibration was 80°C. Below 150°C, the system accuracy starts to diminish. To enhance the accuracy, different curves were used to fit the calibration data below and above the temperature limit 150°C for both the one-color and two-color methods.

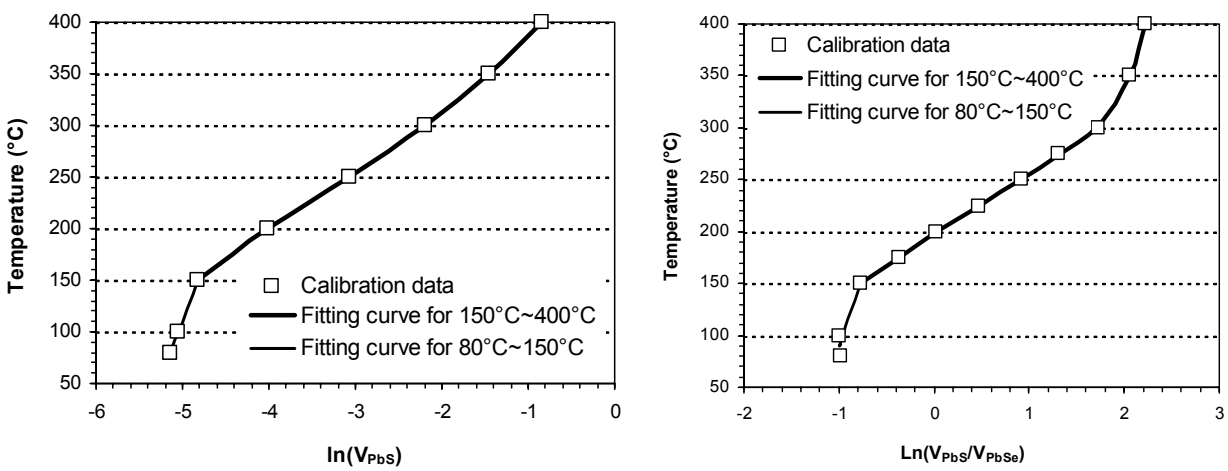

(a) One-color calibration curve (b) Two-color calibration curve

Figure 3. Results of blackbody calibration curves.

4. Discuss and future work

Efforts have also been made to measure the effective intrinsic emissivity of the filter material. The sensor has a wide spectral operating band. The effective intrinsic emissivity is designated as the weight averaged emissivity observed by PbS and PbSe detectors. Using the voltage outputs of viewing the filter surface and the blackbody at the same temperature, the effective intrinsic emissivity can be evaluated by taking the ratio of the PbS and PbSe detector voltage outputs.

The ceramic filter was first heated in a furnace to 900°C and then removed from the furnace and promptly placed in front of the optical fiber with 45° angled tip. A type K thermocouple was placed closed to the region observed by the optical fiber. As shown in Figure 4, the fiber measured the temperature at point C and the thermocouple recorded temperature at point D, close to point C. The transient voltage outputs of both the PbS and PbSe sensors and the temperature of thermocouple are sampled simultaneously using a PC-based data acquisition system. The temperature reported by the thermocouple was referenced as the temperature at which the amount of the filter surface radiance was reported by PbS and PbSe sensor ouput voltages. The voltage outputs were then used to compare with the voltage recorded at the same temperature using blackbody radiance.

The calculated emissivity values were all beyond one, which is against the physical law of thermal radiation. The discrepancy of temperature at region C and D in Figure 4 is identified as the possible cause. Since the filter was set in a room temperature, the surface temperature was rapidly reduced. The thermocouple itself also acts as the heat sink to draw temperature from region C. Therefore, the temperature gradient between C and D cannot be neglected. The temperature at point C was higher than that at point D, which, in turn, caused that the filter surface radiance at a higher temperature. This indicates the setup in Figure 4 for calibration was not successful unless better contact surface temperature measurement method at point C can be developed.

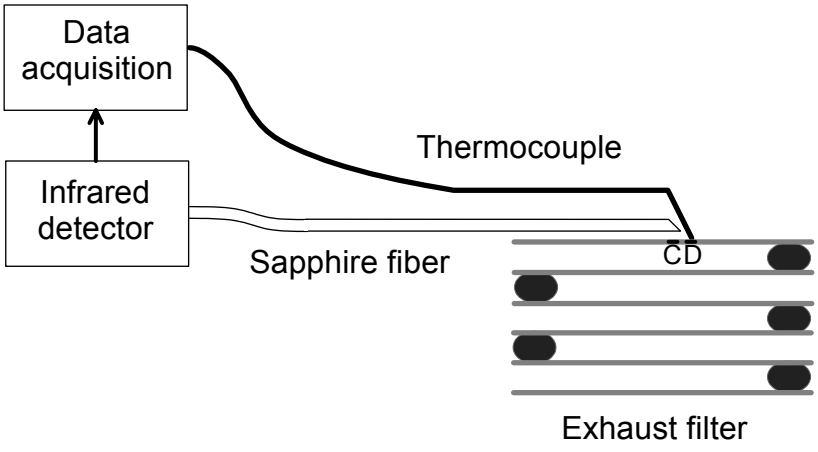

Figure 4. Setup of emissivity test.

The calibration curves presented in Figure 3 will be used to measure the heating history of the temperature in a microwave heated diesel exhaust aftertreatment filter. Initial results indicated that the temperature distribution is not uniform, higher in cavities in the middle of the filter.

Experiments to use silica light-pipe and single color Si-based sensor has also been explored in collaboration with Cummins Technical Center. Test results will be report in the next quarterly report.

Status of Milestones

Milestone 1: Develop a temperature measurement system using sapphire fiber and infrared sensors for diesel exhaust filter.

Status: A fiber optic temperature measurement system consisting of angled sapphire fiber, PbS/PbSe two-color sensor, and DAQ system has been developed. With the 45° angled tip, the sapphire fiber is able to precisely collect the radiation emitted from the internal wall surface of filters. Tests are underway to study the capability to measure temperature below 150°C.

Milestone 2: Establish calibration methods for the infrared temperature measurement system.

Status: Calibration methods have been studied and reported. The system is capable to accurately measure temperature in the range of 150 ~400°C. Study will be conducted to further enhance the low temperature sensing ability of the system down to 100°C level.

Milestone 3: Identify the sensitivity and external noise in infrared temperature measurement.

Status: Nothing to report in this quarter.

Milestone 4: Investigate the cylindrical abrasive waterjet machining of titanium alloys.

Status: Nothing to report in this quarter.

Milestone 5: FEM modeling and setup cutting experiments to evaluate new cutting tools and coatings for machining of titanium alloys

Status: The direction of the titanium machining research has been shifted to the friction stir joining of titanium alloys. Literature search has been planned for summer.

Communications/Visit/Travel

John Kong, the PhD student from NC State Univ., continues working at the Cummins Technical Center in Spring 2003 semester.

Albert Shih visited ORNL in Feb. 21 and April 22 to update the progress on the project. Albert Shih visited Cummins on April 21 to review the progress and continue collaboration of temperature measurement.

Publications

B. J. Boothe, A. J. Shih, J. Kong, W. L. Roberts, 2003, "Goniometric Characteristics of Optical Fibers for Temperature Measurement in Diesel Engine Exhaust Filters," *Measurement Science and Technology,* Vol. 14, No. 5, pp. 563–572.

A.C. Curry, A.J. Shih, R.O. Scattergood, and S.B. McSpadden, 2003, "Grinding Temperature Measurements in MgO PSZ Using Infrared Spectrometry," *J. Am. Ceram. Soc*., Vol. 86, No. 2, pp. 333–341.

References

[1] A. Mayer, T. Lutz, C. Lammle, et. al., 2003, "Engine Intake Throttling for active Regeneration of Diesel Particle Filters," *SAE2003-01-0381*

[2] H. Okazoe, K. Shimizu, Y. Watanabe, et. al., 1996, "Development of a Full-Flow Burner Regeneration Type Diesel Particulate Filter Using SiC Honeycomb," *SAE960130*

[3] A. G. Konstandopoulos, M. Kostoglou, E. Skaperdas, et. al., 2000, "Fundamental Studies of Diesel Particulate Filters: Transient Loading, Regeneration and Aging," *SAE2000-01-1016*

[4] J.C. Richmond, D.P. Dewitt, and w.D. Hayes, 1964, "Procedures for the Precise Determination of thermal Radiation Properties November 1962 to October 1963," *National Bureau of Standards Technical Note 252*, Nov. 20.

[5] R.F. Gansman, 1991, "Using Reflection Measurement to Calculate Emissivity for Improved In-Situ Temperature Measurement in Rapid Thermal Processing," *MS Thesis*, North Carolina State University.

Advanced Cast Austenitic Stainless Steels for High Temperature Components

P. J. Maziasz, R. W. Swindeman, and N. D. Evans
Oak Ridge National Laboratory
and
M. J Pollard
Caterpillar, Inc.

Objective/Scope

The objective of this new CRADA project is commercial scale up of the new modified cast austenitic stainless steels developed by Caterpillar and ORNL as cost-effective high-performance alternatives to the standard SiMo ductile cast iron used for most diesel engine exhaust manifold and turbocharger housing components. Cast austenitic stainless steels can withstand prolonged exposure at temperatures of 750°C or above, and are much stronger than SiMo cast iron above 550-600°C. The new modified stainless steels (CF8C Plus and CN12 Plus) have better aging resistance and ductility after creep that standard commercial grades of the same steels. This would indicate better fatigue and thermal fatigue resistance than commercial cast stainless steels, and much better than SiMo cast iron, and resistance to cracking during the severe thermal cycling that exhaust components experience. This project will provide the more comprehensive properties data needed by designers to qualify these new alloys, and optimize component designs. This new advanced diesel engine CRADA (Cooperative Research and Development Agreement) project (ORNL02-0658) began on July 21,2002, and will last at least three years. More detailed information on this project must be requested directly from Caterpillar, Inc.

Technical Highlights, 2nd Quarter, FY2003

Background

Advanced large diesel engines must have higher fuel efficiency as well as reduced exhaust emissions, without sacrificing durability and reliability. They require exhaust manifolds and turbocharger housings made from materials that can withstand temperatures ranging from 70 to 750°C or higher in a normal duty cycle. Such materials must withstand both prolonged, steady high-temperature exposure as well as more rapid and severe thermal cycling. New technology to reduce emissions and heavier duty cycles will push temperatures in these critical components even higher.

Current diesel exhaust components are made from SiMo ductile cast iron, and higher engine temperatures would push such materials well beyond their current strength and corrosion limits. The previous CRADA produced systematic data comparing cast CN12 stainless steel and SiMo cast iron for such diesel exhaust component applications. The data demonstrated a clear tensile strength advantage of standard CN12 steel above 550-600°C, and even larger advantages in creep strength and fatigue life above 700°C. The previous CRADA project also developed new modified CN12 and modified CF8C steels with better creep strength, and significantly better aging resistance and thermal fatigue resistance than standard CN12. The purpose of this new CRADA project is commercial scale up of these new modified stainless steel heats, and development of the systematic and thorough database required by designers to optimize component design, and to qualify them for trial component production.

Approach

Prior work on lab-scale (15 lb induction melts with argon cover gas) heats of modified CN12 and modified CF8C and screening tests (aging, tensile, creep) at 800-850°C at ORNL provided a composition of each alloy for commercial scale up. High-temperature fatigue testing at Caterpillar Technical Center has identified a significant advantage of the modified CN12 steel. Two commercial stainless steel foundries have produced 500 lb heats of the modified CN12 and modified CF8C steels for testing and evaluation.

Technical Progress

Creep tests of standard CN12 and the modified CF8C (CF8C Plus) at 850°C and 35 MPa ended this quarter. The modified CF8C ruptured after 23,600 h with about 7.8% creep strain, and the test of the standard CN12 was stopped at 15,500 h without failure and less than 1% creep strain. The CF8C Plus had much better creep resistance than standard, commercial CF8C at 850°C, and was comparable to CN12.

Tensile and fatigue testing were completed last quarter, and thermal fatigue testing continued this quarter at Caterpillar. Tensile data on the new commercial scale-up heats of the standard and modified cast stainless steels show that the CF8C Plus is about as strong as the standard and modified CN12 steels, but still has high ductility similar to the standard CF8C steel (Fig. 1). The "engineered microstructure" of the as-cast CF8C Plus steel is also quite different than that of standard CF8C steel (Fig. 2); the CF8C Plus has mainly carbides (NbC and a little $Cr_{23}C_6$) in an austenite parent phase matrix in contrast to the large amounts of □-ferrite found in standard CF8C steel. Achieving this remarkable combination of good strength and ductility at both higher and lower temperatures was an important first step in achieving the best thermal fatigue resistance from the CF8C Plus or CN12 Plus steels. Aging of tensile/fatigue specimens for 1,000 and 10, 000 h at 700-850°C began at ORNL last quarter. Aging to 1000 h was completed this quarter, and the specimens were sent to Caterpillar for tensile and possibly some fatigue testing. Aging to 10, 000 h continues this quarter. Microstructural analysis of aged or creep-tested specimens of the new modified CN12 and modified CF8C steels was nearly completed this quarter.

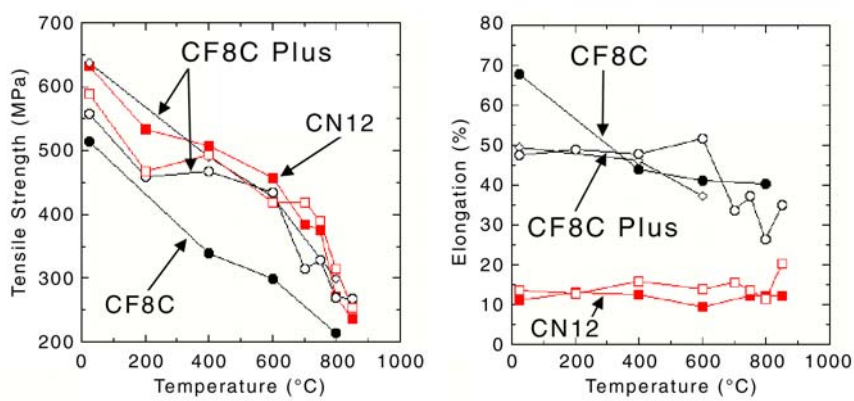

Figure 1 – Tensile properties measured by Caterpillar for the commercial scale-up heats of the new modified CN12 and CF8C stainless steels at room temperature to 850°C in air.

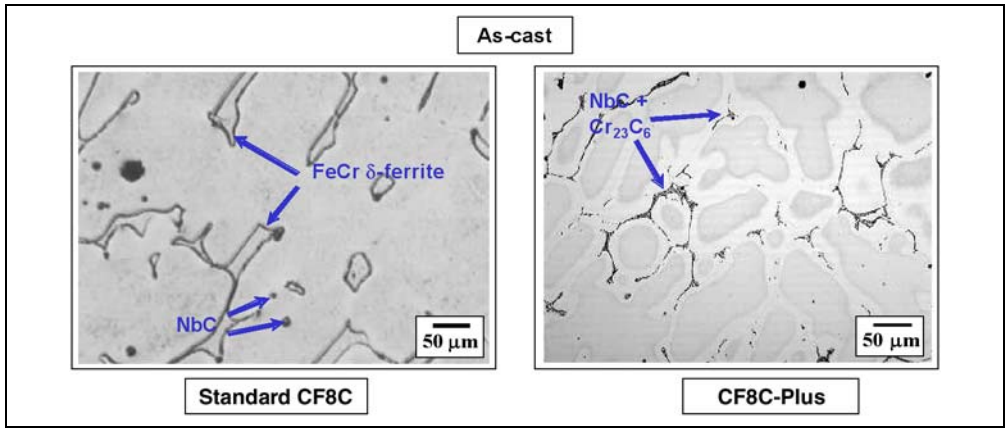

Figure 2 – Optical metallography of as-cast microstructures of standard CF8C and the new CF8C-Plus steels.

Isothermal fatigue testing and data analysis of the new commercial scale-up heats of CF8C Plus and CN12 Plus were completed this quarter at Caterpillar, and data will be given next quarter. Planning for additional heats of the new alloys is underway, including variations in processing to test centrifugal casting as well as static sand casting behavior.

Communications/Visits/Travel

Detailed team communications between ORNL and Caterpillar occur regularly, at least once or twice a week. The new 3 year CRADA began on July 21, 2002, when the previous CRADA ended.

An invention disclosure and patent application on cast austenitic stainless alloys with improved performance were completed by Caterpillar and filed with the U.S. Patent Office in December 2000. It is entitled "Heat and Corrosion Resistant Cast Stainless Steels With Improved High Temperature Strength and Ductility," by P. J. Maziasz (ORNL), T. McGreevy (U. of Bradley/CAT), M. J. Pollard (CAT), C. W. Siebenaler (CAT), and R. W. Swindeman (ORNL). Last quarter, two separate new patent applications were developed and submitted to the U.S. Patent Office, one on the CF8C Plus steel and the other on the CN12 Plus steel.

Status of Milestones

Formal milestones were imbedded in the previous CRADA and in the new CRADA, which is part of the DOE/OFCVT Heavy Vehicle Propulsion Materials Program, but a task in the ORNL FWP. However, all milestones have been achieved on or significantly ahead of schedule.

Publications/Presentations

A final ORNL report for CRADA ORNL99-0533 was prepared last quarter, and was approved this quarter by Caterpillar for unrestricted release, entitled: "Development of Low-Cost Austenitic Stainless Gas-Turbine and Diesel Engine Components With Enhanced High-Temperature Reliability," P. J. Maziasz and R. W. Swindeman, ORNL, P. F. Browning, Solar

Turbines, Inc., and M. E. Frary, M. J. Pollard, C. W. Siebenaler, and T. E. McGreevy, Caterpillar, Inc.

An R&D 100 Award Nomination Package was submitted to R&D Magazine entitled "CF8C-Plus, Cast Stainless Steel for High-Temperature Performance," by ORNL and Caterpillar this quarter.

IN-SITU TEM OBSERVATIONS OF STRAIN-INDUCED INTERFACE INSTABILITY IN TiAl/Ti_3Al LAMINATE COMPOSITE

Luke L. Hsiung
Lawrence Livermore National Laboratory

Objective/Scope

The stability of interfaces in lamellar TiAl (or TiAl/Ti_3Al laminate composite) by straining at ambient temperatures has been investigated using in-situ staining techniques performed in a transmission electron microscope in order to obtain direct evidence to support the previously proposed creep mechanisms in refined lamellar TiAl based upon the interface sliding in association with the cooperative motion of interfacial dislocations. It has been reported previously that the mobility of interfacial dislocations can play a crucial role in the creep deformation behavior of refined lamellar TiAl [1,2]. Since the operation of lattice dislocations within refined α_2 and γ lamellae is largely restricted, the motion of interfacial dislocations becomes the major strain carrier for plasticity. Results of ex-situ TEM investigation have revealed the occurrence of interface sliding in low-stress (*LS*) creep regime and deformation twinning in high-stress (*HS*) creep regime. These results have led us to propose that interface sliding associated with a viscous glide of pre-existing interfacial dislocations is the predominant creep mechanism in *LS* regime and interface-activated deformation twinning in γ lamellae is the predominant creep mechanism in *HS* regime. Stress concentration resulted from the pileup of interfacial dislocations is suggested to be the cause for the interface-activated deformation twinning. Accordingly, the creep resistance of refined lamellar TiAl is considered to depend greatly on the cooperative motion of interfacial dislocations, which in turn may solely be controlled and hindered by the interfacial segregation of solute atoms (such as W) or interfacial precipitation. Furthermore, through the in-situ TEM investigation, we also found that the lamellar interfaces could migrate directly through the cooperative motion of interfacial dislocations. That is, the γ/γ and γ/α_2 interfaces can migrate through interface sliding and lead to the coalescence or shrinkage of constituent lamellae (i.e. microstructural instability), which results in a weakening effect when refined lamellar TiAl is employed for engineering applications. Although it is anticipated that interface sliding and migration are prevalent at elevated temperatures, the present in-situ straining study reveals the instability of lamellar interfaces at ambient temperatures.

Technical Highlights

Refined lamellar TiAl with a nominal composition of Ti-47A1-2Cr-lNb-lTa (at.%) was used for this investigation. Interfacial substructures were examined using JEOL-200CX transmission electron microscope. Dislocation structure and the core structure of interfacial dislocations were also examined using weak-beam dark field (WBDF) and high-resolution (HRTEM) imaging techniques. To investigate strain-induced interface sliding, an in-situ straining experiment was performed at room temperature in a JEOL-200CX transmission electron microscope using a single-tilt straining holder. A gear-drive translation mechanism was activated through the foot pedals with the deformation rate controlled by the speed of y-axis tilt. Plastic deformation took place and was recorded right after a short period of time in which elastic deformation was first distinguished from the motion of bend extinction contours. A hi-8 videocassette recorder attached to a TV rate camera in the microscope was used to record the straining events (e.g., dislocation motion/interaction, interface migration). After completing the experiment, video images of special interest were printed out for analysis.

Interfacial substructures

There are in general two types of lamellar interfaces within $TiAl/Ti_3Al$ laminate composite, i.e. (1) the γ/α_2 interphase interface which has an orientation relationship: $(0001)_{\alpha 2} \parallel (111)_\gamma$ and $\langle 11\bar{2}0\rangle_{\alpha 2} \parallel \langle 1\bar{1}0\rangle_\gamma$, and (2) the γ/γ interfaces which include true twin, pseudo twin, and order-fault interfaces. Types (2) interface is also referred as twin-related interfaces hereafter. A typical TEM observation of lamellar interfaces viewed from the $[011]_\gamma$ edge-on orientation is shown in Fig. 1. Notice that interfacial dislocations (IDs hereafter) can be found in both γ/γ and γ/α_2 interfaces. Figure 1(b) was imaged with a tilting angle of ~15° from Fig. 1(a). Several dislocation tips (appeared as white dots) in Fig. 1(a), and the corresponding dislocation lines appeared in Fig. 1(b) are marked by arrows. In general, the dislocation density in γ/α_2 interphase interfaces is higher than that in γ/γ twin-related interfaces as a result of a greater lattice and thermal misfit between γ and α_2 lamellae. The core of each ID in γ/α_2 interface contains a small step (ledge) with the step height two layer thickness of the $(111)_\gamma$ plane (d_{111} = 0.232 nm) is shown in Fig. 2(b), which is consistent with the observations reported elsewhere in literature. Accordingly, if an ID moves along the interface, the step moves along with the dislocation and thus, the interface is displaced (advanced) perpendicular to its plane, i.e. the interface will migrate by the distance of a step-height. Therefore, the cooperative motion of IDs will always cause a combination of interface sliding and interface migration as illustrated schematically in Fig. 2(c). Since the Burgers vector ($b = 1/6\langle\bar{1}\bar{1}2\rangle$) of IDs is parallel to the $(111)_\gamma$ plane, the dislocations need only to glide to cause the interface to slide. Similar properties are also true for γ/γ interfaces, and a small step is associated with the core of each ID ($b = 1/6[\bar{1}\bar{1}2]$) in γ/γ interface with the step height one layer spacing of the $(111)_\gamma$ plane [Fig. 3(a)]. The IDs in γ/γ_T true-twin interface compensate a small angle departure of the γ/γ_T interface plane from the exact (111) twin plane, which is schematically illustrated in Fig. 3 (a). The inclination angle (θ) of the interface plane to the exact twin plane is therefore given by

$$\tan\theta = \frac{\boldsymbol{h}}{\boldsymbol{s}} \qquad (1)$$

where $\boldsymbol{h}$ is the step height, and $\boldsymbol{s}$ is the average spacing of IDs. Accordingly, as illustrated in Figs. 2(b) and 3(b), it is anticipated that the cooperative motion of interfacial (Shockley partial) dislocations can result in the migration of lamellar interfaces, and thereby lead to the coalescence/shrinkage of the constituent lamellae. The migration rate ($\boldsymbol{v_i}$) of an interface can be expressed as

$$\boldsymbol{v_i} = \boldsymbol{\rho v_d h} \qquad (2)$$

where $\boldsymbol{\rho}$ is the dislocation density, $\boldsymbol{v_d}$ the dislocation velocity, and $\boldsymbol{h}$ the step height.

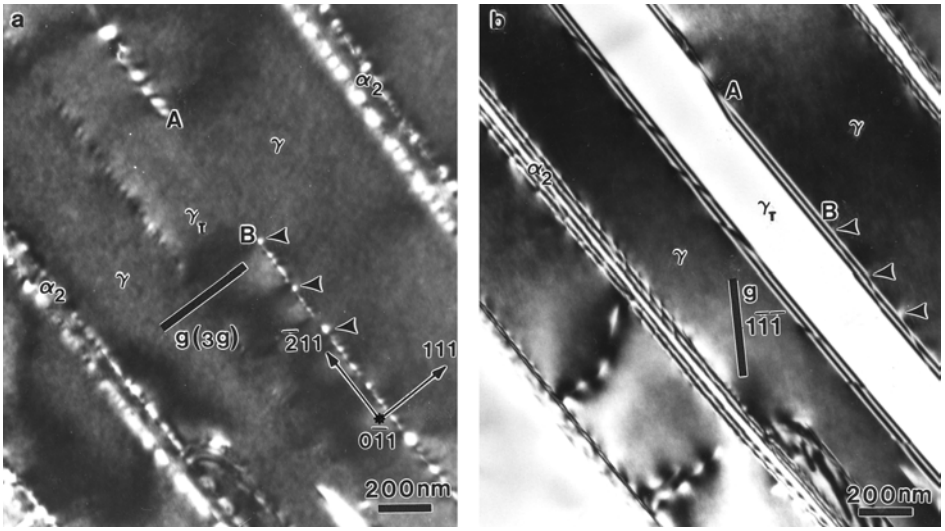

Fig. 1 (a) A WBDF TEM image showing a typical edge-on lamellar structure consisting of γ, γ_T and α_2 lamellae within an as-fabricated alloy sample, Z (zone axis) = $[0\bar{1}1]_\gamma$. (b) A bright-field TEM image showing the existence of interfacial dislocations in both γ/α_2 and γ/γ_T interfaces, Z = $[1\,\bar{2}\,1]_\gamma$.

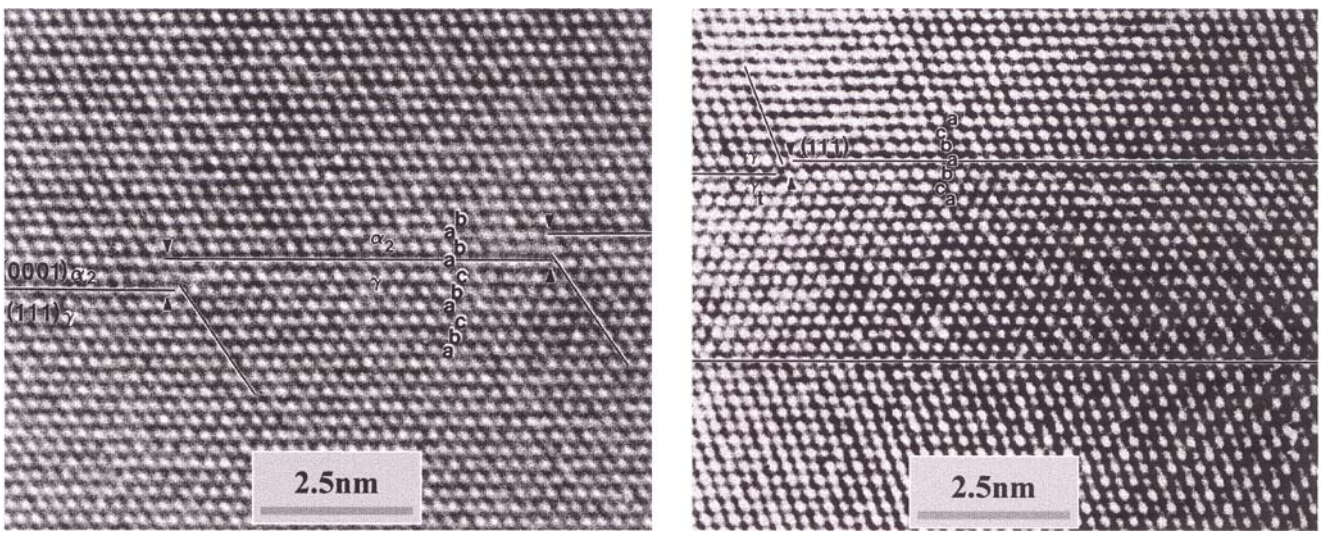

(a) (b)

Fig. 2. HRTEM images showing the core structure of interfacial dislocations in (a) γ/α_2 and (b) γ/γ_T interfaces. The letters **abab** and **abcabc** stand for the stacking sequence of α_2 and γ lamellae, respectively.

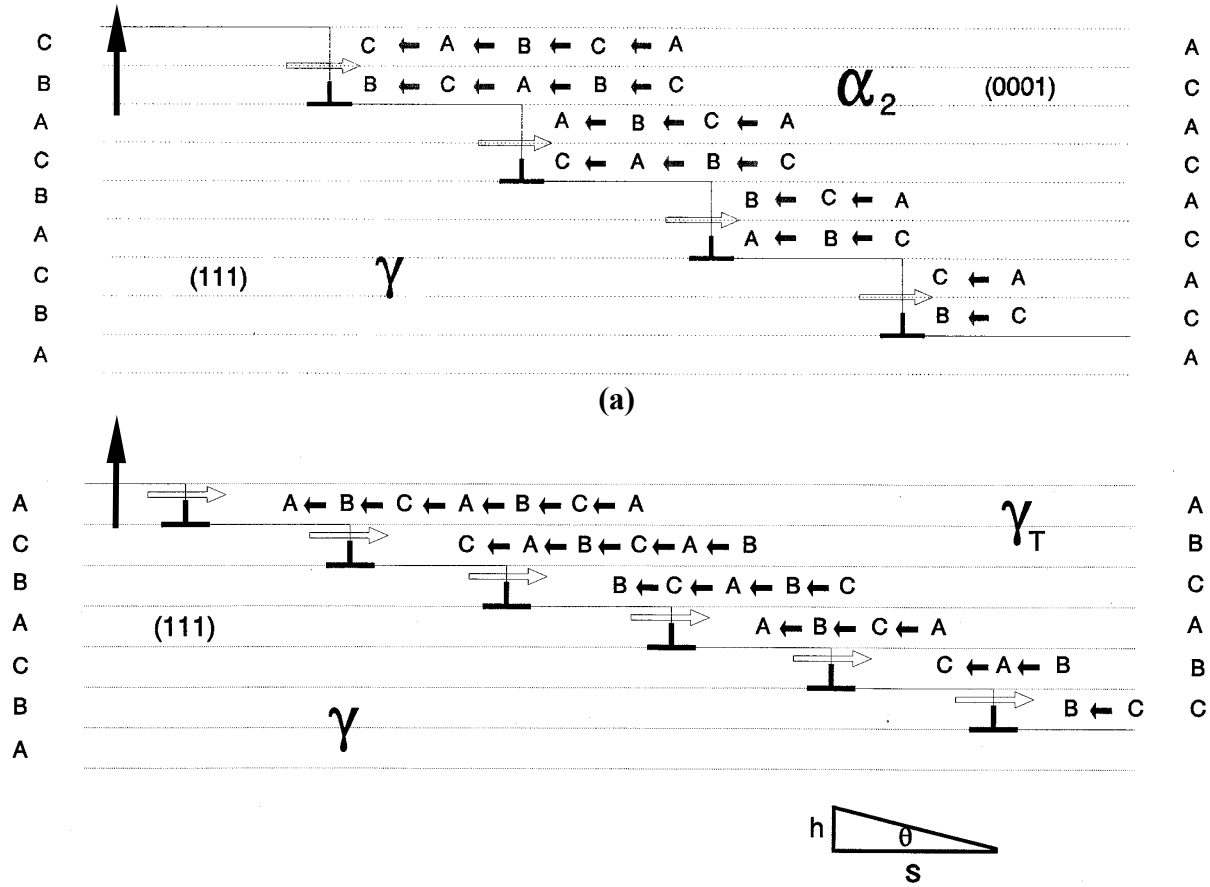

Fig. 3. Schematic illustrations of (a) an array of interfacial (Shockley partial) dislocations forming a glissile α_2/γ interface and (b) an array of interfacial (Shockley partial) dislocations in a glissile γ/γ_T interface. Both interfaces can be migrated by the cooperative motion of the interfacial dislocations. The letters **ACAC** and **ABC** stand for the stacking sequence of α_2-lamella and γ-lamella, respectively. The direction of interface migration is indicated by ↑.

In-situ observations of interface sliding and migration

A direct observation of interface sliding and migration has been obtained from an in-situ straining experiment. Throughout the in-situ straining experiment (conducted at room temperature), the motion of IDs was mainly observed in γ/γ twin-related interfaces. This indicates that the mobility of IDs in γ/α_2 interface is much lower than that of IDs in γ/γ twin-related interfaces at room temperature. Typical video images recorded from the in-situ straining experiment for the motion of IDs in a pair of edge-on twin interfaces are demonstrated in Figs. 4 (a) and (b), in which the identical IDs are marked by arrows. It is seen that dislocations in the left interfaces moved cooperatively about 17 nm downward after 11 seconds, while those in the right interfaces moved cooperatively about an equal distance upward. The average dislocation velocity (v_d) is estimated to be 1.5 nm/s. With a known dislocation density at the interface ($\rho \sim 0.033$ nm^{-1}), the interface migration rate (v_i) can be evaluated [according to eqn. (2)] to be 0.012 nm/s, which is so slow that the interface migration is not detectable within a short period of time. An in-situ observation of interface migration is demonstrated in Figs. 5(a) – 5(d), in which the images were taken in a region close to a crack tip. The velocity of dislocation motion in a γ/γ twin-related interface was found to be much faster than that shown in Fig. 4 because of a stress concentration caused by the crack. In fact, the dislocation velocity was so fast that it became difficult to track the motion of each dislocation in the dislocation array.

The twin interface initially migrated with a high rate [Figs. 5(a) and 5(b), v_i ~19 nm/sec (1580 times faster than that in Fig. 4!)], and after 10 second the migration became much slower [Figs. 5(c) and 5(d), v_i ~0.16 nm/sec]. The interface subsequently migrated close to a γ/α_2 interface. This rate change is presumably resulted from the interaction of stress field between γ/γ and γ/α_2 interfaces. Coarsening of the γ lamella occurred as a result of the migration of γ/γ interface.

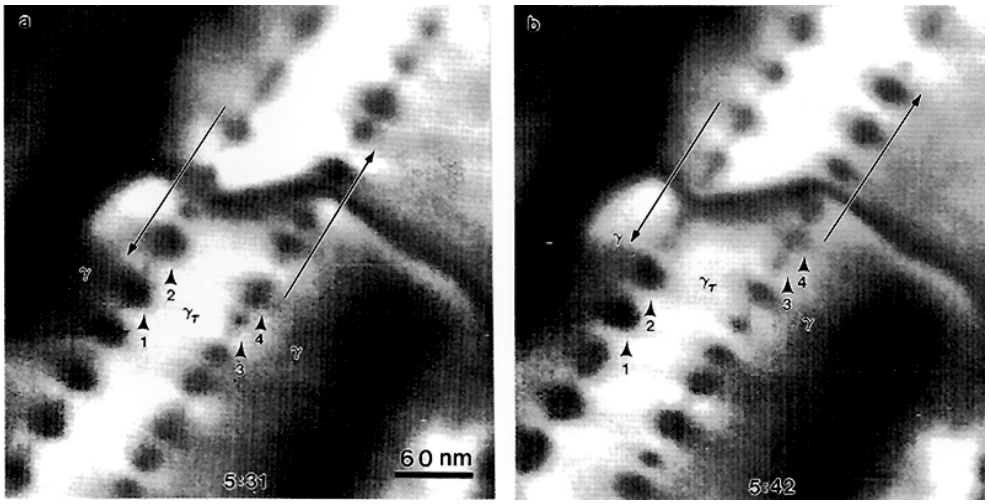

Fig. 4. Two consecutive in-situ video images showing the cooperative motion of interfacial dislocation tips (appeared as black dots) in a pair of γ/γ interfaces; the moving directions are labeled by long arrows.

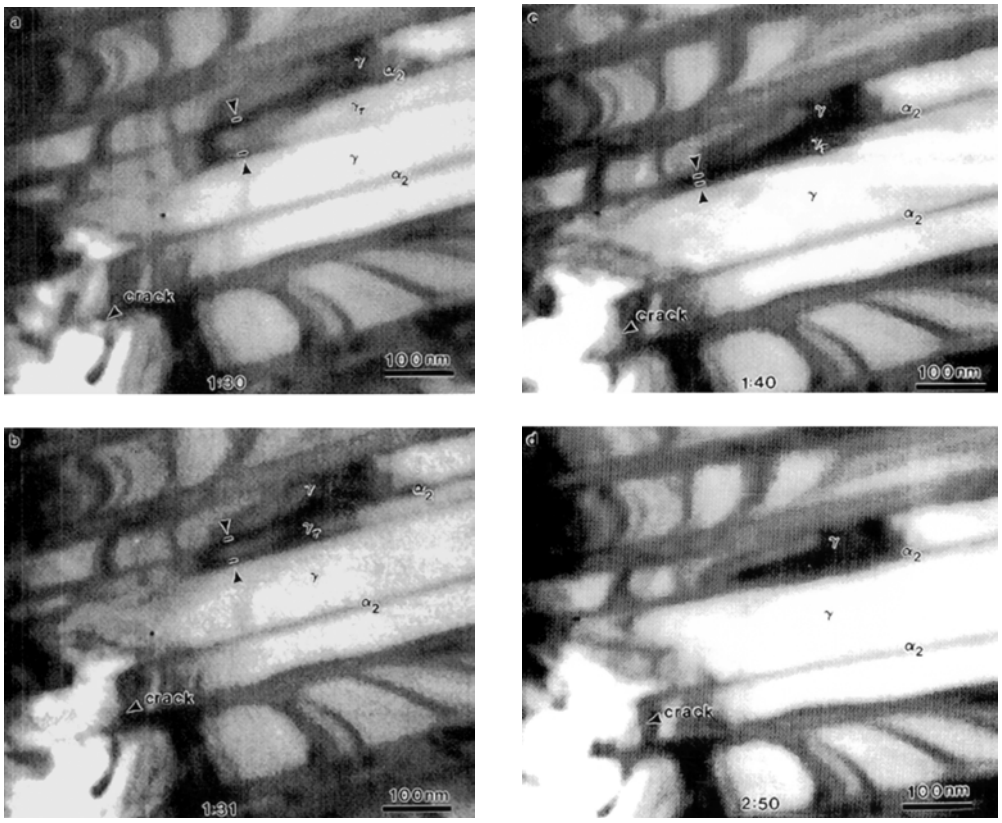

Fig. 5. Consecutive in-situ video images showing the migration of a twin-related interface near a crack tip; (a) t = 0, (b) t = 1 s, (c) t = 10 s, (d) t = 80 s.

Status of FY 2003 Milestones

Milestone: "Conduct in-situ TEM experiment to record a direct observation of interface sliding" was completed.
Milestone: "Continue to collaborate with ORNL (Dr. C.T. Liu) to fabricate refined $TiAl/Ti_3Al$ laminate composites from cast Ti-46.5Al-3Nb-1.0W-0.1B and Ti-46.5Al-3Nb-2W-0.1B alloys using hot-extrusion processing techniques" was completed.
Milestone: "Continue TEM characterization and microanalysis to measure the extent of solute segregation at lamellar interfaces" was on schedule and will be completed in June 2003.
Milestone: "Continue characterize the effect of alloying modification on creep resistance of the composite materials" was on schedule and will be completed in September 2003.

Travel

2003 TMS Annual Meeting, San Diego, CA (3/2 – 3/6, 2003).

Publications

L.M. Hsiung, A. J. Schwartz, and T.G. Nieh "In-Situ TEM Observations of Interface Sliding and Migration in a Refined Lamellar TiAl Alloy," presented in International Symposium on Intermetallic and Advanced Metallic Materials – A Symposium Dedicated to Dr. C. T. Liu, TMS Annual Meeting San Diego, CA, March 3, 2003; to be published in *Intermetallics*.

References

[1] L. M. Hsiung and T. G. Nieh, *Intermetallics* **7**, 821 (1999).
[2] L. M. Hsiung, T. G. Nieh, B.W. Choi, and J. Wadsworth, *Mater. Sci. Eng.*, A329-331, (2002), 637.
[3] M. Yamaguchi and Y. Umakoshi, *Progress in Materials Science, 34,* 1 (1990).

DISCLAIMER

This document was prepared as an account of work sponsored by an agency of the United States Government. Neither the United States Government nor the University of California nor any of their employees, makes any warranty, express or implied, or assumes any legal liability or responsibility for the accuracy, completeness, or usefulness of any information, apparatus, product, or process disclosed, or represents that its use would not infringe privately owned rights. Reference herein to any specific commercial product, process, or service by trade name, trademark, manufacturer, or otherwise, does not necessarily constitute or imply its endorsement, recommendation, or favoring by the United States Government or the University of California. The views and opinions of authors expressed herein do not necessarily state or reflect those of the United States Government or the University of California, and shall not be used for advertising or product endorsement purposes.

AUSPICE

This work was performed under the auspices of the U.S. Department of energy by University of California, Lawrence Livermore National Laboratory under contract No. W-7405-Eng-48.

Synthesis of Powders for Titanium Carbide/Nickel Aluminide Cermets

Michelle Zeles, Christopher Gump, and Alan Weimer (PI)
University of Colorado

Objective/Scope

The purpose of this research is to find a cheap, efficient way to produce titanium carbide (TiC) and nickel aluminide (NiAl or Ni_3Al) cermets. ORNL is interested in this cermet for possible use in diesel engine parts due to its wear and high temperature resistance. Current research has been focused on two different methods for making the pure materials and the cermet. One of the methods is a scale up of the research previously conducted in the large cup capacity Thermogravimetric Analyzer (TGA) using a modified SHS process called Thermally Ameliorated Rapid Powder Synthesis (TARPS). It was discovered that this process could synthesize a submicron cermet with a tight particle size distribution even when starting with significantly larger feed particles with a wide particle size distribution. A new reactor was engineered to test if the quality of the product could be reproduced on a larger scale. The other method involves continuous rapid reaction processing to synthesize the titanium carbide, nickel aluminides, and their cermets. These reactions are carried out in an aerosol transport tube reactor. This reactor design has been used on both the laboratory and industrial scale to synthesize high quality submicron ceramic and metal powders.

Technical Highlights

Task 1

The new reactor was designed for use in a horizontal tube furnace. Since it was made from graphite, it had to be sealed inside the furnace to prevent it from reacting at high temperature with oxygen in the air, while still allowing for the flow of purge gas in and out of the reaction mass. The initial sealing methods proved inadequate, as the ends of the muffle tube were quite rough. Eventually, a set of permanent end caps were machined and attached to the tube to improve the seal. Once the reactor was up and running, several experiments were run. The first few experiments involved creating TiC from titanium dioxide (TiO_2) and carbon pellets via carbothermal reduction. The final product looked very similar to the product obtained from the TGA. However, after analyzing the mass lost during the reaction (due to the evolution of carbon monoxide) it was determined that the product still contained oxygen bound to the titanium, and some free carbon. According to the mass balance, the final product contained 76% TiC, 17% TiO_2, and 7% free carbon. Leco elemental analysis (carbon and oxygen) will be performed later to confirm the composition of the product. Most likely, the reaction failed to go to completion because of incomplete heating of the reaction mass. As the carbothermal reduction began, the temperature in the reactor would have dropped since the reaction is endothermic. Although the reaction mass was held at the final temperature for 15 minutes, this may have been insufficient time to overcome the heat transfer limitations of the reactor. Indeed, these heat transfer limitations are one of the main reasons for running the reaction in the aerosol transport tube. Such a reactor design can eliminate heat transfer limitations. Additional runs were conducted with nickel and aluminum combined with the TiC product in order to create the TiC and Ni_3Al cermet. Most of resulting product came out of the reactor in a small clump that was easily broken into powder. A small quantity of material came out in loose power form and appeared to have not reacted. XRD analysis has yet to be performed on any of the above reaction products

because of equipment malfunction. Therefore, the exact product composition remains undetermined.

Task 2

Prior to beginning the rapid reaction processing of the nickel aluminides, initial work on the rapid carbothermal reduction of titania and carbon was performed. Based on experience with the rapid carbothermal synthesis of boron carbide, it was felt that feed rate of precursors into the reactor would be critical. Therefore, significant efforts were made to improve the particle feeding methods into the transport tube. These improvements would also carry over to the synthesis of the aluminides, since there is a safety issue running an exothermic reaction at high temperatures (>1000°C). A new feed reservoir and feeder were constructed in order to allow for the controlled, dispersed feeding of powders into the reactor. Previous feeders had significant shortcomings in both aspects. Once constructed, the new design proved effective in other studies, and a provisional patent on its design has been filed with the US Patent Office.

Using this feeder, a brief exploratory experimental matrix was design to determine what temperature range should be studied. The carbothermal reductions of boron oxide and titanium oxide both become thermodynamically favorable at comparable temperatures. For boron oxide, the transition temperature is about 1540°C, and for titanium dioxide the transition temperature is about 1340°C. Since it is known from experience that boron carbide can be synthesized in a continuous rapid reaction system in the range of 1800-2300°C, it was decided to begin the titanium carbide experiments in the 1900-2100°C range.

The feed was synthesized using the same method described in the FY 2000 Final Report (Synthesis of Ceramic Powders and Coating, Buechler et. al.). In short, a stoichiometric ratio of Degussa P25 titania and carbon black were milled using titanium media along with a fraction of corn and wheat starch to serve as a binding agent (the amount of carbon black used was reduced by the carbon content of the starches to maintain the stoichiometric ratio). Once well mixed, water was added to the dry powder, creating a slurry. The slurry was heated, causing the starch to congeal. The congealed solution was then dried in a tube furnace at 150°C to drive off the water. The dry mixture was then heated further to 300°C to carbonize the starch. The resulting flaked material was then re-milled using the titanium media to break the particles up. The resulting powder was sieved at 150 μm. The –150 μm fraction was utilized as the feed to the reactor.

The initial experiments were run at a residence time of 2.0 s and at temperatures of 1900, 2000, and 2100°C. After some initial difficulties with the feeder were over come, about 5-20 g of powder were synthesized at these conditions. In each case, the reaction could be monitored in real time by measuring the total gas flow of the system and the power drawn by the furnace, both of which are monitored by the computer control system for transport tube reactor. Since two moles of carbon monoxide are produced for every mole of titanium carbide, the flow meter on the reactor exit line would register an increase in flow whenever the reaction was occurring. Similarly, since the powder would absorb heat to reach the reaction temperature and the reaction would absorb additional heat (it is endothermic), the power drawn by the furnace would increase when powder was being fed. In previous experiments, this allowed for the calculation of a heat of reaction. However, such calculations require extended feeding times to generate accurate

results. Feeding times were not long enough for these runs to allow for such analysis, but in the future it should be possible. Table 1 shows the results for the elemental analysis of the three runs.

Table 1. Elemental compositions for the products of the three continuous rapid processing experiments

	Feed	1900°C	2000°C	2100°C	Pure TiC
% C	31.1	30.7	23.9	23.6	20.1
% O	27.7	21.1	6.4	4.3	--
% N	--	1.2	0.4	0.3	--
% Ti	41.3	47.0	69.3	71.8	79.9
% TiC	--	14.2	73.0	80.4	100
% free C	31.1	27.9	9.3	7.5	--

The weight percent of C, O, and N were measured using a Leco Corporation total carbon analyzer and N/O fusion analyzer. As can be seen, increasing the temperature reduces the amount of carbon and oxygen in the product. The purity of the resulting titanium carbide also increases. However, the purity is still too low to be of much use.

Figure 1 shows the particle size distributions for the 2000 and 2100°C experiments, along with the particle size distribution for TiC made by the batch process in the TGA. Both show significant amounts of submicron TiC, but the total distribution is quite broad. This has been seen before in the batch process for making TiC in the TGA. In that case it was attributed to mass transfer resistances during the reaction. When the feed preparation was altered to ensure close contact between the raw materials, the particle size distributions became much sharper and centered around 0.4 μm.

Future Plans

Task 1

1. Increase the extent of reaction for the TiC synthesis by increasing the hold time at high temperature and/or the maximum reaction temperature.
2. Produce tens of grams of submicron TiC/nickel aluminide powders.
3. Analyze the product powders using XRD, SEM, PSD, SA, Leco C and O.

Task 2

1. Further explore the synthesis conditions for TiC in the transport tube reactor.
2. Check feasibility of nickel aluminide synthesis in the transport tube.

Travel

2003 American Ceramics Society Annual Meeting in Nashville, TN – presented by Christopher Gump

Status of FY 2003 Milestones

Task 1

1. Graphite reactor received from supplier and integrated into tube furnace.
2. Tens of grams of titanium carbide and cermet material synthesized.
3. Analysis of products begun.

Task 2

1. Preliminary synthesis of grams of titanium carbide performed.
2. Analysis of titanium carbide product begun.
3. Experimental matrix designed.
4. New feedstocks designed to increase conversion.

Publications

Three papers are in the process of being written about each of the following: nickel aluminide, titanium carbide, and their cermet.

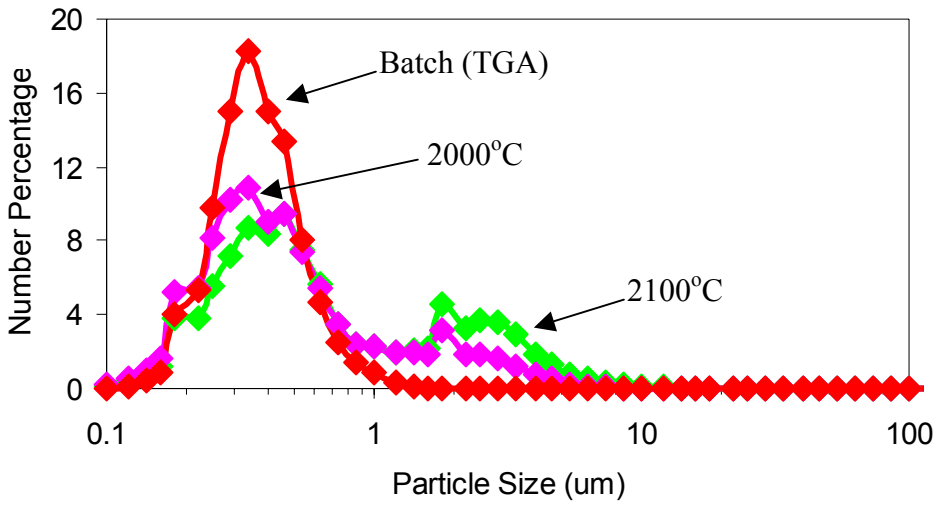

Figure 1. Particle size distributions for the product powders synthesized at 2000 and 2100°C by the continuous rapid process. The particle size distribution for powder synthesized bin the batch process is shown for comparison.

Laser Surface Texturing Of Lubricated Ceramic Parts

Peter J. Blau and Laura Riester
Oak Ridge National Laboratory

Objective/Scope

The objective of this effort is to evaluate the frictional benefits of laser dimple patterns on the lubrication of ceramic surfaces. This project is part of a joint Argonne National Laboratory/ ORNL analysis of the benefits of a laser surface texturing (LST) process developed by Prof. Itzhak Etsion, Surface Technologies, Ltd., Israel. That process uses a computer-controlled laser to produce a pattern of shallow, rounded dimples on bearing surfaces. Based on calculations, preliminary tests, and limited field trials, the developer claims that LST enhances the ability of a lubricated surface to establish a load-bearing hydrodynamic film that decreases friction relative to a non-dimpled surface. The ORNL portion of this joint effort is focused on two aspects of LST: (1) conducting reciprocating tests of ceramic surfaces using lubricating fluids with various viscosities, and (2) determining the microstructural changes that are associated with the LST process.

Technical Highlights

Effects of LST on the Microstructure of Zirconia. As previously reported, experiments were performed to investigate the effects of LST on the frictional response of transformation-toughened zirconia (TTZ) and SiC. This period, additional work was done to characterize the effects of rapid heating and cooling by LST on the TTZ.

Nanoindentation hardness numbers were measured in the zone of thermally disturbed material below the LST surfaces to see whether the local micro-mechanical properties were altered by dimpling. Figure 1 shows an optical image of a dimple on a taper-polished specimen of TTZ. The arrows indicate regions of fine-scale micro-cracks that were previously observed by scanning acoustic microscopy. Using a three-faced Berkovich indenter, 300 nm-deep nanoindentations were made in several of the regions surrounding the dimples, avoiding the micro-cracks. In addition, the load displacement data were used to estimate the modulus of elasticity of the materials in those regions. For reference, nanoindentation hardness was also measured in the bulk material, well away from the laser-treated region.

A summary of the results is provided in Table 1. For the sake of comparison, several distinct regions of the microstructures were identified. The 'bulk' refers to regions well below the surface of the specimen. 'Crater bottom' refers to material that was within the micro-cracked regions surrounding the bowl of the dimple. 'Rim' refers to material that stood above the as-ground surface, resembling a frozen splash created by the rapid laser heating and cooling of the surface material.

Table 1 indicates that, within the standard deviation of the data, the nanoindentation hardness did not vary significantly from one region to another, suggesting that the micro-mechanical properties of the material in the heat-affected zones were not significantly different from those of the bulk. On the other hand, the micro-cracked regions were avoided during these nanoindentation tests. The cracks could affect the properties of the larger volumes of material;

therefore, the fact that the hardness was not clearly different from one place to another does not imply that the integrity of the material was not compromised by microcracks.

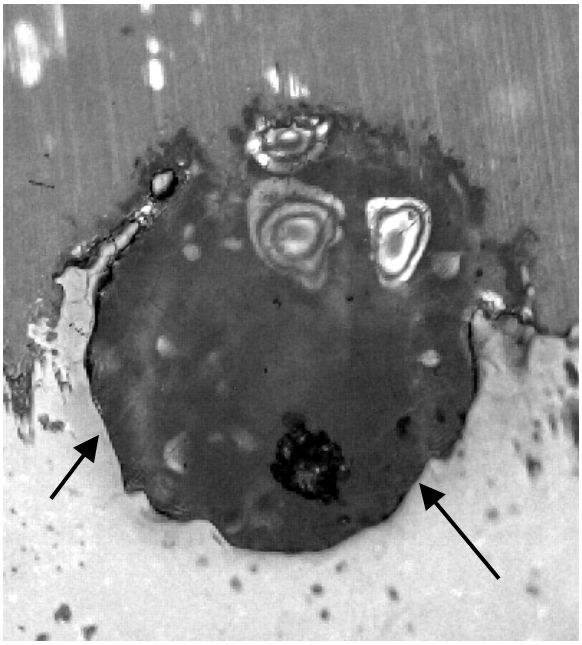

Figure 1. Light optical image of a taper-section of a dimple. Arrows indicate subsurface regions of fine micro-cracks where nanoindentations were placed. The narrow region extending upward from the dimple at the left is part of the crater rim.

Table 1. Nanoindentation Data for Laser-Surface-Treated Zirconia

Region	Ave. Nanoindentation Hardness (GPa)	Standard deviation (GPa)
Bulk region	16.1	1.7
Crater bottom	15.2	1.0
Rim region	15.3	2.2

Future Plans

(1) Continue microstructural analysis of the LST TTZ.
(2) Conduct microstructural analysis of the LST SiC specimens.

Travel

None.

FY 2003 Milestones

Complete studies on the effects of LST on the frictional behavior and microstructural changes produced on ceramic bearing surfaces. Submit final report. **(09/03)**

Publications

None this period.

High Density Infrared Surface Treatment of Materials For Heavy-Duty Vehicles

T. N. Tiegs, D. C. Harper, and C. A. Blue
Oak Ridge National Laboratory

Objective/Scope

High Density Infrared (HDI) technology is relatively new to the materials processing area and is gradually being exploited in materials processing. For many applications in heavy-duty vehicles, superior properties, such as corrosion and wear resistance, are only required at the material surface. The project using HDI technology will be exploratory and will examine (1) application of wear-resistant coatings, and (2) modification of plasma-sprayed coatings.

Technical Highlights

High Density Infrared (HDI) technology is relatively new to the materials processing area and is gradually being exploited in materials processing. The HDI processing facility at ORNL utilizes a unique technology to produce extremely high-power densities of 3.5 kW/cm^2 with a single lamp, which is currently the most powerful one in the world. Instead of using an electrically heated resistive element to produce radiant energy, a controlled and contained plasma is utilized. The advantages of the technology include:

1. Compared to laser technology, it can cover large areas,
2. Consists of short wavelength radiation (0.2-1.2 μm),
3. Fast heating and cooling rates,
4. Capable of attaining very high temperatures,
5. Potential for continuous processing.

Since the technology is relatively new, its utility to the surface treatment of materials for applications in heavy-duty vehicles will be explored. In most cases, the need for wear resistance, or corrosion resistance, or high strength is only necessary in selected areas of the part that is exposed to the working environment or under high stress. Therefore, it would be desirable to use materials that are lighter or less expensive for the bulk of the part and only have the appropriate surface properties where required. The project using HDI technology will be exploratory and will examine a couple of approaches on surface modification that would be of interest to materials for heavy-duty vehicles. The first area would be in the application and formation of adherent, wear/corrosion resistant coatings. The initial tests will be based on hardmetal compositions applied onto iron-based parts that are currently used. The other area that will be examined in the initial study would be the treatment of plasma-sprayed coatings that had been put on iron-based substrates. These types of coatings are presently used extensively in heavy-duty vehicles. Previous work had shown that HDI surface treatment of certain ceramics resulted in columnar grain growth at the surface. Thus, the HDI has the potential to modify the plasma sprayed microstructure to one that is columnar in nature. Such coating microstructures are believed to have better properties than the plasma sprayed coatings. In addition, the HDI approach would be more cost-effective than other competitive processes such as physical vapor deposition. Based on these exploratory studies, further research on the utilization of HDI technology could be ascertained.

The project has been initiated and base materials have procured. Three different iron-based alloys were chosen (gray cast iron, 4140 alloy steel, and D2 tool steel). Slurry coatings including WC-Ni, WC-Co, WC-Ni_3Al and TiC-Ni_3Al, are being fabricated. These will be applied to the metallic substrates and then surface treated in the HDI unit.

Status of Milestones
On schedule.

Communications/Visits/Travel
None.

Problems Encountered
None.

Publications
None.

Standards For Reliability Testing Of Heavy Vehicle Propulsion Materials

Stephen Hsu, William Luecke, Lew Ives, and Jerry Chuang
National Institute of Standards and Technology

Objective/Scope

The objective of this project is to develop international standard test methods for assessing the reliability of ceramic components used in diesel engines and other heavy vehicle propulsion systems. Silicon nitride ceramics offer a unique combination of light weight, high-temperature strength, and wear resistance. These properties make them attractive as roller lifters, valve inserts, and injectors for diesel engines. Their use allows longer durability. Reliability and cost-effectiveness are critical issues in implementing ceramics in the valve train of diesel engines. Ceramic valve train components are subjected to demanding conditions that include high contact loading, elevated temperatures, and corrosive environments. To ensure a reliable service life, standard test methods are needed to evaluate the performance of potential ceramics in highly loaded rolling and sliding contacts. This project will develop test methods for evaluating the contact damage behavior of ceramics under rolling and sliding conditions that simulate the cam roller followers, valves and valve seats. In support of this goal we will pursue four research thrusts: 1) fundamental understanding between microstructure and performance, 2) basic mechanisms of contact damage, 3) modeling and prediction of contact damage under cyclic loading, and 4) development of international standards for assessment of contact damage.

Technical Highlights

IEA Annex III Activities:

Activities under the IEA Annex III, approved by the Executive Committee in July 2002 include various forms of contact damage testing and evaluations relevant to the implementation of advanced materials in engines. These include rolling contact fatigue, sliding and fretting wear, fretting fatigue, and other mechanical performance phenomena that control the reliability of contacts in advanced engines. Materials under consideration may include structural ceramics, composites, and nanostructured friction/wear coatings.

Two Subtasks were initiated under this new annex. The objective of Subtask 1 (Technical Information Exchange) is to achieve a balanced exchange of technical information between the participating countries on contact reliability of ceramics and coatings. The Subtask activities may include (a) Exchange of reports, studies, and software packages as agreed upon in advance by the Executive Committee on an annual basis; (b) Joint technical meetings; (c) Reciprocal invitations to workshops and conferences; and (d) Reciprocal visits to research facilities.

The objective of Subtask 2 (Rolling Contact Fatigue Testing) is to compare the currently employed test methods used for evaluating rolling contact fatigue of advanced ceramics to develop a uniform, internationally agreed-upon testing protocol. Four test configurations are currently in popular use. These include 3-ball-on-rod (mostly used in the U.S.), cylinder-on-cylinder (mostly used in Europe), 4-ball (primarily used for lubrication analysis), and the thrust bearing (mainly used for bearing life testing). Each test configuration has unique attributes. However, no attempt has been made to compare and correlate the data generated by these test

configurations. Many issues require particular attention: defining ‘failure”, understanding the method by which “failure” is detected, distinguishing wear from fatigue, specifying parameters for surface finish, evaluating possible influences from machining damage, and incorporating micro slip and sliding into models.

Plans for an International Interlaboratory Study of Rolling Contact Fatigue:
The original plan was to run an interlaboratory study on the 3-ball-on-rod test (NTN or Federal Mogul) method, but the recent closing of the NTN U.S. Technical Center eliminated one possible participant and cast some doubt on the future of the test technique. As a result we have changed plans from primarily U.S.-based study of the 3-ball-on-rod test to an interlaboratory, inter-test comparison on two materials with participants from U.S.A., Europe and Asia. Rather than attempting to establish the precision and bias of a single test, we will be able to evaluate the suitability of a variety of tests to evaluating rolling contact fatigue. As far as we have been able to determine, such a study has never been conducted.

In pursuit of that goal we held a discussion held March 11, 2003 at NIST with Matt Ferber, Ray Johnson and Andrew Wereszczak of ORNL, and William Luecke and Stephen Hsu of NIST. Our current expectation is to run a test series lasting approximately two years, and involve as many laboratories as are willing to participate. NIST will provide base material, and in some cases, finished specimens, oversee all the administrative tasks, and prepare the final report to the participants.

Fatigue test development:
An important aspect of the standardization process is the evaluation of various relevant parameters that may influence test results. Moreover, the utility of most standards is enhanced by the capability of the test to examine a range of different conditions. Oil has been used almost exclusively in testing with the NTN ball and rod machine. This is not surprising since the test was originally developed to evaluate steel bearing materials. A distinct advantage of ceramic bearings (especially all-ceramic bearings) is that they permit use in environments that may be quite corrosive to steel. A series of tests was conducted with water as the lubricant. It has long been known that silicon nitride yields an interesting tribological response during sliding under water lubrication.[1] Depending on the contact stress and speed, after a short induction period of relatively high and irregular friction, a relatively rapid transition occurs to a condition of very low coefficient of friction (<0.01) and low wear. It is found that during the initial period of sliding, wear occurs yielding an extremely smooth surface. Measured surface roughness values on the order of a few nanometers Ra have been obtained. This polishing mode of wear is attributed to a tribochemical reaction between water and silicon nitride. The mechanism responsible for the ensuing extremely low coefficient of friction is controversial. The extremely smooth mating surfaces are conducive to the hydrodynamic regime. On the other hand, it has been argued that generation of a thin lubricious film in the sliding contact area due to the tribochemical reaction responsible for smoothing is responsible for the low coefficient of friction.[2]

In order to conduct water-lubricated tests, a simple gravity fed delivery system was installed. In function, the setup essentially duplicated the built-in oil drip-feed delivery arrangement. During operation, the water drip rate was adjusted to obtain approximately the same volume rate of delivery as is normally used for oil. The only additional modification was the installation of an o-ring between the collet nut and test rod to prevent water from entering the collet chuck. This

was done both to protect the steel collet components against corrosion by water and to prevent egress of oil from the collet and consequent "oil contamination" of the contact. The steel cups and bronze separator normally used in oil-lubricated tests were also used for water-lubricated tests. New cups were used for each test. All components were carefully solvent cleaned to eliminate oil from the contact.

A series of five tests were conducted employing NBD200 silicon nitride balls and a Ceradyne 147-31n HP silicon nitride rod. HP designates final finishing of the rod by hand polishing. A test load of 495 N was used yielding an initial Hertzian contact stress of 6.3 GPa. The results are

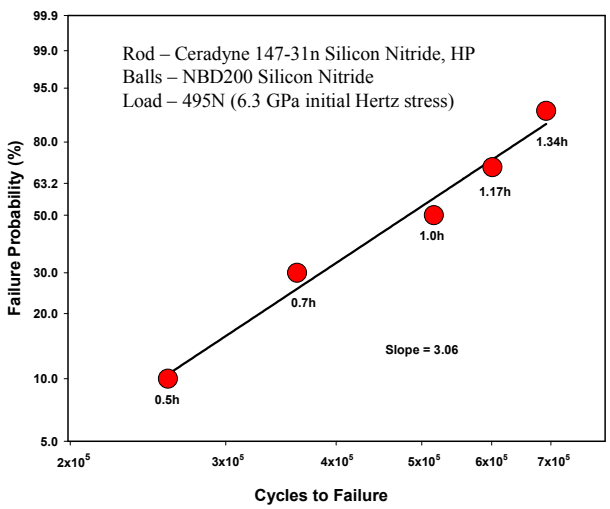

Fig. 1 Cycles to fatigue failure under water lubrication.

shown in Fig. 1. Fatigue failure occurred after a relatively short test duration in all cases. Under oil lubrication with CFI silicon nitride balls and HP rods all tests ran to suspension even at a higher 761 N load. That is, fatigue failure was not obtained with oil lubrication. We doubt that the use NBD 200 balls in the water-lubricated tests had any influence; however, tests will be conducted in the future to confirm this.

The amount of wear on the rods was relatively small. This is not surprising due to the short duration of the tests. Nevertheless, this also indicates that the presence of water did not lead to excessive wear. The fatigue spalls were several millimeters in length, similar to spalls that occurred with oil lubrication on rods that had not been hand polished after grinding.

The early onset of failure might be ascribed to a higher coefficient of friction and consequently higher tangential stresses associated water lubrication. This would be expected if transition to the low coefficient of friction regime, noted above, had not occurred. On the other hand, a deep pit was observed at the initial end of the spall in every case. Such pits were not observed in fatigue spalls formed under oil lubrication. Structural silicon nitrides, due to the presence of a glassy intergranular phase, are known to be susceptible to stress corrosion cracking. Thus, it may be that stress corrosion cracking was responsible for the large pit at the beginning of the spall, and the early fatigue failure with water lubrication.

In its current design, the NTN ball/rod machine does not incorporate the capability to measure such important variables as friction force and load variation during testing. Knowledge of these variables would provide an important asset in connection with the evaluation of test results. Moreover, knowledge of these test variables is necessary for support of the modeling activity that is being carried out in this project. For these reasons, force sensors will be inserted to monitor friction force and load. This can be done with only minor modification of the machine itself and will not affect the normal operation of the machine. Parts for the modification had been ordered.

On modeling the rolling contact fatigue in ceramic rods

The objective of this project is to predict fatigue life of a ceramic rotating rod subjected to rolling contacts by ball bearings, using analytical or numerical approaches such as finite element techniques and Weibull statistical analysis guided by experimental observations. Extensive literature search reveals that there are two major attributes affecting fatigue life: (1) As-received conditions and (2) Environments. The major parameters in the former category include: pre-existing defect distribution in the microstructure, surface topography such as surface roughness, asperity distribution, surface texture, etc., residual stresses induced by processing such as due to thermal expansion mismatches and machining or sample preparation and finish. Environments include: applied load, temperature, rotating speed if the material in consideration is rate-sensitive, lubrication or contaminants and temperature. Literature review also shows that a majority of work in this area is concerned with metallic materials such as steels, and moreover, the approaches they adopted were purely empirical; they seldom revealed insights with regards to the fundamental understanding on the failure mechanisms as well as predictive capability. Thus, there is a need to construct a model validated by experiment to predict life of a ceramic rod subjected to rolling contacts fatigue.

In general, there are two approaches used to attack contact fatigue problems of ceramics. The first is deterministic in nature using finite element stress analysis coupled with fracture or damage mechanics methodology. The second one involves Weibull statistic analysis preferred by ceramic researchers in their experimental work, since fatigue of ceramics in general is probablistic in nature due to inherent flaws already existed in the body. Our work will follow these two approaches depending on the experimental results of the project. In the stress analysis portion, we will develop two levels of model in terms of size scale: (1) Macro/continuum model; and (2) Micro-contact sliding model. In the former model, a 2D finite element model will be constructed with the material's constitutive laws incorporated damage or fracture mechanics. Thus, the problem is high non-linear, and the analysis will be carried out in a step-by-step fashion. In the micro model, contact mechanics principle will be injected to assess the effects of surface asperity and lubrication. The appropriateness of each model will be judged by comparing with the data produced from the current experimental program.

The following experimental data will be used to construct a preliminary model:

(1) The initial conditions including built-in residual stresses, porosity, and surface roughness.
(2) Periodic test samples obtained at 25%, 50%, 75%, 90% of life and post-test analyses.

References:
1. H. Tomizawa and T. E. Fischer, "Friction and Wear of Silicon Nitride and Silicon Nitride in Water," ASLE Trans. **30** (1987) pp. 41-46.
2. J. Xu, K. Kato, and T. Hirayama, "The Transition of Wear Mode During the Running-In Process of Silicon Nitride Sliding in Water," Wear 205 (1997) pp. 55-63.

Travel
None

Status of FY 2003 Milestones
1.) Organize a symposium on contact reliability to compare testing procedures used in different countries **(Oct. 2002).**

–done-- Completed a symposium among the participating countries on IEA activities on Oct. 29, 2002, during the ASME Tribology Conference in Cancun, Mexico.

2.) Propose to the IEA Executive Committee the formation of a new Subtask related to performance testing of nanostructured coatings for friction reduction **(Jan. 2003).**

Proposed a new subtask to the DOE program managers on an integrated surface technology. A workshop was held at NIST on March 11, 2003 in which ORNL, ANL, BNW and DOE headquarters were represented. A general agreement was reached to embark on this technology.

3.) Prepare draft progress report on international collaboration on rolling contact fatigue testing **(March 2003)**

The proposed IEA international round robin was modified at the March 11 meeting because of the closing of NTN Technical Center in the US. The new round robin is being initiated and solicitation of participants are requested from various country representatives.

4.) Complete preliminary round robin rolling contact fatigue testing **(June 2003).**

--deleted—due to change of plans

5.) Report progress of IEA Annex III activities to the Executive Committee **(July 2003)**

6.) Develop a preliminary analytical model for prediction of rolling contact fatigue lifetime **(September 2003)**

Publications
None

Implementing Agreement For A Programme Of Research And Development On Advanced Materials For Transportation Applications

M. K. Ferber
Oak Ridge National Laboratory

Objective/Scope

The International Energy Agency (IEA) was formed via an international treaty of oil consuming countries in response to the energy crisis of the 1970s. A major objective of the IEA is to promote secure energy supplies on reasonable and equitable terms. The governing board of the IEA, which is composed of energy officials from each member country, regularly reviews the world energy situation. To facilitate this activity, each member country provides energy experts who serve temporary staff assignments at IEA headquarters. These staff or secretariat support the governing board by collecting and analyzing energy data, making projections in energy usage, and undertaking studies on specialized energy topics. The governing board is also assisted by several standing groups, one being the committee on energy research and technology (CERT), which encourages international cooperation on energy technology. Implementing agreements (IAs) are the legal instruments used to define the general scope of the collaborative projects. There are currently 40 active implementing agreements covering research topics such as advanced fuel cells, coal combustion science, district heating and cooling, enhanced oil recovery, fluidised bed conversion, fusion materials, solar heating and cooling, pulp and paper, hydropower, heat pumping technologies, hybrid and electric vehicles, high temperature super conductivity, wind turbines, and high temperature materials. A complete listing can be found at the IEA website, www.iea.org.

This progress report summarizes recent activities in the implementing agreement entitled, "Implementing Agreement For A Programme Of Research And Development On Advanced Materials For Transportation Applications." This implementing agreement currently consists of one active annex entitled," Annex II: Co-Operative Program on Ceramics for Advanced Engines and Other Conservation Applications". The motivation for this IA is the development of new and improved ceramic materials, brittle material design methods, and life prediction methodology. The objective of Annex II is coordinated R&D on advanced ceramics leading to standardized methods for testing and characterization.

The Executive Committee for the IA on Advanced Materials is also exploring the possibility of adding new efforts (Annex III and Annex IV). Annex III focuses on the characterization of contact damage (fatigue) while Annex IV deals with materials for hydrogen storage.

Technical Highlights

A working group meeting for Subtasks 11 and 13 was held on Wednesday, January 29th from 6:00-8:00 p.m. in conjunction with the American Ceramic Society's 27th Annual Cocoa Beach Conference and Exposition on Advanced Ceramics & Composites. The following were in attendance:

- Matt Ferber - Oak Ridge National Laboratory (ORNL),
- Rolf Wäsche - Bundesanstalt für Materialforschung und-Prüfung (BAM),
- Mineo Mizuno - Japan Fine Ceramics Center,

The meeting began with a discussion of Subtask 11. Dr. Mizuno indicated that the work was now completed and he provided a draft copy of the Japanese Final report for Subtask 11. Next Dr. Wäsche summarized recent results obtained in Germany. Preliminary thermal fracture tests were conducted using SN282 silicon nitride. Due to range limitations of the temperature measurement device, it was necessary to correct the rim (outer diameter) temperature. Subsequent fractography also proved to be difficult. A key issue that must be addressed before the thermal fatigue experiments are initiated is the control of the laser heating required to generate the desired temperature-time (and thus stress-time) profiles.

Figure 1 compares the Weibull plot obtained by BAM with results generated for the SN282 in Subtask 9. The group also discussed potential reasons for the discrepancy observed in the thermal shock strengths. It was thought that the failure locations (edge versus near-edge) may have been different. Dr. Ferber suggested that in order to remove the edge effect, a set of thin disk specimens should be annealed prior to testing. He also indicated that another source for the discrepancy might be differences in the effective load factor for the various experimental setups. Recent work at NASA-Glenn has shown that unlike in conventional flexure tests where the load factor is constant for a fixed geometry and Weibull modulus, the load factor for the centrally heated disk specimen can change as a function of time. The group agreed that it would be worthwhile to re-examine the Subtask 9 thermal shock data.

Dr. Ferber summarized the results for the Subtask 11 effort in the United States. Flexural dynamic fatigue testing (strength measured as a function of stressing rate) indicated that the GS44 was susceptible to slow crack growth at 20, 500, 700, and 850°C. The slow crack growth exponent, N, at 850°C was 32. The Rotary Bend Fatigue (RBF) specimens were also evaluated (in the absence of rotation) using dynamic fatigue testing. The N values measured at 700 and 850°C tended to be higher than those determined from the flexure specimens. One factor affecting the validity of the results was the deformation of the grip located farthest from the applied external load. This deformation was assumed to be caused by the combined affects of high stresses and temperatures. To address the stress issue, a new loading scheme involving the application of equal but opposite loads is being investigated.

The next discussion topic was Subtask 13, which involves a round-robin assessment of burner rig testing. Dr. Mizuno described the system to be used in Japan, which operates at 1 atm total pressure and a velocity of 160-220 m/s. Preliminary tests were conducted on SN282 bars exposed to a 1200-1240°C combustion gas having a velocity of 175.7 m/s. To date 70 h of exposure have been accumulated.

Dr. Ferber then described the progress on Subtask 13 made in the United States effort (see Attachment B). Two approaches for implementing the burner rig studies are being pursued. In the first approach, a high-pressure, high-velocity combustion facility located at GE Global Research Center is being used to evaluate the environmental stability of SN282 silicon nitride. Operating conditions include a test temperature of 1120-1150°C, a total pressure of ~4.0 atm, and a gas velocity of ~100.0 m/s.

The second approach has focused on the design and fabrication of hardware required to adapt the existing creep/stress rupture test machines to accommodate a steam injection system. Currently an

alumina or SiC tube is used to inject steam directly onto the midspan of the gage section. This facility has been extremely effective in simulating recession and enhanced oxidation. The reason for the relatively high recession may be a result of the higher than expected velocity of the water vapor resulting from the confinement of gas in the small volume of the injection tube and forced flow through the narrow gap that separates the injection tube from the tensile specimen.

Dr. Wäsche indicated that he was had not yet located a partner for the burner rig testing in Germany. Dr. Ferber suggested that Germany could compliment the burner rig round robin by conducting static oxidation tests on SN282 in order to establish the baseline behavior.

The third order of business was to discuss the location of the next Executive Committee meeting. Both Dr. Wäsche and Dr. Mizuno proposed to hold this meeting in conjunction with the 8th ECerS European Conference & Exhibition, 29 June – 3 July 2003, Istanbul, Turkey. The group also agreed that it would be appropriate to conduct a Subtask 11 and 13 working group meeting during the same conference.

The final order of business was to discuss new activities in Annex II. Dr. Ferber suggested that group focus on the characterization of ceramic coatings. This activity, which would be conducted as Subtask 15-Annex II) would consist of a round-robin laboratory evaluation of the thin film adhesion test standards. The results would be used to evaluate and document the repeatability and reproducibility of the adhesion test. Dr. Ferber agreed to prepare a formal test plan for Subtask 15 to be presented at the next Executive Committee meeting.

Status of Milestones

All milestones are on track.

Communications/Visits/Travel

None.

Publications

None.

References

None

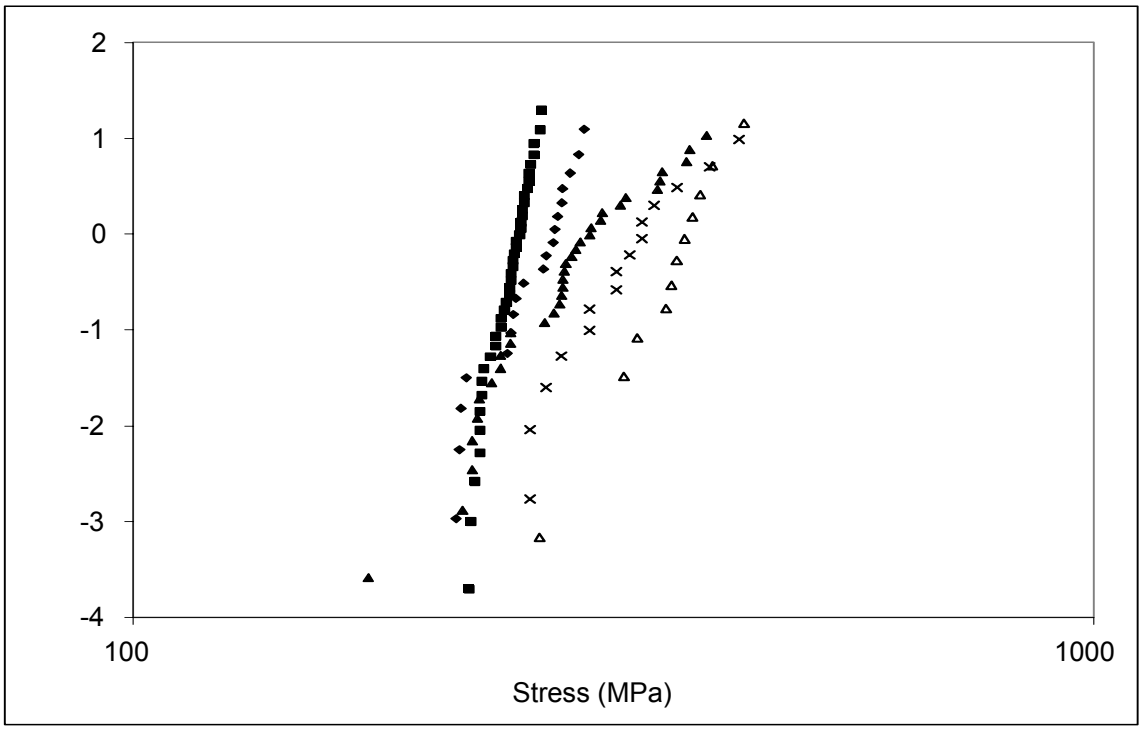

Figure 1: Comparison of Weibull plots generated from thermal shock tests conducted in Subtasks 9 and 11.

Mechanical Property Test Development

George Quinn
NIST

Objective/Scope

This task is to develop mechanical test method standards in support of the Propulsion Systems Materials Program. Test method development should meet the needs of the DOE engine community but should also consider the general USA structural ceramics community as well as foreign laboratories and companies. Draft recommendations for practices or procedures shall be developed based upon the needs identified above and circulated within the DOE engine community for review and modification. Round robins will be conducted as necessary. Procedures will be standardized by ASTM and/or ISO.

Technical Highlights

1. General

In this quarter, work was done to finish some manuscripts and reports, to revise some ASTM and ISO standards, to finish preparation of the new Vickers hardness standard reference material, and to plan for a new Applications Subcommittee in ASTM Committee C 28, Advanced Ceramics. We are hopeful we can get past these paper exercises and resume new test method development and experimental work in the next quarter.

2. Fracture Toughness

a. ISO FDIS 18756, Fracture Toughness by the SCF method

The final draft international standard (FDIS) was polished up in late 2002. Some editorial polishing work on the draft was done in February 2003 in cooperation with the secretariat. This document is done and is ready for final ISO balloting.

b. R-curve of Ceradyne SRBSN

Detailed discussions were held with Professor Jurgen Rödel of the Technical University Darmstadt, Germany about their new R-curve results for Ceradyne's SRBSN 147-31N. Mr. Quinn had sent some specimens to Prof. Rödel for evaluation in connection with the NIST study on machining g damage cracks in rods and bars. How does the low end of the R-curve relate to the performance of the machining cracks?

This same material was also featured in the 2003 first quarterly report (October 2002 – December 2003) by H. T. Lin and others at ORNL, along with M. Andrews at Caterpillar in their Life Prediction of Diesel Engine Components project for the Heavy Vehicles Propulsion Materials program. We already have collected fracture toughness data by the three methods in the ASTM standard for this silicon nitride, but we are keen on learning whether a short crack R-curve can be determined. Evidence from Darmstadt indicates there is a steep R curve.

Table 1 Standard Reference Materials

SRM	Specifics	Availability	Images
# **2100** Fracture Toughness of Ceramics K_{Ic}	(5) silicon nitride bend specimens with certified fracture toughness values: 4.57 MPa√m. Any method may be used.	Immediate $355	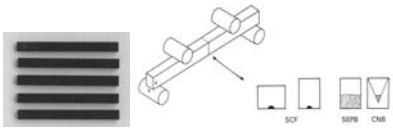
# **2830** Knoop Hardness of Ceramics HK2	(1) hot-isopressed (NBD-200) silicon nitride disks with 5 NIST 19.6 N (2 kgf) indentations HK ~ 14.0 GPa; 1,400 kgf/mm^2	Immediate $581	
# **2831** Vickers Hardness of Ceramics and Hardmetals HV1	(1) hot-isopressed tungsten carbide disk (12% cobalt) with (5) NIST 9.8 N (1 kgf) indentations. HV ~ 15.0 GPa; 1500 kgf/mm^2	Estimated April. 2003 Estimated $450	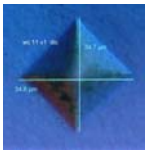

For more information about these SRMs, or any of the NIST power size standards, contact:

http://ts.nist.gov/ts/htdocs/230/232/232.htm

c. Manuscript on SRM 2100

We finished a manuscript on the fracture toughness Standard Reference Material 2100 for the 8th International Fracture Mechanics of Ceramics Conference in Houston in February. **Table 1** shows the three mechanical property SRMs that have been developed.

This new manuscript is the longest, most comprehensive report yet written on this SRM. Earlier papers were constrained by paper limitations. The goal of the new manuscript was to better document the creation and background of the reference material and to spread the news that the reference materials was available to as broad an audience as possible. The manuscript was a good complement to one given by Dr. Jonathan Salem of NASA-Glenn on the ASTM standard test method C 1421.

d. ISO DIS 15732 fracture toughness standard by the SEPB method

This Draft International Standard was reviewed this quarter. This was the first test method for fracture toughness to be advanced I ISO committee 206. It was written by Tetsuro Nose of Nippon Steel in 1997 and was reviewed in the USA by Professor Isa Bar-On of Worcester Polytechnic. Unfortunately, after a few years of active work, the document has languished ever since. The British had started to complain. We heard that a new draft was being circulated in TC 206, but a search of the TC web site failed to find the latest rendition. A copy was received from England, and Mr. Quinn made a quick review to ensure nothing had been slipped in or any changes made that ran counter to the ASTM version of this test method.

The new draft does indeed have corrections compared to the 1999 version and it was gratifying to see that a lot of changes we had recommended in 1999 had in fact been incorporated. The USA recommended changes had been ignored or lost by the Japanese secretariat in 1999. An old requirement that all testing had to be done in inert environment has been relaxed. Lab ambient testing is allowed, but new provisions to check for specimen compliance change and to check of the fracture surfaces for evidence of slow cracks growth have been added. Overall, the new draft is a useful improvement and is by and large consistent with the ASTM version. Messages about this were sent to Jon Salem and Mike Jenkins.

3. Flexural Strength of Advanced Ceramics – Rectangular Specimens

a. ASTM C 1161 Room Temperature Flexural Strength Final Revisions

Major revisions to this standard were made in 2001 – early 2002 including revisions to the standard machining requirements for a bend bar. During this quarterly period, the final proofs came back from ASTM headquarters for this final revision. The latest version will be C 1161-02c, where the "02" denotes 2002 and the "c" denotes the third version 2002. This work is complete. This last round of changes incorporated some elements copied over from the ISO version which was adopted in 2000. We also eliminated the old 1/8- x 1/4- x 2-in. specimen once and for all. We added some links to other related ASTM standard for slow crack growth

parameter determination (dynamic fatigue) and so forth. We expect C 1161-02c will be definitive version. No further changes will be necessary in the foreseeable long term.

b. ISO 14704 Room Temperature Flexural Strength

There was no activity. This standard is complete.

c. ASTM C 1211, Elevated Temperature Flexural Strength Revisions

This standard, which is the elevated temperature version of C1161, was overhauled in late 2002. Twenty separate revisions were balloted in late 2002 and comments or negatives were received from Jon Salem, Mike Jenkins, Sung Choi, and Vic Tennery. All the feedback was reviewed at the November ASTM Committee C-28 meeting in Miami. After about 1 hour of discussion, satisfactory solutions were found for all input received. The proof of the revised C 1211 came in early April 2003. Unfortunately it was poorly done and six typewritten pages of corrections had to be prepared and sent back to the ASTM editor. Once these changes are made, C 1211 will be released as C 1211-03 where the "03" denotes 2003. This version incorporates some of the same changes mentioned in the room temperature standard C 1161 above, and we expect C 1211-03 will also become the definitive version that will be stable for the foreseeable long term.

d. ISO DIS 17565, Elevated Temperature Flexural Strength

After the early 2002 enquiry stage ballot for conversion to a FDIS, the ISO secretariat seems to have forgotten about this document. It is nearly complete and there is little left that is controversial. The ISO secretariat was contacted in January 2003, and agreed to resume the final phase of getting this document fully approved. In January and February we worked on polishing up the document. We had to redo many of the figures in order to get them into ISO format. This work is finished. This document will be sent out by the secretariat for a 5-month enquiry stage ballot phase as a FDIS "Final Draft International Standard."

4. Fractography

a. ASTM Standard C 1322, Fractographic Analysis of Advanced Ceramics

The proofs for the second round of revisions in 2002 for this document have not yet been prepared by ASTM.

b. New NIST Guide to Practice for Fractographic Analysis

Although the ASTM Standard Practice for Fractographic Characterization of Fracture Origins has been on the books for six years now, NIST management felt that there was still a need for a

separate user-friendly "Guide to Best Practice" for fractographic analysis. Work will commence on this topic in FY 2003.

5. Flexural Strength Testing of Cylindrical Ceramic Specimens

A major 104-page NIST Special Publication on the findings of the fractography of machining damage cracks in Ceradyne SRBSN has been approved for publication. A short condensed article was written for Ceramic Engineering and Science Proceedings and was presented at the Engineering Science Division meeting of the American Ceramic Society in Cocoa Beach in January 2003.

The paper on the Weibull effective volumes and surfaces of rods loaded in flexure was published by the Journal of the American Ceramic Society in March 2003. It is a good complement to the test method standardization work.

6. Hardness

a. New Standard Reference Material SRM 2831 for Vickers Hardness

In October 2002, we finished preparing SRM 2831, Vickers Hardness of Ceramics and Hardmetals. Ninety-six disks were accepted for distribution by the NIST Reference Materials Office. The Statistical Engineering Division reviewed the data collected in order to prepare the uncertainty estimates for the certificate. They approved the data in January. SRM 2831 should be available in late April or early May. **Table 1** shows SRM 2831.

b. Update ASTM C 1326 Knoop Hardness and ASTM C 1327 Vickers Hardness

The process of updating and revisions ASTM Committee C-28 standards continued. This time the two hardness standards C 1326 for Knoop and C 1327 for Vickers will be updated. The changes are minor. Only four changes are being made to the Vickers standard and three to the Knoop standard. One involves relaxing the numerical aperture of the objective lens of the microscope used to measure the indentations slightly to make the ASTM version compatible wit the ISO 14705 standard that was adopted two years ago. Also, a specification for the allowable asymmetry of a Vickers indentation, also taken from the ISO standard, will be added to C 1327. Statements encouraging collection of hardness at more than one indentation load will be added to both standards.

c. U. S. Customs Service Use of ASTM C 1326 Knoop hardness standard

ASTM Committee C-28 standards for advanced ceramics are increasing being used. An interesting example is the U. S. Customs Service, which now cites C 1326 in their in-house

laboratory test work to assess import ceramics for possible tariffs. A clause in the Harmonized Tariff Schedule for the United States has a hardness stipulation. If certain import ceramics have a hardness greater than 9 on the Mohs scale, then duties may be adjusted from 4% to 4.5% or vice-versa. The Customs Service has decoded to convert the Mohs 9 requirement (the hardness of sapphire) to a more modern Knoop hardness requirement and an equivalent hardness of 1500 has been chosen. The Customs Service has acquired SRM 2830 Knoop hardness reference blocks from NIST and is using them to verify their own hardness testers.

7. New Applications Subcommittee for ASTM Committee C-28 Advanced Ceramics

ASTM Committee C 28 decided to reorganize itself at the November 2002 meeting in Miami. The sense was that the committee had done a good job in preparing generic standard test methods since the committee's inception in 1986, but that interest was petering out on the generic property work, in part since many of the key properties have indeed been standardized. Through the years, we had been aware that industry was desirous of having test methods and standards for specific components and applications. These are not generic property standards such as strength of a laboratory test piece such as a button-head tension specimen or a bend bar, but instead the strength of a honeycomb structure for a diesel filter or a catalytic converter substrate. Indeed, in the early days of committee C-28 in 1986-1990, there had been a performance subcommittee C-28.03 led by Don McGrath and Terry Richardson of Airesearch -Garrett, which contemplated applications or performance standards, but emphasis shifted in those early days back to the generic standards.

The new applications subcommittee can also craft materials specifications standards. Such specifications standards, based in part on Committee C-28's generic standards, have already been prepared in ASTM by committees F-34 on Bearings and F-04 on Surgical and Medical Devices. The executive committee of C-28 decided that the time had come to organize a C-28 subcommittee devoted to just such new applications and specifications standards. A new applications subcommittee chairman is being recruited as this was written and it is hoped the Committee can get this new imitative up and running in 2003.

To help the new subcommittee get off to a good start, we have started discussions about a task group on catalytic converter substrate strength or performance standards. Engineers at Corning have expressed a keen interest in this and have said they would be willing to actively participate.

8. Other

G. Quinn reviewed Kristen Breder's new ASTM draft standard test method on static fatigue testing and send comments back to Breder.

Status of Milestones

412146	Ballot major revisions to ASTM C 1161 flexural strength	September 2001
		Completed , October 2002✓
412147	Prepare ballot revisions for ASTM C 1322, Fractographic Analysis	April 2002
		Completed, January 2002✓
412148	Prepare follow on specimen machining revisions to ASTM C 1161 flexural strength if needed	April 2002
		Completed, April 2002✓
412149	Prepare ballot-ready first ASTM draft of cylindrical rod flexure strength test	April 2002
		Delayed
412150	Prepare paper on effect of machining on strength of SRBSN rods.	May 2002
		Completed, Nov. 2002 ✓
412151	Prepare review paper on flexural testing of cylindrical rods.	October 2002
		Delayed by completion of SRM 2831, HV

Communications/Visits/Travel

- Mr. Quinn attended the February 2003 conference in Houston on Fracture Mechanics of Ceramics.
- Extensive discussions were held with Dave Carruthers and Mike Jenkins about the formation of a new subcommittee for Applications in ASTM Committee C2-8.
- Collaborations with Technical University Darmstadt are underway to reconcile R-curve data they have generated on the SRBSN with our strength, fracture toughness.
- G. Quinn talked with A. Wereszczak about the possibility of doing fractographic analyses of Hexoloy SP silicon carbide.
- G. Quinn met with V. Pujari and also had a long discussion with N. Corbin of St. Gobain/Norton about the machining findings from the grinding study of rods and bars in Ceradyne's SRBSN.
- Discussions with Corning and Ford engineers were held about the possible applications standards subcommittee and their companies' interests in applications standards.
- Detailed technical discussions were held with Professor Jurgen Rödel of Technical University Darmstadt, Germany about R-cure characterization in Ceradyne's SRBSN 147-31N.
- Information on the effect of grinding flaws and lapping on biaxial ring on ring strengths were sent to Mark Andrews at Caterpillar.

Publications and Presentations

1. G D. Quinn, K. Xu, J. A, Salem, and J. J. Swab, "SRM 2100: the World's First Fracture Toughness Reference Material," subm. to 8th International Conference on the Fracture Mechanics of Glasses and Ceramics, Houston, Feb. 2003.
2. J. A. Salem, G. D. Quinn, and M. G. Jenkins, "Measuring the Real Fracture Toughness of Ceramics –ASTM C 1421," subm. to 8th International Conference on the Fracture Mechanics of Glasses and Ceramics, Houston, Feb. 2003.
3. G. D. Quinn, "Weibull Strength Scaling for Standardized Rectangular Flexure Specimens," J. Am. Ceram. Soc., 86 [3] (2003) pp. 508-510.
4. G. D. Quinn, "Weibull Effective Volumes and Surfaces for Cylindrical Rods Loaded in Flexure," J. Am. Ceram. Soc., 86 [3] (2003) pp. 475-478.
5. G. D. Quinn, L. K, Ives, and S. Jahanmir, "On the Fractographic Analysis of Machining Cracks in Ground Ceramics: A Case Study on Silicon Nitride," NIST SP 966, 2003.
6. G. D. Quinn, L. K, Ives, and S. Jahanmir, "Machining Damage Cracks: How to Find and Characterize Them by Fractography, " to be publ. Ceram. Eng. Sci Proc., Vol. 24, Issue 3 or 4, 2003.
7. G. D. Quinn, L. K, Ives, and S. Jahanmir, "On the Nature of Machining Cracks in Ground Ceramics: Part I: SRBSN Strengths and Fractographic Analysis," subm to Machining Science and Technology, Dec. 2002.
8. G. D. Quinn, L. K, Ives, and S. Jahanmir, "On the Nature of Machining Cracks in Ground Ceramics: Part II: Comparison to Other Silicon Nitrides and Damage Maps subm to Machining Science and Technology, Jan. 2003.